Active sites on the surface of nanocrystalline semiconductor oxides ZnO and SnO_2 and gas sensitivity*

A. V. Marikutsa, N. A. Vorob´eva, M. N. Rumyantseva, and A. M. Gas´kov*

Department of Chemistry, M. V. Lomonosov Moscow State University, Building 3, 1 Leninskie Gory, 119992 Moscow, Russian Federation. Fax: +7 (495) 939 0998. E-mail: artem.marikutsa@gmail.com

The data on active sites on the surface of nanocrystalline semiconductor oxides ZnO and SnO_2 are reviewed. Their interrelation to the gas sensitivity of the materials toward the main air pollutants, *viz.*, CO, NO_2, NH_3, and H_2S, is analyzed. The influence of the synthesis conditions, microstructure parameters, content of dopant impurities, and the presence of catalytic modifiers on the concentration of various active sites on the oxide surface is considered. Relationships between the concentration of the surface sites and sensitivity of the oxides to gases with various chemical properties are revealed. The active sites responsible for the formation of a sensory signal upon the selective interaction with molecules of the detected gases are determined.

Key words: active site, tin dioxide, zinc oxide, gas sensor, oxide surface, nanocrystals.

1. Introduction

Nanocrystalline metal oxides ZnO, SnO_2, WO_3, In_2O_3, and TiO_2 are of significant interest for the development of gas sensors. These materials are unique due to a combination of fundamental physical and chemical properties. The listed oxides are wide band gap semiconductors with conductivity of n-type and a band gap of 2.5—4.5 eV under standard conditions, which makes it possible to detect a change in the electrophysical properties of the oxides in the temperature range from room temperature to 600 °C when redox reactions solid—gas are observed on the surface. The oxide surface has high adsorption properties and reactivity caused by the presence of free electrons in the conduction band of the semiconductor, surface and volume oxygen vacancies, and active chemisorbed oxygen. All oxides are stable in air on heating to 600 °C and can be obtained in the highly dispersed state with a crystallite size of 3—50 nm and the specific surface up to 100—150 $m^2\,g^{-1}$.

Gas sensitivity of nanocrystalline semiconductor oxides are determined by effects of the electrochemical interaction of molecules in the gas phase with the semiconductor surface. For example, the electric conductivity of materials decreases with an increase in the oxygen content in the gas phase because of chemisorption on the surface of acceptor molecules of O_2 (gas-oxidant) and localization of electrons in the sub-surface layer. The gases with the electron-donor properties CO, NH_3, and H_2S (gas-reducing agents) interact with chemisorbed oxygen, which results in a decrease in the negative charge density on the surface and an increase in the electric conductivity. For the major pollutants of air CO, NH_3, H_2S, and NO_x, a noticeable change in the conductivity (sensor signal) can be detected in the presence of trace concentrations of pollutants (0.1—10 ppm) in air.

In spite of the high sensitivity to the content of impurities in air, the use of broad-band semiconductor oxides in the production of gas sensors is restricted for several reasons. The main of them is low selectivity, since molecules of gases with similar redox properties toward the oxide surface make indiscernible contributions to the sensor signal. This impedes the use of semiconductor sensors for the detection in air of dangerous impurities from a large group of gas-reducing agents, such as CO, NH_3, and H_2S on the background of interfering impurities that are present, as a rule, in high concentration.

The fundamental approach to the solution of the problem of selectivity of sensor materials is based[1] on the statement that the character of interaction of the material with gas molecules is determined by the nature and concentration of active sites on the surface. Active site is a local area on the surface possessing specific chemical properties. Single atoms, atomic groups, molecules or their derivatives, defects of the crystal structure, and electron orbitals of surface atoms can act as these sites.[1—3] The presence of non-compensated bonds in atomic groups and saturation of the coordination environment of sur-

* Based on the Materials of the XX Mendeleev Congress on General and Applied Chemistry (September 26—30, 2016, Ekaterinburg, Russia).

Published in Russian in *Izvestiya Akademii Nauk. Seriya Khimicheskaya,* No. 10, pp. 1728—1764, October, 2017.

1066-5285/17/6610-1728

face cations and anions determine the adsorbability and reactivity of active sites. On the one hand, active sites interact with gas molecules from the external medium; on the other hand, they are in the electron interaction with the semiconductor matrix. On the whole, these sites form so-called "molecular ensembles," [1] the composition and electronic state of which determine the key functional properties of the sensor: sensitivity and selectivity. According to the earlier published classification,[4,5] active sites are responsible for the first stage of sensor sensitivity, so-called "reception" including the chemisorption of gas molecules and the redox interaction with them. The role of the semiconductor matrix is the conversion of electronic pulses appeared on the surface to the integral electric signal and transmission of this signal into the external chain, so-called "transduction."

The following three approaches are distinguished in the works devoted to the chemical modification of sensor materials as a method of enhancing selectivity.

(1) Cross-linking of synthetic organic receptors, whose chemical properties and topology are complementary to the properties of target gas molecules in such a way that interactions between them would proceed *via* the "key—lock" principle.[6] For this purpose, the surface of semiconductor oxides is modified by organometallic complexes mainly based on metal porphyrins and phthalocyanines "tuned" to molecular recognition of dangerous gases, the cavity size and adsorbability of which can be controlled depending on the sizes and properties of target gas molecules.[6—9] For instance, bivalent iron and cobalt cations have high affinity to coordination of gaseous oxygen and oxidation of hydrocarbon molecules.[10,11] Copper and zinc phthalocyanines manifest selectivity in the interaction with ammonia,[8,12] and copper and nickel cations are also efficient for hydrogen sulfide detection.[13]

(2) Enhancement of the reactivity of the material by the formation of new specific sites on the surface. As applied to semiconductor oxides, this takes place most frequently by the deposition of catalytic additives in the form of clusters or nanoparticles of noble metals and their oxides or transition metal oxides on the surface of the semiconductor matrix.[14—16] It is assumed that the catalytic clusters on the surface of the sensor material perform functions similar to the functions of the active sites of the heterogeneous catalysts: the formation of the molecule—site chemical bond and weakening of interatomic bonds inside the molecule, the formation of a labile intermediate and its transformation into the reaction product, desorption of the product, and regeneration of the active site.[17,18] Catalyst selectivity is determined by the chemical properties and sizes of active sites and reactant molecules, as well as the thermodynamics of chemisorption and chemical transformation of the initial molecules and intermediates.[18] Note that the modification of the sensor material surface by catalytic additives is efficient for both enhancing selectivity to certain molecules and decreasing the temperature necessary for their detection, since the mechanism of catalysis implies a decrease in the activation barriers to the interaction with gas. In this case, it is necessary that catalytic clusters would provide the electrochemical interaction involving electrons of the semiconductor support.

(3) Enhancement of the adsorbability by the modification of acid-base properties. For example, to increase the selectivity of detection of basic ammonia and amine molecules, it seems reasonable to increase purposefully the concentration of strong acidic (Lewis) sites, while the concentration of basic sites on the sensitive material surface should be increased when acidic molecules (hydrogen sulphide, sulphur dioxide) are detected.[19,20]

As shown previously,[21] it is important that the adsorbability and reactivity of the surface would be balanced. For example, the highest sensor sensitivity of semiconductor oxides toward alcohol molecules is achieved if comparable amounts of OH groups and oxygen anions acting as adsorption and oxidative sites, respectively, are present on the surface. The modification of adsorption sites of the surface can be performed by the chemical way, for example, by the formation of superacid centers on the SnO_2 surface by sulfation[22] or by the introduction of acidic oxides of transition metals, which is often accompanied by a change in both the adsorption and catalytic properties of the surface.[23]

Note that the methods of modification of oxide surfaces listed above do not allow one to control separately the receptor and transduction functions of the sensor materials. The modifiers deposited on the surface affect the concentration and activity of surface sites. At the same time, modification results in a change in the state of intergranular barriers, diffusion of modifier atoms into the volume, and doping and, thus affects the value of the sensor signal caused by a change in the composition of the gas phase.

In spite of practical significance and numerous scientific works on the sensor theme, the "chemical" approach to the consideration of gas sensitivity focused on the study of active sites on the surface of sensor materials is not popular. The most part of experimental and theoretical works is devoted to the physical aspects of sensor signal formation. The physical approaches make it possible to predict the dependence of the sensor signal on the shape and size of particles of nanocrystalline oxide and morphology and thickness of the sensitive layer.[4,24] They also allow the specific resistance of the material to be efficiently motored by doping.[14] For instance, donor additives of Sb^V or fluorine are introduced to enhance the conductivity in SnO_2, while ZnO is doped with Al^{III}, Ga^{III}, or In^{III} for the same purposes. However, the influence of dopants on the chemical properties and reactivity of the surface interacting with gases is completely ignored.

The data on the influence of catalytic modifiers and doping impurities on active sites of nanocrystalline semiconductor tin(IV) and zinc oxides and their gas sensitivity are systematized for the first time in this review.

The study of active sites on the surface of gas-sensitive oxides is conjugated with a series of difficulties. Presently there is no distinct concept about their nature and it is not clear what of the surface sites are "active" indeed, *i.e.*, directly react with gas molecules. In spite of the high fraction of the surface in the total number of atoms in the nanomaterials (up to 10—30% with decreasing the average particle size within 3—4 nm), the equilibrium concentration of active site on the surface is low and, therefore, their presence does not affect the fundamental chemical properties of semiconductor oxides.[1] The study of the properties of the surface requires using sensitive physicochemical methods of analysis directly under the operation conditions of sensors *operando*, at the working temperature of the sensor in air in the presence of a trace concentration of target gases. The small size of active sites compared to the size of atom or cluster (0.1—1 nm) results in a difficult of their visualization, especially when studying the surface of highly dispersed materials, the size of structural units of which is comparable with the size of active site. It should be mentioned that quantitative analysis of the nanomaterial surface is difficult. In these cases, to determine the concentration of active sites, it seems reasonable to use procedures of spectroscopy of probe molecules, for example, thermodesorption mass spectrometry (TDS),[25] temperature-programmed desorption (TPD),[26] IR diffuse reflectance spectroscopy,[27,28] spectrophotometric titration,[28,29] and *in situ* ESR spectroscopy. Probe molecules interact with certain active sites and thus serve as markers, and a change in their concentration allows one to judge about the concentration of these sites. A particular type of probe molecules are isotope-labeled oxygen molecules widely used in the method is isotope oxygen exchange $^{18}O/^{16}O$ when studying active sites of heterogeneous catalysts.[30] This method makes it possible to analyze the mechanism and kinetics of the interaction of the catalytic centers with oxygen and determine quantitatively the degree of participation of lattice oxygen of the support in these processes. It is evident that the study of the oxygen exchange of sensor materials with the gas phase is reasonable taking into account that gas sensors are used under atmospheric conditions and chemisorbed oxygen is a direct participant of the interaction of the surface with molecules of analyzed gases. However, data on the oxygen exchange for sensor materials are not met in the literature and were obtained by us for the first time.

2. Types of active sites on the surface of semiconductor oxides and investigation methods

Taking into account the structural concepts, active sites on the surface of metal oxides can be classified as follows[2,3]: coordinately unsaturated metal cations and oxygen anions and point defects (cationic and anionic vacancies, interstitial atoms). These "intrinsic" sites are typical of the solid surface that was not subjected to special preparation, for example, chemical modification. Two more types of sites are always present on the real oxide surface as a result of gas adsorption from air: chemisorbed forms of oxygen and hydrate—hydroxyl layer (HHL) including all possible products of molecular and dissociative adsorption of water molecules on the oxide surface. The chemical modification by catalytic additives forms extrinsic active sites on the oxide surface: clusters of noble metals or their oxides. According to the manifested chemical properties and methods of their investigation, the active sites can conventionally be divided into redox and acid-base sites. The types of active sites on the surface of modified tin dioxide are schematically shown in Fig. 1.

2.1. Acid-base sites. Acid-base sites of two types exist on the oxide surface: Lewis (strong) and Brønsted (weak) sites. Lewis sites are surface atoms being donors (basic

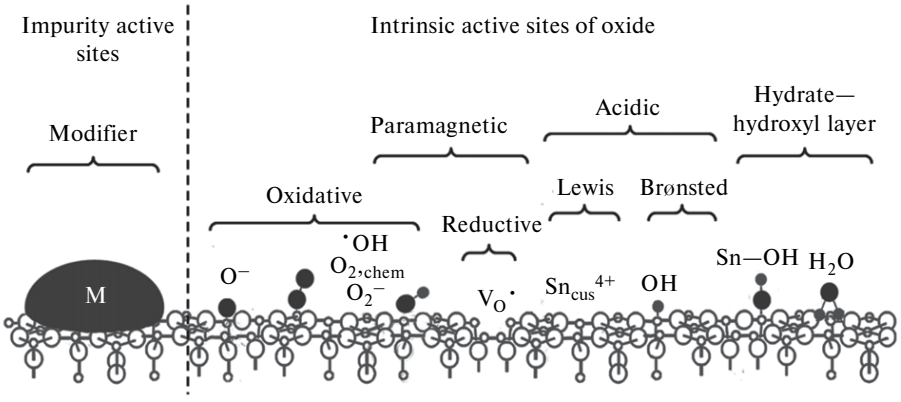

Fig. 1. Types of active sites on the modified SnO_2 surface; $O_{2,chem}$ are chemisorbed O_2 molecules, and Sn_{cus}^{4+} are coordinately unsaturated surface cations.

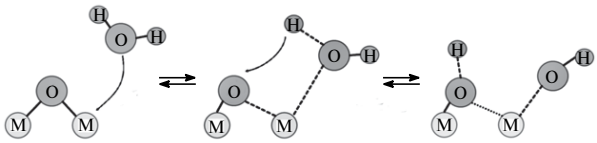

Fig. 2. Scheme of dissociative adsorption of water molecules on the metal oxide surface with the formation of bridging and terminal hydroxyl groups.

sites) or acceptors (acidic sites) of an electron pair during the interaction with gas molecules. During chemisorption of gas molecules, Brønsted acidic sites tend to donate proton, whereas Brønsted basic sites accept proton from chemisorbed molecules. Lewis sites on the surface of SnO_2 and ZnO oxides can be of two types: (1) acidic coordinately unsaturated tin and zinc cations and (2) basic lattice oxygen anions. The Brønsted sites are acidic (bridging OH groups formed upon the protonation of surface anions (Fig. 2)) and terminal OH groups representing a residue of the water molecule upon dissociative adsorption capable of exhibiting both acidic and basic properties.

The methods of investigation of surface acid-base sites can conventionally be divided into the following, depending on the crystalline state and morphology of oxide: (1) methods of investigation of single crystal surfaces close to ideal and thin films; and (2) methods of investigation of nanocrystalline material surface characterized by high lability of the chemical state of active sites. The first group of methods includes quantum chemical calculation methods that make it possible to predict some properties of Lewis sites: coordination numbers of surface cations and anions, degree of covalence of their bond with adsorbates, *etc*. Among experimental procedures of studying Lewis acid-base sites one can distinguish the methods of determination of the oxidation state and coordination environment of surface cations and anions, such as X-ray photoelectron spectroscopy (XPS),[31] electron paramagnetic resonance spectroscopy (ESR),[32] and Mössbauer spectroscopy.[33] The methods using basic probe molecules (ammonia, amines, pyridine) under the *in situ* conditions are efficient for the study of acidic sites of nanocrystalline oxides: spectrophotometric titration in the presence of indicators,[26,34] TDS,[25] and TPD (see Ref. 26). In the indicator methods, the parameter of strength of acidic and basic sites is the Hammett function (H_0), whereas the desorption temperature of probe molecules from the sites is the strength parameter in thermodesorption methods. An ammonia molecule is a convenient probe molecule in the investigation of acid-base properties of nanocrystalline tin dioxide by the TPD method. From the viewpoint of thermodynamics, desorption takes place under the following condition:

$$\Delta G_{des} = \Delta H_{des} - T\Delta S_{des} \leq 0, \quad (1)$$

where ΔG_{des}, ΔH_{des}, and ΔS_{des} are the Gibbs energy, enthalpy, and entropy of desorption, respectively. In this case, $\Delta H_{des} > 0$ (desorption is the endothermic process) and $\Delta S_{des} > 0$, because upon desorption the entropy of the system increases due to an increase in the concentration of gas-phase molecules. The enthalpy of desorption is determined by the bonding energy of molecules with adsorption sites. Since the entropy factor depends poorly on the type of adsorption sites, the temperature $T \geq \Delta H_{des}/\Delta S_{des}$, at which the desorption of NH_3 becomes possible, can be considered as a characteristic of the strength of acidic sites. The concentrations of acidic sites of various strength are determined using the earlier described model[35] under the assumption that one NH_3 molecule desorbs from one site.

The quantum chemical simulation of the oxidized and reduced $SnO_2(110)$ surfaces shows the presence of the following Lewis acidic sites on them: Sn^{IV} cations with the coordination number equal to 5 designated as Sn^{IV}_{5c} and Sn^{II} cations with the coordination number 4 designated as Sn^{II}_{4c}.[36—38] The existence of coordinately unsaturated Sn^{II}_{4c} cations is caused by oxygen vacancies in the nearest environment, the concentration of which in tin dioxide is very low (10^{-4}—10^{-3} at.%). Therefore, Sn^{II}_{4c} can experimentally observed only after the special treatment of the surface aimed at increasing the degree of oxygen deficient for example, heating *in vacuo*, thermal treatment in the reductive medium, and etching with argon plasma.[31] The IR spectrum of tin dioxide kept *in vacuo* at 450 °C after contact with oxygen contains a band assigned to vibrations[3] of the Sn^{II}—O_2 bond at $\nu = 1060$ cm^{-1}. The coordinately unsaturated cations Sn^{IV}_{5c} and Sn^{II}_{4c} are among adsorption sites on the SnO_2 surface. The adsorption properties of the cations are manifested toward both acceptor (oxygen,[39,40] nitrogen dioxide[41]) and donor molecules (CO,[42] H_2O,[43] NH_3 (see Refs 36 and 44)). It was assumed that the adsorbability of the Sn^{II}_{4c} sites is higher than that of Sn^{IV}_{5c} and this affects a higher energy of adsorption and energy of the bond with adsorbates.[36,39,45,46] The presence of free electron orbitals at the surface tin cations results in their Lewis acidity, which manifests itself for the chemisorption of molecules containing lone electron pairs: ammonia,[36,44] water, ethanol,[44,47] and oxygen.[39] The variable valence of tin determines the redox properties of the SnO_2 surface.[17] The Sn^{IV}_{5c} cations can be partially reduced during chemisorption of donor molecules or can accept electrons released upon the desorption or interaction of lattice oxygen with other molecules exhibiting reductive properties.[48] In turn, the Sn^{II} cations are characterized by the reductive properties determining the enhanced adsorption activity of the oxygen-deficient SnO_2 surface toward acceptor gases.[39,41]

The study of the single crystal surface of zinc oxide by the experimental and theoretical methods was carried out

mainly for polar (0001), (000$\bar{1}$) and nonpolar (10$\bar{1}$0), (11$\bar{2}$0) planes of which the ZnO(10$\bar{1}$0) surface is most energetically favorable.[49] The basis planes of the single crystals (0001) and (000$\bar{1}$) are polar: the ZnO(0001) surface is restricted by zinc cations (Zn—ZnO), whereas the ZnO(000$\bar{1}$) surface is restricted by oxygen anions (O—ZnO). Their electrostatic instability can be compensated by the reconstruction of the Zn—ZnO surface with the formation of triangular "terraces." The O—ZnO surface can be stabilized by the formation of either ordered oxygen vacancies,[49] or OH groups upon the interaction of the O—ZnO surface with hydrogen atoms or water molecules.[50] Surface OH groups can also be formed for other faces of zinc oxide. For example, the study of water adsorption on the ZnO (10$\bar{1}$0) surface showed that some portion of water molecules existed directly in the form of H_2O and another portion exists in the dissociated form.[51] It was established[52] by the study of polycrystalline zinc oxide that the material had no strong acidic sites with $H_0 \le 5$; however, weak acidic sites ($5 \le H_0 \le 7$) are present on the surface in a concentration of 0.004 mmol g^{-1}. The thermal treatments *in vacuo* and in air enhance the concentration of weak acidic sites to 0.009—0.010 mmol g^{-1}. A significant number of strong acidic sites for the samples annealed at $T = 300$—400 °C was found by an analysis of nanocrystalline ZnO obtained from zinc chloride by precipitation with aqueous solution of ammonia followed by the thermal treatment. The titration of a suspension of nanocrystalline ZnO with a solution of *n*-butylamine in benzene in the presence of indicators allowed the acidic strength of the surface to be estimated as medium,[53] and annealing at 300 and 600 °C does not change the ration of acidic sites and an increase in the annealing temperature to 900 °C results in a decrease in the concentration of acidic sites ($H_0 \le 7$) and the formation of stronger acidic sites with $H_0 \le 5$.

Bridging anions O^{2-} are considered as Lewis basic sites on the surface of oxides SnO_2 and ZnO, which is explained by their coordination unsaturation, a weak bond with the adjacent cations, and, hence, enhanced reactivity. Their basic properties are manifested in that the bridging O^{2-} anions are precursors of bridging hydroxyl groups formed by proton addition[17,54]:

$$O_2^- + H^+ \rightleftharpoons OH^-. \qquad (2)$$

Dissociated water molecules (see Fig. 2) or molecules of hydrogen,[54,55] methane,[48] and other hydrogen-containing compounds can be sources of H^+ in similar processes. The basic properties of surface anions appear also in the formation of surface carbonates in the presence of carbon dioxide,[56] which is used in the study of basic Lewis sites by the TPD-CO_2 method. In the work[53] where the strength and concentration of basic sites on the surface of nanocrystalline zinc oxide was evaluated by the titration of a suspension of powders with trichloroacetic acid in benzene in the presence of indicators, it was shown that a change in the annealing temperature of ZnO (300, 600, and 900 °C) did not change the concentration of basic sites with $H_0 \ge 3.3$, but at an annealing temperature of 900 °C the basic sites with $H_0 \ge 4.8$ disappear.

2.2. Chemisorbed oxygen. Chemisorbed forms of oxygen are most significant as active sites directly involved in redox processes on the surface of semiconductor oxides and determining their sensor sensitivity. These forms are conventionally divided as follows:

(a) physically adsorbed molecules ($O_{2,phys}$) retained by van der Waals bonds;

(b) chemisorbed molecules ($O_{2,chem}$) bound to tin cations by the covalent bond *via* the local transfer of the electron density;

(c) ionosorbed molecular (O_2^-, O_2^{2-}) and atomic (O^-, O^{2-}) oxygen species.

The character of oxygen adsorption is determined by temperature as follows:

(1) at $T < 200$ K physical adsorption predominates[57];

(2) in the temperature range from room temperature to 150—200 °C molecular chemisorption[39] and formation of superoxide anions[15,17] O_2^- prevail;

(3) at $T = 200$—350 °C dissociative ionosorption[15,39] with the formation of O^- and O^{2-} predominates;

(4) at $T > 350$ °C complete ionization of atomic species[37] to O^{2-} predominates.

Chemisorption of oxygen on the tin dioxide surface was studied using quantum chemical modeling that describes the interaction with the ideal SnO_2(110) surface and by experimental methods. The studies of oxygen adsorption on the single crystal surface and on nanocrystalline tin dioxide were conducted by both spectral methods (ESR,[58] IR spectroscopy,[3] XPS,[59] and thermodesorption[60]) and indirect methods (measurement of electric conductivity[39,59,61] and work function of electron[39,62]).

The quantum chemical calculations predict that oxygen adsorption is endothermic on the ideal stoichiometric surface SnO_2(110) and the energy of the Sn^{IV}_{5c}—O_2 bond is –0.02 eV.[63] On the oxygen-deficient surface adsorption is energetically favorable due to the charge transfer from Sn^{II} cations. The transfer can be direct in the case of binding with Sn^{II}_{4c} or indirect for the coordination of O_2 on the Sn^{IV}_{5c} cations located near the Sn^{II}_{4c} cations.[57] According to the calculation results, horizontally oriented peroxide ions (O_2^{2-}) bound by two oxygen atoms with the Sn^{II}_{4c} cations should be most stable.[40,45,57,59] Other possible adsorbates but with a lower bond energy are ions O_2^- coordinated to the cations by one end and oriented at an angle to the surface.[39,57] Although the calculations predict low activation barriers for the dissociation of O_2^{2-} and higher bond energies of atomic ionosorbates compared to molecular ionosorbates,[40,57] the concentration of surface O^- ions is expected to be low because of their instability and high electron affinity.[40,57]

However, the results of spectroscopic studies do not confirm the conclusion about the existence of O_2^{2-} groups on the real SnO_2 surface.[40] On the contrary, the presence of superoxide anions at the temperature <160 °C was proved by ESR (see Ref. 58) and IR spectroscopy.[3] The formation of dipolar (uncharged) chemisorbates $O_{2,chem}$ at the temperature <200 °C was monitored by a decrease in the electron affinity of SnO_2 during oxygen adsorption.[39]

Chemisorption of oxygen on the zinc oxide surface occurs similarly. It is shown that in the temperature range 100—180 °C oxygen is chemisorbed on the surface of polycrystalline ZnO doped with gallium to form O_2^-, and atomic ionosorbates O^- predominate on the surface at >230 °C in this case.[64] It was proved by the ESR method[65,66] that with the temperature increase the type of the predominant form of oxygen adsorbed on the ZnO surface changed as follows:

$$O_{2,chem} + 4\,e^- \rightleftharpoons O^-_{2,surf} + 3\,e^- \rightleftharpoons \rightleftharpoons 2\,O^-_{surf} + 2\,e^- \rightleftharpoons 2\,O^{2-}_{surf}, \qquad (3)$$

where $O^-_{2,surf}$ and O^-_{surf} are O_2^- and O^- ions, respectively, on the oxide surface. Thus, at high temperatures oxygen of the gas phase is equilibrated with zinc oxide. At low partial pressures of O_2 lattice oxygen transits to the gas phase, increasing the deviation of the ZnO composition from the stoichiometric one. When the concentration of oxygen increases, the processes of its adsorption on the zinc oxide surface and incorporation into the structure occur, which causes a decrease in the concentration of intrinsic donor defects (oxygen vacancies and interstitial zinc atoms). All these processes affect the electric conductivity and gas sensitivity of zinc oxide, and the highest effect is observed in the case of the nanocrystalline samples, where the role of the surface is significant.

The oxidative activity for the interaction with gas-reducing agents (CO, H_2, NH_3, H_2S, CH_4) is the most important property of chemisorbed oxygen from the viewpoint of gas sensitivity. Atomic species O^- are considered to be the strongest oxidants.[45,59] The interaction of chemisorbed $O_{2,chem}$ molecules with gases is ignored when the sensor sensitivity is considered, because the working temperature of sensors, as a rule, is in the range of predominant ionosorption of oxygen (>250 °C).

A convenient method for the investigation of chemisorbed oxygen on the surface of nanocrystalline oxides is temperature-programmed reduction using probe molecules of hydrogen (TPR-H_2). The hydrogen uptake from the gas passed through the sample is measured during experiment. Temperature dependences of the hydrogen uptake rate make it possible to reveal temperature ranges in which different oxidative sites are formed, and the temperature of the H_2 uptake maximum is a qualitative characteristic of the oxidative activity of the corresponding sites.[67,68]

2.3. Hydrate—hydroxyl layer. The concentration of the active sites formed by adsorption of molecules and having the general name HHL is the highest on the surface of oxides contacting with atmospheric air. The HHL includes two types of adsorbates: (1) molecular adsorbates are adsorbed molecules of H_2O and their protonated species H_3O^+ and $H_5O_2^+$,[69] (2) dissociated hydrate forms are isolated OH groups and associates of hydroxyl groups OH...OH joined by hydrogen bonds.[59]

Similarly to the case of other active sites, the HHL is studied using both quantum chemical calculations that make it possible to predict the bond energy of H_2O molecules and OH groups with various adsorption sites on the model $SnO_2(110)$ surface[70] and polar and nonpolar surfaces O—ZnO and $ZnO(10\bar{1}0)$, respectively, and experimental methods. Among the latter is IR spectroscopy,[54,69] which allows one to determine the type of adsorbed hydrate species and semiquantitatively estimate their concentration. Thermodesorption mass spectrometry[37] and temperature-programmed desorption of water[43] are quantitative methods using which the total concentrations of hydrate species differed in energy of the bond with the surface are determined. According to the data of thermodesorption, hydroxyl groups prevail in the HHL on the polycrystalline SnO_2 surface.[37] Adsorbed H_2O molecules bound by hydrogen bonds with the surface O^{2-} anions exist at low temperatures. On heating at temperatures higher than 200 °C, water molecules desorb or dissociate to form hydroxyl groups.[17]

Two types of hydroxyl groups are observed on the single crystal $SnO_2(110)$ surface: terminal (OH_{ter}) and bridging (OH_{bridge}).[54,71] The former are residues of dissociated H_2O molecules bound to the Lewis acidic sites (surface cations Sn^{IV}_{5c}). The bridging hydroxyl groups are derivatives of bridging O^{2-} anions on the SnO_2 surface. Adsorption of water on SnO_2 resulting in the formation of terminal and bridging hydroxyl groups[37,54] and in an increase in the electric conductivity is described by the following equation[72]:

$$H_2O + Sn_{Sn}^{\times} + O_O^{\times} \rightleftharpoons \rightleftharpoons (Sn{-}OH)_{Sn}^{\times} + (OH)_O^{\bullet} + e', \qquad (4)$$

where $(Sn{-}OH)_{Sn}$ is the terminal group on the Sn site, $(OH)_O^{\bullet}$ is the bridging hydroxyl group, e' is electron, $\times$ is the neutral charge of the cation relative to the charge that should be on the site, and superscripts "point" and "stroke" imply that the charge on the ion is by unity higher or lower than should be in this site. The terminal OH_{ter} groups on the SnO_2 surface are presented as isolated groups, whose vibrations appear in the IR spectra as particular narrow bands in the high-frequency range (Table 1).[54,69,73] Unlike them, the bridging hydroxyl

groups form so-called families consisting of series of bridging O^{2-} anions bound to delocalized protons ($mO^{2-}...nH^{+}$),[43] whereas another interpretation considers them as associates of bridging hydroxyl groups bound by hydrogen bonds ($OH_{bridge}...OH_{bridge}$).[74] Their delocalized character causes broad absorption bands in the IR spectra shifted to lower frequencies (see Table 1).[54,73] The composition of the HHL on the surface of nanocrystalline tin dioxide is much more diverse than in the case of single crystals due to the high surface area. This leads to the appearance of broad bands in the IR spectra of nanocrystalline SnO_2 in the ranges of wave numbers 3700—2000 and 1700—1600 cm^{-1}. The oxide surface includes a wide set of adsorption sites (tin cations with different coordination numbers, surface oxygen anions, vacancies of lattice oxygen). The set becomes larger when defects and structural heterogeneities, whose concentration increases on going to nanosized particles, contribute to the local environment of the sites.

A comparison of the O—H vibration frequencies (see Table 1) indicates that in the families ($OH_{bridge}...OH_{bridge}$) protons are bound to oxygen more weakly than in terminal OH_{ter} groups, so that the bridging hydroxyl groups are stronger Brønsted acids.[54] This can enhance water adsorption by hydrogen bond formation. The acidity of OH groups is manifested for ammonia chemisorption.[19,44] In addition of the acidic properties, the surface hydroxyl groups is characterized by oxidative activity for the interaction with CO.[37,72,75] The oxidative properties of hydroxyl groups are more pronounced than those of the oxygen ionosorbates.[76] Bridging hydroxyl groups can directly oxidize H_2 to enlarge the families ($OH_{bridge}...OH_{bridge}$) on the SnO_2 surface with new protonated groups.[54]

Table 1. Parameters of IR spectral vibrations of adsorbed hydrate species on the nanocrystalline tin dioxide surface

Hydrate species	Wave number/cm^{-1}	Type of vibrations	Reference
OH_{ter}	3630, 3662—3700, 3728—3780	ν(O—H)	54, 69, 73
OH_{bridge}	3555, 3524, 3483	ν(O—H)	69, 73
$OH_{bridge}...OH_{bridge}$	3400—3200	ν(O—H)	37, 54, 69, 73
H_2O	3400—3200	ν(O—H)	37, 54
	1620	δ	
H_3O^+	3300—3150, 2650—2470	ν(O—H)	69
	1700—1670	δ	
$H_5O_2^+$	3000—2850, 2250—2200	ν(O—H)	69
	1700—1660	δ	

It was found[49] by the methods of He atom scattering (HAS) and IR spectroscopy that both the monolayer and bilayer consisting of H_2O molecules can be formed on the single crystal polar surface O—ZnO due to the chemisorption of water. Surface OH groups can be formed on the nonpolar surface of zinc oxide, for instance, $ZnO(10\bar{1}0)$. The study of water adsorption on this surface by high resolution electron energy loss spectroscopy (HREELS), HAS, and thermodesorption showed that one portion of water molecules existed directly in the form of H_2O and another portion was dissociated.[51,77]

The results of studying the interaction of water vapors with nanocrystalline ZnO by IR spectroscopy show that both molecular and dissociative chemisorption of H_2O occur at 50 °C.[34] A comparison of the wavelengths of bond vibrations and thermal stabilities of various sites allowed us to distinguish the following processes: (1) formation of OH groups on the polar O—ZnO surface upon water dissociation on oxygen vacancies; (2) partial dissociation of water on the $ZnO(10\bar{1}0)$ surface to form chemisorbed H_2O molecules and OH groups; (3) formation of isolated OH groups on the $ZnO(10\bar{1}0)$ surface; and (4) interaction of water with defects to form hydroxyl bonds or O—H···O bonds.[34]

2.4. Paramagnetic centers. Paramagnetic active centers on the surface of gas-sensitive oxides is of special interest, since they are highly reactive due to unpaired electrons. They can significantly affect the character of interaction with gas molecules, but at the same time are labile and, hence, exist in low concentrations, so that it is difficult to study them experimentally.

Quantum chemical calculations show the possibility of formation on the $SnO_2(110)$ surface of such paramagnetic centers as partially ionized oxygen vacancies[40,45] and ionosorbed oxygen species.[59] The only method for the direct experimental study of paramagnetic centers is ESR spectroscopy. However, in this case, data can be interpreted ambiguously. The ESR signal with $g = 1.95$—1.96 in the spectra of tin dioxide was attributed[78] to the singly ionized vacancies $V_O^{\bullet}$ (Table 2), whereas it was earlier[45] assigned to the Sn^{III} state. Indirect results can be obtained by other experimental methods: measurement of electric conductivity,[48,85] impedancemetry,[86] and luminescence spectroscopy.[87]

The formation of the following types of paramagnetic centers is probable for single crystal tin dioxide: ionosorbed forms of oxygen (O_2^-, O^-) and singly charged oxygen vacancies ($V_O^{\bullet}$). The former are rigidly surface sites. Oxygen vacancies can exist both on the surface and in the volume of oxide. In the case of their shifting onto the surface, the singly charged oxygen vacancies play the role of adsorption sites for acceptor molecules.[40,86] In the presence of air, they adsorb oxygen producing ionosorbates of O_2

$$V_O^{\bullet} + O_2 = V_O^{\bullet\bullet}—O_2^{\prime}. \qquad (5)$$

Table 2. Types of paramagnetic centers in polycrystalline oxides SnO_2 and ZnO and the corresponding ESR signals

Oxide	Paramagnetic center	*g*-Factor	Reference
SnO_2	O_2^-	$g_1 = 2.0210$, $g_2 = 2.0030$, $g_3 = 1.9833$	79
	O^- (existence is not proved)	2.002	80
	$OH^{\bullet}$	$g_1 = 2.0021$, $g_2 = g_3 = 2.0009$	79
	$V_O^{\bullet}$	1.9812	78, 79
	Sn^{III}	1.98	32
ZnO	$V_O^{\bullet}$ of axial symmetry	$g_1 = 1.963$, $g_2 = 1.9921$	81, 82
	$(V_{Zn}')_2$ of non-axial symmetry	$g_1 = 2.0075$, $g_2 = 2.0060$, $g_3 = 2.0009$	83
	V_{Zn}' of axial symmetry	2.013	84
	$(V_{Zn}'—Zn_i^x)$	2.02	83

On the whole, the description of these paramagnetic centers in single crystal tin dioxide is based on the quantum chemical models using the oxygen-deficient surface $SnO_2(110)$ as an example. The compensation of the surface vacancy by the O atom is one of the reasons for dissociative oxygen adsorption on the defect pairs $Sn^{II}{}_{4c}—VO^{\bullet\bullet}$ or $Sn^{IV}{}_{5c}—V_O{}^x$.[40,48]

During adsorption air oxygen stimulates the volume diffusion of oxygen vacancies and related long-term change in the electric conductivity of SnO_2.[85,88] According to the quantum chemical calculations,[85] the presence of CO or H_2O impurities in air enhances the concentration of oxygen vacancies on the oxide surface. The simulation of the interaction of NO_2 with the oxygen-deficient surface $SnO_2(110)$ shows that the vacancies of bridging oxygen favor the more efficient charge transfer to the adsorbate and a higher energy of adsorption than the vacancies of oxygen anions arranged in the crystallographic plane.[41,87]

It follows from the results of the ESR study of nanocrystalline tin dioxide that the predominant type of paramagnetic centers on the surface is presented by molecular ionosorbates O_2^-.[79] However, hydroxyl groups $OH^{\bullet}$ were observed along with ionosorbates on the SnO_2 surface (Fig. 3). The concentration of $OH^{\bullet}$ hydroxyl groups correlates with the relative humidity in air (Fig. 4). This indicates that they are equilibrated with adsorbed water molecules

$$H_2O + O^{2-} \rightleftharpoons OH^{\bullet} + OH^- + e^-. \qquad (6)$$

The release of electrons, in this case, is consistent with an increase in the electric conductivity of tin dioxide

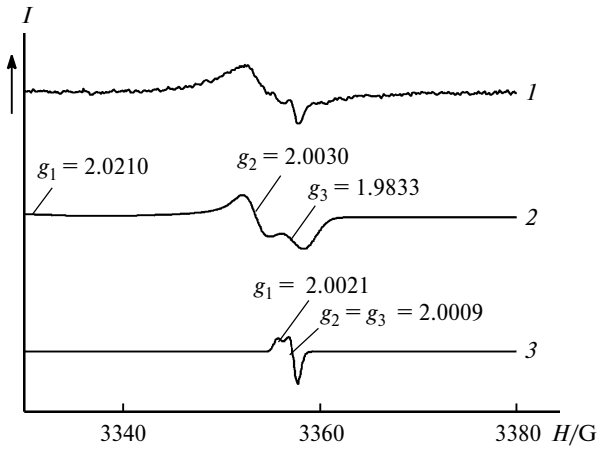

Fig. 3. Experimental ESR spectrum of nanocrystalline tin dioxide (*1*) and modeled signals of paramagnetic centers O_2^- (*2*) and $OH^{\bullet}$ (*3*).[79]

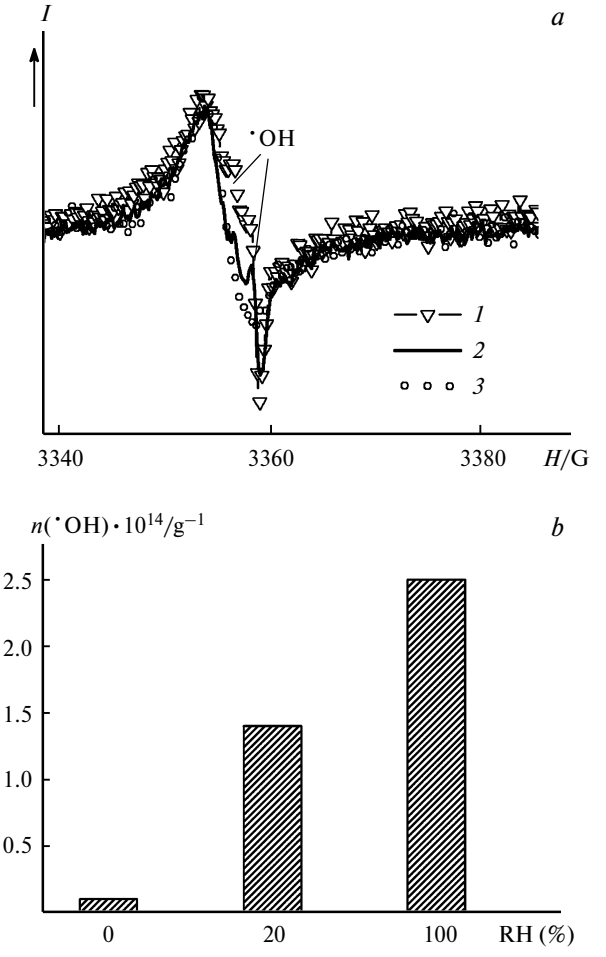

Fig. 4. (*a*) ESR spectra of nanocrystalline tin dioxide kept at different humidity contents: 100 (*1*), 20 (*2*), and 0% (*3*); (*b*) concentration of $OH^{\bullet}$ centers on the SnO_2 surface ($n(OH^{\bullet})$ *vs* relative humidity (RH).[79]

with an increase in the humidity content.[17,37] In terms of the Heiland—Kohl model,[89] the conductivity increases due to the formation of electron-deficient associates (Sn—OH) upon the dissociative adsorption of water on the SnO_2 surface.

Signals of singly charged oxygen vacancies $V_O^{\bullet}$ are detected in the ESR spectra of nanocrystalline tin dioxide.[90] However, they are detected only by ESR spectra recording at the temperature of liquid helium (5 K). The temperature affects the frequency of phonon vibrations of the solid lattice, which determines the lifetime of the excited state before spin-lattice relaxation. According to the principle of uncertainty,[91] the lifetime of excited spin ($\Delta\tau$) is inversely proportional to the width of the ESR signal (ΔH)

$$\Delta E \Delta\tau = g\mu_B \Delta H \Delta\tau \geq \hbar, \qquad (7)$$

where ΔE and $\Delta\tau$ are the uncertainties of the energy of electron in the excited state and lifetime of the excited state, respectively; g is the g-factor (proportionality coefficient); μ_B is the Bohr magneton; ΔH is the uncertainty of the magnetic field strength; and $\hbar$ is the reduced Planck constant. At a constant concentration of spin centers, signal broadening induces the corresponding decrease in intensity. As a result, signals of spin centers in the volume of the solid are characterized by higher broadening and sensitivity to temperature. The ESR spectra of nanocrystalline SnO_2 detected at $T = 5$ K exhibit a low-intensity broad signal of vacancies $V_O^{\bullet}$ along with narrow and intense signals of O_2^- and $OH^{\bullet}$ (Fig. 5). Thus, unlike radicals, *viz.*, derivatives of adsorbed oxygen and water molecules, paramagnetic centers $V_O^{\bullet}$ exist in the volume of SnO_2 nanoparticles. The application of SnO_2 in sensors assumes their heating to 200—450 °C. According to the ESR data, radicals O_2^- and $OH^{\bullet}$ exist at these temperatures on the surface of nanocrystalline SnO_2, and their concentration cannot be estimated because of strong peak broadening; however, no new signals appear.

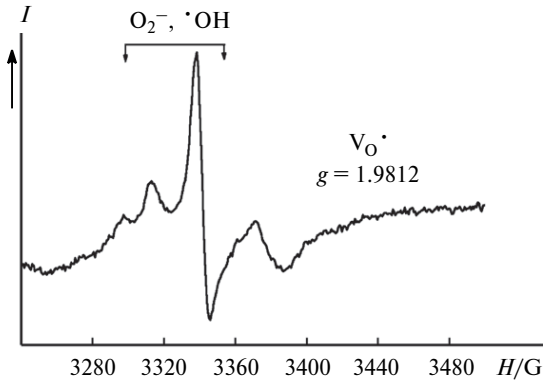

Fig. 5. ESR spectrum of nanocrystalline tin dioxide recorded at 5 K.[90]

There are no direct experimental data on the reactivity of paramagnetic centers on the surface of nanocrystalline SnO_2. Oxidative properties are characteristic of the O_2^- sites as of other forms of chemisorbed oxygen. The $OH^{\bullet}$ hydroxyl sites possess, most likely, the same properties[54,92] and appear on interaction with gas-reducing agents H_2 and CO.

In the case of crystalline oxide ZnO with the wurtzite structure characterized by oxygen deficient, a zinc excess can appear due to the partial transition of oxygen to the gas phase. The calculation methods show the probability of formation of both anionic vacancies and also interstitial zinc atoms (Zn_i).[93] This can be illustrated by the quasi-chemical equations in the Kröger—Vink notation

$$Zn_{Zn}^{\times} + O_O^{\times} \rightleftharpoons Zn_i^{\bullet} + 0.5\,O_2\,(g) + e', \qquad (8)$$

$$O_O^{\times} \rightleftharpoons V_O^{\bullet} + 0.5\,O_2\,(g) + e', \qquad (9)$$

where O_2 (g) is O_2 in the gaseous state.

The semiconductor properties of the n-type and increasing concentration of electrons on heating or treatment of ZnO in the reductive medium are explained by the formation of $Zn_i^{\bullet}$ and/or $V_O^{\bullet}$ donor sites.[94,95] However, there is no concept what defects predominate. An analysis of the probability of defects according to Frenkel by the shift from regular positions into interstices (reactions (10) and (11)) by comparing atomic and ionic radii of zinc and oxygen gave no unambiguous conclusion about prevailing defects because of uncertainty in the degree of ionicity of the Zn—O bond.[65] The calculations of the energy of defect formation in zinc oxide showed that the oxygen vacancies had a lower energy of formation than the interstitial zinc atoms, but the ionization energy of the latter is lower, so that the electron conductivity can be caused by the formation of $Zn_i^{\bullet}$.[96]

$$Zn_{Zn}^{\times} \rightleftharpoons Z\,n_i^{\bullet} + V_{Zn}' \qquad (10)$$

$$O_O^{\times} \rightleftharpoons O_i' + V_O^{\bullet} \qquad (11)$$

The ESR investigation of nanocrystalline zinc oxide is impeded by a high concentration of defects, which can differ in nature and local environment. This causes a set of closely arranged signals in the spectra (Fig. 6) and ambiguity of their interpretation. The signals with the g-factor equal to 1.95—1.96 are ascribed by independent authors to point defects of the ZnO structure: ionized oxygen vacancies $V_O^{\bullet}$, interstitial zinc $Zn_i^{\bullet}$, their complexes $V_O^{\bullet}$—$Zn_i^{\bullet}$, free electrons e' or electrons localized at the zinc interstices, and interstitial oxygen ions.[98,99] It is difficult to unambiguously attribute the ESR signal, because the calculated g-factor for electron bound to the oxygen vacancy is about 2.0002 (free electron)[100] or 2.01 (see Ref. 101). It is known that the signal with $g = 1.956$ corresponds to the donor centers determining the con-

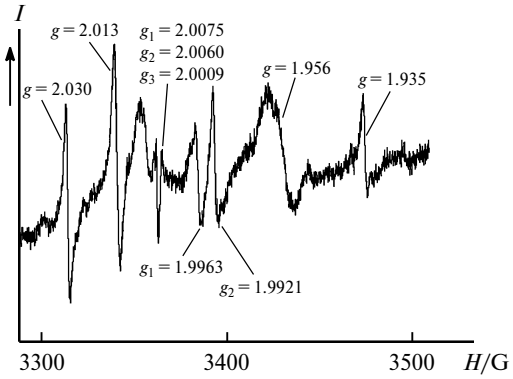

Fig. 6. ESR spectrum of nanocrystalline zinc dioxide.[97]

centration of conductivity electrons.[102,103] The interpretation according to which this signal belongs to the oxygen vacancies $V_O^{\bullet}$, since its intensity increases on annealing in an inert atmosphere and decreases in the oxygen-containing atmosphere, seems to be most reliable.[104] The ESR signal with $g = 1.935$ belongs to similar centers but with a different geometry, for example, for the arrangement of oxygen vacancies on the nanocrystalline surface. In addition to oxygen vacancies, the ESR spectrum of nanocrystalline ZnO (see Fig. 6, Table 2) contains signals of singly charged zinc vacancies V_{Zn}', doubly charged zinc bivacancies $(V_{Zn}')_2$, and complex defects of negatively charged zinc vacancies with interstitial atoms $(V_{Zn}'—Zn_i^x)$.[97]

In order to identify the nature of active sites and the properties characteristic of them, the listed types of "intrinsic" sites were analyzed in this section using mainly ideal (model) and real mono- and polycrystalline surfaces of tin and zinc oxides. It is assumed that for nanocrystalline materials the nature of active sites is the same in essence as that in the cases considered: coordinately unsaturated cations and anions, point defects, and oxygen and hydrate—hydroxyl adsorbates. On going to the nanocrystalline form, the principal distinction is a significant increase in the fraction of the surface over the volume in the real structure of the material. The corresponding decrease in the degree of crystallinity and, on the contrary, an increase in the number of extended defects (steps, boundaries, edges) favor, most likely, the diversification of the properties of active sites. For instance, the surface cations with diverse local environments can differ strongly in acidic strength, which, in turn, favors the formation of a set of various hydrate derivatives due to the chemisorption of water. Thus, the reactivity and concentration of active sites on the surface of semiconductor oxides are interrelated to the microstructure parameters (morphology, particle size, specific surface), which are determined by the synthesis conditions. In addition, the content of volume-doping and surface-modifying additives affects the active sites. Then these relationships were analyzed for nanocrystalline oxides SnO_2 and ZnO using as examples on the basis of the experimental results published by the authors of the present review in the recent decade.

3. Relationship of the synthesis conditions, microstructure parameters, and active sites on the surfaces of nanocrystalline oxides SnO_2 and ZnO

The experimental results considered in the present review were obtained for the nanocrystalline oxides synthesized by precipitation from aqueous solutions of salts followed by annealing at $T = 250—1000$ °C.[61,97,105,106] In all cases, the obtained samples contained only one crystalline phase SnO_2 (cassiterite) or ZnO (wurtzite). The average size of crystallites of the oxide matrix (SnO_2 or ZnO) increased and the specific surface, on the contrary, decreased as the annealing temperature increases (Fig. 7).

3.1. Influence of the synthesis conditions and microstructure of oxides on the type and concentration of acidic sites. Acidity of the material surface was studied by TPD of ammonia. The TPD spectra (Fig. 8) represent the temperature dependences of the specific rate of NH_3 desorption from surfaces of SnO_2 and ZnO oxides pre-saturated with ammonia and obtained at different annealing temperatures. Desorption of NH_3 from weak (Brønsted) acidic sites, *i.e.*, OH groups, occurs in the low-temperature range ($T < 200$ °C).[19,44,97] At a higher temperature ($T > 200$ °C), ammonia molecules bound to the Lewis acidic sites, *viz.*, coordinately unsaturated cations on the surface, are desorbed. Lewis acidic sites of medium strength (desorption of NH_3 at $T = 200—400$ °C) and strong acidic sites, ammonia desorption from which needs heating to $T > 400$ °C, are distinguished.[44] It is considered that on the reduced surface of single crystals of SnO_2 the Lewis sites of medium strength correspond to the Sn^{IV} cations and the strong sites correspond to the Sn^{II}

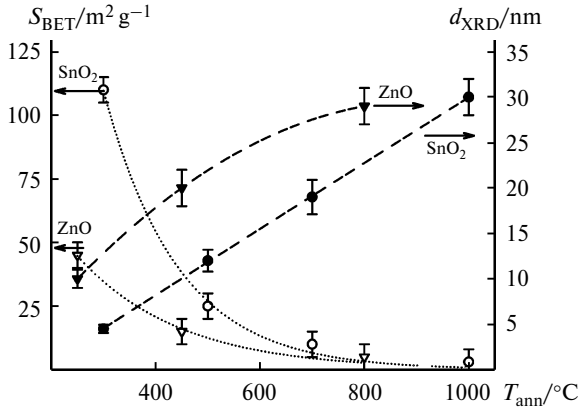

Fig. 7. Influence of the annealing temperature (T_{ann}) on the size of crystalline grains (d_{XRD}) and specific surface area (S_{BET}) of nanocrystalline oxides SnO_2 and ZnO.

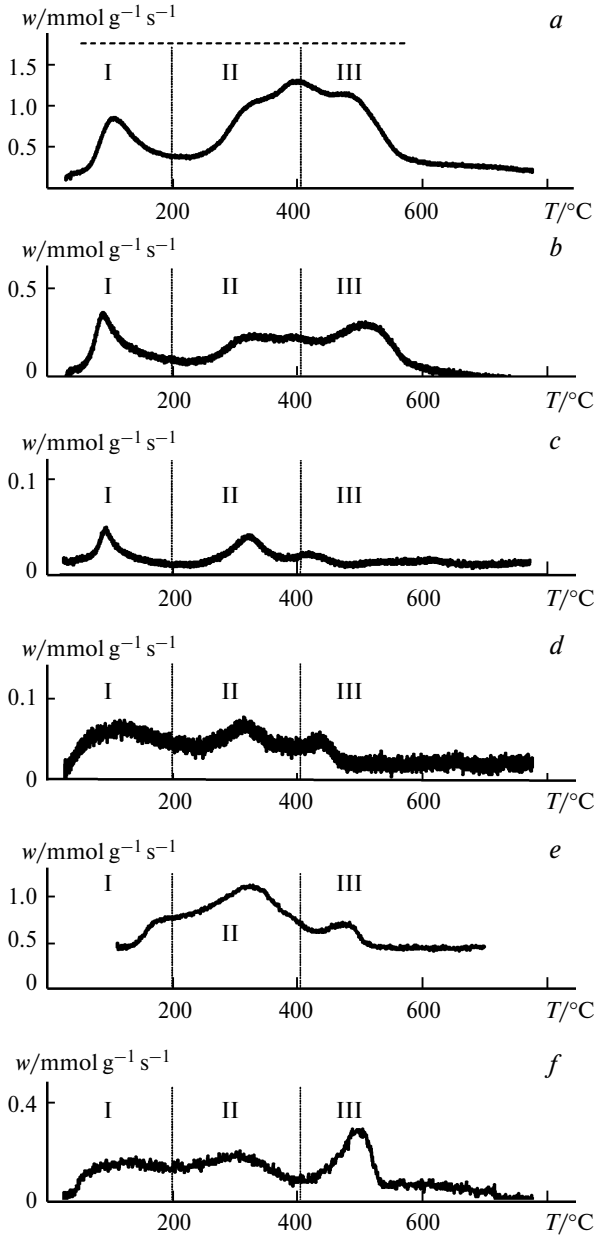

Fig. 8. Temperature dependences of the specific rate of ammonia desorption (w) during TPD from the surface of nanocrystalline oxides SnO_2 and ZnO with different microstructure parameters: (*a*) $d_{XRD}(SnO_2)$ = 3—5 nm, S_{BET} = 100—110 $m^2\ g^{-1}$; (*b*) $d_{XRD}(SnO_2)$ = 10—12 nm, S_{BET} = 20—25 $m^2\ g^{-1}$; (*c*) $d_{XRD}(SnO_2)$ = 16—20 nm, S_{BET} = 5—10 $m^2\ g^{-1}$; (*d*) $d_{XRD}(SnO_2)$ = = 26—35 nm, S_{BET} = 1—5 $m^2\ g^{-1}$; (*e*) $d_{XRD}(ZnO)$ = 10—12 nm, S_{BET} = 40—45 $m^2\ g^{-1}$; and (*f*) $d_{XRD}(ZnO)$ = 19—21 nm, S_{BET} = 10—15 $m^2\ g^{-1}$. The regions of weak (I), medium (II), and strong acidic sites (III) are distinguished.[61,97,109]

cations.[36] However, for nanocrystalline SnO_2 in air, the presence of the Sn^{II} cations that would be accessible for the adsorption of NH_3, is poorly probable, because they being electron-donor centers, should be blocked by chemisorbed oxygen. In this case, the presence of a set of Lewis sites of various strength appeared in broad bands of NH_3 desorption at T = 300—600 °C (see Fig. 8) can be explained by differences in local environment of Sn^{IV} cations on the nanocrystalline surface. The concentration of Brønsted sites remains unchanged within the error limit as the average crystallite size increases (Table 3). The total amount of Lewis sites decreases, and the fraction of acidic sites of medium strength increases, A probable reason for this can be a decrease in the concentration of coordinately unsaturated tin cations with a decrease in the degree of dispersion of SnO_2. It is most likely that the number of structural defects and, hence, strongly acidic surface cations Sn^{IV} with low coordination numbers decrease with the crystallization of oxide particles.[19,44] At the same time, the fraction of "regular" surface cations Sn^{IV} with the minimum number of coordination vacancies and, therefore, less pronounced acidic character increases.[36]

Zinc cations on the ZnO surface are characterized by a lower acidic strength than the Sn^{IV} cation on the SnO_2 surface. Therefore, the desorption of ammonia bound to the Lewis sites on the surface of nanocrystalline ZnO occurs at the temperatures corresponding to acidic sites of medium strength (see Fig. 8). The peak of highly dispersed ZnO at T = 480—500 °C in the TPD spectrum is caused by the desorption of ammonia thermolysis products.[97,107] On heating NH_3 molecules adsorbed on the ZnO surface can decompose to form NH, NH_2, and OH groups, which are more strongly bound to the surface than molecular-adsorbed ammonia.[108] The fraction of these sites increases significantly with an increase in the average size of ZnO particles (see Fig. 8). A decrease in the fraction of molecular-adsorbed NH_3 correlates with a lower concentration of coordinately unsaturated cations on the surface of larger ZnO crystallites. It can be assumed that Zn^{II} cations with low coordination numbers facilitate the molecular adsorption of ammonia, since their oxidative dissociation is impeded in this case. At the annealing temperature resulting in an increase in the ZnO crystallite sizes increases, the concentrations of Brønsted acidic sites and Lewis sites responsible for molecular ammonia adsorption decrease.

3.2. Influence of the synthesis conditions and microstructure of oxides on the concentration of chemisorbed oxygen. The data on the concentration of chemisorbed oxygen on the surface of nanocrystalline oxides SnO_2 and ZnO were obtained by the TPR-H_2 method.[67,68] The TPR spectra (Fig. 9) represent a temperature dependence of the hydrogen uptake rate from the gaseous mixture in which oxides are reduced. The major peak of H_2 uptake by the SnO_2 samples at T = 400—800 °C corresponds to the bulk reduction of the SnO_2 phase to tin[67]

$$SnO_2\ (s) + 2\ H_2\ (g) = Sn\ (l) + 2\ H_2O\ (g), \qquad (12)$$

where s, g, and l are the solid, gaseous, and liquid states, respectively.

Table 3. Concentration of acidic sites (C_{ac}) on the surface of nanocrystalline oxides SnO_2 and ZnO doped with various amounts of donor impurities and modified by catalytic additives of Pd and Ru (1 wt.%)

Matrix	T_{ann}/°C	Modifier (1 wt.%)	Dopant (C (at.%))	C_{ac}/μmol m^{-2}			
				Brønsted (weak)	Lewis		
					medium	strong	totally
SnO_2	300	—	—	0.6±0.2	1.3±0.2	1.1±0.3	2.4±0.5
		Pd	—	0.9±0.2	2.7±0.4	0.5±0.1	3.2±0.5
			Sb (0.5)	1.2±0.2	3.1±0.3	0.6±0.2	3.7±0.5
			Sb (1.0)	1.0±0.2	2.9±0.3	0.1	3.0±0.4
			Sb (2.0)	0.8±0.2	2.9±0.3	0.1	3.0±0.4
			Sb (4.0)	1.0±0.2	3.3±0.3	0.1	3.4±0.4
			Sb (8.0)	1.2±0.2	3.4±0.4	0.6±0.1	4.0±0.5
		Ru	—	0.6±0.2	2.1±0.2	—	2.1±0.2
	500	—	—	0.5±0.2	0.9±0.2	0.6±0.2	1.5±0.4
		Pd	—	0.8±0.2	2.1±0.3	—	2.1±0.3
		Ru	—	0.5±0.2	1.3±0.2	—	1.3±0.2
	700	—	—	0.5±0.2	1.0±0.2	0.2±0.1	1.2±0.3
		Pd	—	0.9±0.2	1.3±0.2	—	1.3±0.2
		Ru	—	0.6±0.2	1.3±0.2	—	1.3±0.1
	1000	—	—	0.6±0.3	0.5±0.3	0.2±0.1	0.7±0.4
		Pd	—	0.9±0.4	1.1±0.5	—	1.1±0.5
		Ru	—	0.6±0.3	0.8±0.4	—	0.8±0.4
ZnO	250	—	—	0.4±0.1	1.9±0.3	0.2±0.1	2.5±0.4
			Ga (0.5)	0.3±0.1	2.1±0.3	0.2±0.1	2.6±0.5
			Ga (4.3)	0.4±0.1	2.0±0.4	—	2.4±0.4
			In (0.5)	0.3±0.2	1.6±0.3	0.4±0.1	2.3±0.4
			In (1.0)	0.4±0.1	1.7±0.3	0.3±0.1	2.4±0.4
			In (5.0)	0.6±0.1	1.8±0.3	0.2±0.1	2.6±0.5

The amount of H_2 absorbed in this temperature range is independent of the dispersion of the samples, but the uptake maximum shifts to the high-temperature range with an increase in the size of SnO_2 particles. This is caused by kinetic hindrances for the interaction of dihydrogen with atoms in the crystallite bulk. The broad shoulder at the beginning of the high-temperature peaks is associated, most likely, with the formation of intermediate tin oxides: Sn_2O_3, Sn_3O_4, and SnO. The bulk reduction of nanocrystalline ZnO occurs at a higher temperature: 900—1100 °C. This is due to the enhancement of the stability of the oxide crystal lattice with an increase in the degree of iconicity of the M—O bond. The TPR study of zinc oxide is difficult because of zinc vapors, which are the product of bulk reduction under these conditions

$$ZnO\ (s) + H_2\ (g) = Zn\ (g) + H_2O\ (g). \qquad (13)$$

Hydrogen absorption at 100—300 °C during TPR is observed only for dispersed materials (particle size ≤20—25 nm, specific surface area ≥20 m^2 g^{-1}), and its intensity decreases with a decrease in the specific surface area of the materials (see Fig. 9). This indicates that the low-temperature hydrogen absorption corresponds to the reduction of oxidative sites on the oxide surface. They can include chemisorbed oxygen molecules $O_{2,chem}$, ionized species O_2^- and O^-, and reactive OH groups. The concentration of oxidative sites (Table 4) was evaluated assuming the chemisorbed oxygen molecule prevail among them and react with hydrogen *via* the equation

$$O_{2,chem} + 2\,H_2 \longrightarrow 2\,H_2O. \qquad (14)$$

This assumption is based on the fact that at room temperature in air diatomic forms of oxygen predominate on the surface of oxides SnO_2 and ZnO.[17,40,64] At the same time, it is proved by the ESR method that the concentration of ionosorbates O_2^- on the SnO_2 surface does not exceed ~$1.5 \cdot 10^{-11}$ mol m^{-2}, which is by six orders of magnitude lower than the total concentration of oxidative sites (~10 μmol m^{-2}). As follows from the data presented in Table 4, for similar average particle sizes of the oxides, the concentration of chemisorbed oxygen on the SnO_2 surface is higher than that on the ZnO surface. The concentration of chemisorbed oxygen decreases considerably with an increase in the crystallite size.

3.3. Relationship of the microstructure parameters of the oxides to the composition of the hydrate—hydroxyl layer. For the chemisorption of water molecules on nanocrystalline oxides, there is a series of possible routes for the interaction of adsorbates with the surface leading to its coverage with various hydrate forms. Some of them

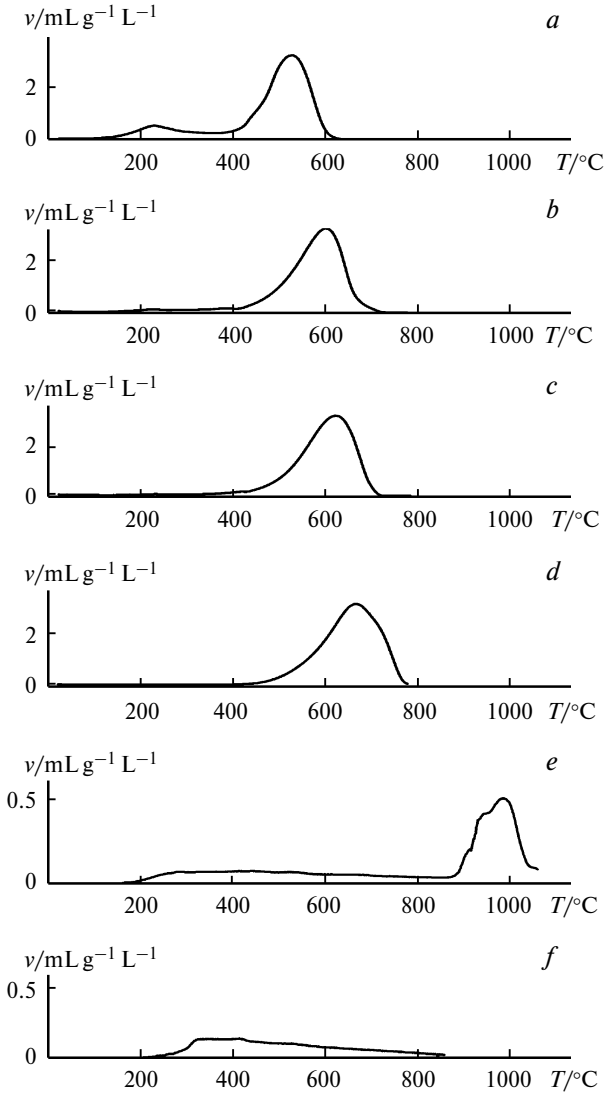

Fig. 9. Temperature dependences of the specific rate of hydrogen uptake (v) during TPR of nanocrystalline oxides SnO_2 and ZnO with different microstructure parameters: (*a*) $d_{XRD}(SnO_2)$ = = 3—5 nm, S_{BET} = 100—110 $m^2 g^{-1}$; (*b*) $d_{XRD}(SnO_2)$ = 10—12 nm, S_{BET} = 20—25 $m^2 g^{-1}$; (*c*) $d_{XRD}(SnO_2)$ = 16—20 nm, S_{BET} = = 5—10 $m^2 g^{-1}$; (*d*) $d_{XRD}(SnO_2)$ = 26—35 nm, S_{BET} = 1—5 $m^2 g^{-1}$; (*e*) $d_{XRD}(ZnO)$ = 10—12 nm, S_{BET} = 40—45 $m^2 g^{-1}$; and (*f*) $d_{XRD}(ZnO)$ = 19—21 nm, S_{BET} = 10—15 $m^2 g^{-1}$.[9]

are presented by Eqs (5) and (7) that illustrate the formation of Brønsted acidic sites: bridging OH groups and paramagnetic $OH^{\bullet}$ centers on the SnO_2 surface. The most complete information about the qualitative composition of the HHL can be obtained by IR absorption spectroscopy. The IR spectra of samples of nanocrystalline oxides SnO_2 and ZnO with various microstructure parameters are presented in Fig. 10. For comparison, the absorption bands of the surface groups (3600—1000 cm^{-1}) were normalized to the peaks of lattice vibrations metal—oxygen (400—700 cm^{-1}). A comparison of the IR absorption

Table 4. Concentration of oxidative centers $O_{2,chem}$ ($C(O_{2,chem})$) on the surface of nanocrystalline oxides SnO_2 and ZnO doped with various amounts of donor impurities Sb (C) and modified by catalytic additives of Pd and Ru (1 wt.%)

Matrix	T_{ann}/°C	Modifier	C (at.%)	$C(O_{2,chem})$ /μmol m^{-2}
SnO_2	300	—	—	11.8±0.4
		Pd	—	13.6±0.5
			1.0	11.8±0.5
			1.5	14.2±0.5
			2.0	11.2±0.5
			3.0	9.6±0.5
			4.0	14.8±0.5
			6.0	13.5±0.5
			7.0	13.4±0.5
		Ru	—	14.9±0.5
	500	—	—	7.6±0.6
		Pd	—	8.8±0.7
		Ru	—	12.2±0.5
ZnO	250	—	—	3.3±0.4
	450	—	—	0.4±0.1

bands with the data in Table 1 shows that the HHL of tin dioxide includes diverse dissociated groups (terminal OH groups, isolated bridging OH groups, and families of bridging hydroxyl groups OH...OH joined by hydrogen

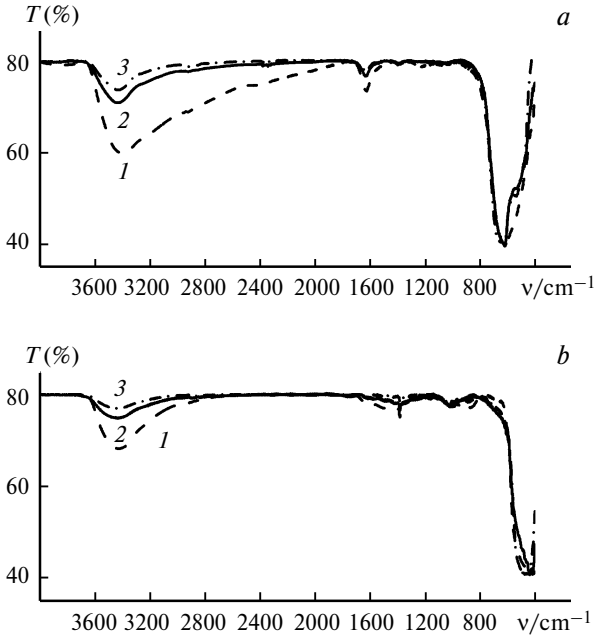

Fig. 10. IR absorption spectra of nanocrystalline oxides SnO_2 (*a*) and ZnO (*b*) with different microstructure parameters: (*a*) d = 3—62 nm, S_{BET} = 100—110 $m^2 g^{-1}$ (*1*), d = 10—12 nm, S_{BET} = 20—25 $m^2 g^{-1}$ (*2*), and d = 16—20 nm, S_{BET} = 5—10 $m^2 g^{-1}$ (*3*); (*b*) d = 10—12 nm, S_{BET} = 40—45 $m^2 g^{-1}$ (*1*), d = 19—21 nm, S_{BET} = 10—15 $m^2 g^{-1}$ (*2*), and d = 26—32 nm, S_{BET} = = 2—5 $m^2 g^{-1}$ (*3*).[61,105]

bonds) and molecular hydrate species (H_2O molecules, hydroxonium ions H_3O^+, and their derivative $H_5O_2^+$).[105,109] According to the width and intensity of the bands corresponding to stretching (3600—2000 cm^{-1}) and bending vibrations (1700—1600 cm^{-1}) of various adsorbates, the family of bridging hydroxyl groups (OH...OH) is the predominant hydrate species on the surface of highly dispersed SnO_2. The amount of chemisorbates decreases significantly with an increase in the size of SnO_2 crystallites, so that for the samples with the specific surface area <20 $m^2\ g^{-1}$ the corresponding absorption bands are almost absent from the IR spectra.

An analysis by IR spectroscopy of the content of molecular-adsorbed water on the surface of nanocrystalline ZnO (see Fig. 10) is impeded by the fact that the peaks of bending vibrations of H_2O (1650 cm^{-1}) are superimposed on both the stretching vibration bands of carbonate (1350 and 1530 cm^{-1})[110] and hydrocarbonate groups formed due to CO_2 chemisorption on oxygen anions and Zn—OH groups (1635 cm^{-1})[111] on the ZnO surface and the peaks of stretching vibrations of adsorbed CO_2 (1370 cm^{-1} (see Ref. 111) and 1360—1450, 1540—1650 cm^{-1} (see Ref. 112)). Carbonate pollutants can be caused by the adsorption of CO_2 from air, which is favored, in this case, by a higher basicity of zinc oxide than that of tin dioxide and by the incomplete decomposition of basic zinc hydrocarbonate during the synthesis of nanocrystalline ZnO.[61] In addition, the Zn—O—H bending vibrations (1320, 1395, 1410, 1560, 1605, and 1640 cm^{-1}) can contribute to the IR absorption bands of zinc oxide in a range of 1300—1700 cm^{-1}.[112] Not only isolated OH groups (3500—3700 cm^{-1})[107,112] and associates (OH...OH) joined by hydrogen bonds (3400 cm^{-1})[107] but also the complexes of OH groups with zinc vacancies (3220—3230 cm^{-1})[112] and defects (3450, 3555 cm^{-1})[113] can be in the composition of the hydroxyl layer of nanocrystalline ZnO, which results in a broad band of O—H stretching vibrations in a range of 2400—3700 cm^{-1}. The intensity of the IR absorption bands of all surface-bound groups and molecules decreases for the ZnO samples with a large size of crystalline (see Fig. 10). This indicates that an increase in the annealing temperature favors the removal of OH groups and carbonate pollutants from the surface and a decrease in the specific surface area of the material prevents their repeated adsorption.

The superimposition of the absorption peaks of various adsorbates creates difficulties for the quantitative determination of the composition of the HHL by IR spectroscopy. Thermodesorption methods make it possible to evaluate the total content of dissociated and molecular hydrate species, since they differ in the strength of the bond with the surface and, hence, in the desorption temperature.[43] Thermogravimetry is most available among these methods. The thermograms of the samples of nanocrystalline SnO_2 with different degrees of dispersion are presented in Fig. 11. A comparison with the data of DSC and mass spectrometry of evolved gases allows one to assert that the mass loss in the low-temperature range (50—200 °C) is caused by the desorption of molecular-adsorbed hydrate species, whereas in the high-temperature range (250—600 °C) the desorption of the OH groups bound to the oxide surface by stronger covalent bonds is responsible for the mass loss.[109] The calculation of concentrations of the molecular (H_2O) and dissociated (OH) hydrate species by the mass loss confirms that the latter prevail on the surface of nanocrystalline SnO_2 (Table 5). The total content of OH groups on the surface of highly dispersed SnO_2 with a particle size of 3—6 nm and the specific surface area equal to 90—100 $m^2\ g^{-1}$ is ~10 μmol m^{-2}, of which ≤10% hydroxyl groups exhibit Brønsted acidity (can adsorb NH_3 at low temperatures) and only an insignificant portion (~10^{-4} %) represents paramagnetic $OH^{\bullet}$ centers. For the SnO_2 and ZnO materials with a lower dispersion, the mass loss does not exceed error limit, and the content of hydrate species cannot be estimated by this method.

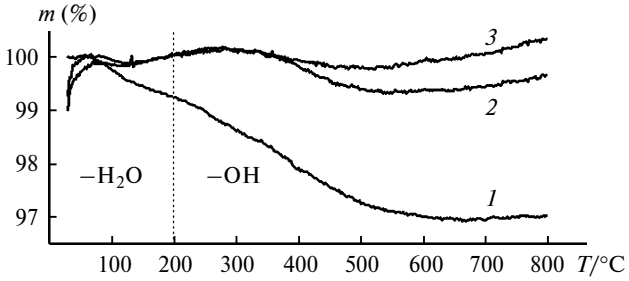

Fig. 11. Thermograms of nanocrystalline tin dioxide with different microstructure parameters: d = 3—6 nm, S_{BET} = = 100—110 $m^2\ g^{-1}$ (*1*); d = 10—12 nm, S_{BET} = 20—25 $m^2\ g^{-1}$ (*2*); and d = 16—20 nm, S_{BET} = 5—10 $m^2\ g^{-1}$ (*3*). The regions corresponding to the desorption of the molecular and dissociated hydrate species are separated.[105,109]

3.4. Relationship of the microstructure parameters of the oxides and the type or concentration of paramagnetic centers. The paramagnetic $OH^{\bullet}$ and O_2^- centers on the surface of nanocrystalline tin dioxide result in the appear-

Table 5. Concentration of hydrate species (C_h) on the surface of nanocrystalline SnO_2 modified by catalytic additives of Pd and Ru (1 wt.%)*

Modifier	C_h/μmol m^{-2}	
	dissociated OH_{surf}	molecular H_2O_{surf}
—	8.5—8.8	3.0—3.5
Pd	14.0—14.5	4.1—4.7
Ru	12.0—12.4	3.5—4.0

* T_{ann} = 300 °C.

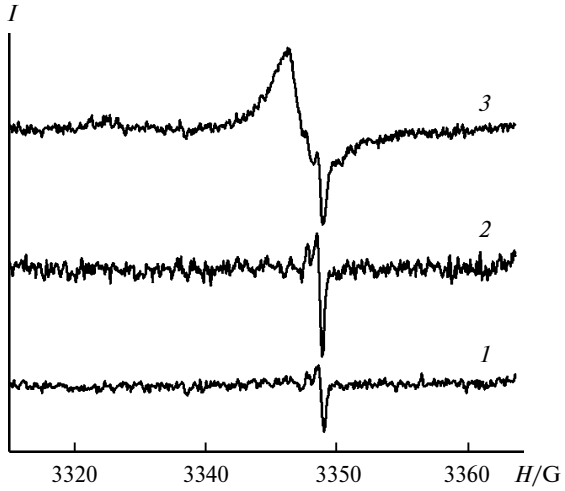

Fig. 12. ESR spectra of nanocrystalline tin dioxide with different microstructure parameters: d = 3—6 nm, S_{BET} = = 100—110 $m^2 g^{-1}$ (*1*); d = 16—20 nm, S_{BET} = 5—10 $m^2 g^{-1}$ (*2*); and d = 26—33 nm, S_{BET} = 1—5 $m^2 g^{-1}$ (*3*).[79]

ance of a complicated signal, whose intensity increases with a decrease in the particle size and an increase in the specific surface area of SnO_2, in the range of H = = 3350—3360 G of the ESR spectra (Fig. 12). The total concentration of surface paramagnetic centers increases by two orders of magnitude with a decrease in the size of SnO_2 particles from 35—50 to 3—6 nm and the respective increase in the specific surface area from 2—5 to 90—100 $m^2 g^{-1}$ (Table 6). The following concentrations of the sites are observed on the surface of highly dispersed SnO_2 (particle size 3—6 nm): $n(O_2^-) = 1.3 \cdot 10^{-11}$ mol m^{-2} and $n(OH^{\bullet}) = 2.5 \cdot 10^{-12}$ mol m^{-2}. The equivalent coverage of SnO_2 with ionosorbates O_2^- is ~10^{-6} monolayer if assuming their orientation to the normal to the surface and atomic radius as that of the O^- ion (1.76 Å), which is lower than the Weitz limit for the coating of the semiconductor with charged adsorbates (10^{-2}—10^{-3} monolayer).[14] The concentration of $V_O^{\bullet}$ oxygen vacancies in this material is estimated as $2 \cdot 10^{16}$ g^{-1}.

Such surface paramagnetic centers as $OH^{\bullet}$ and O_2^- cannot be detected in nanocrystalline zinc oxide, because, most likely, of a lower degree of dispersion compared to oxide SnO_2 and diverse defects (see section 2.4), the content of which in the material with a particle size of 10—12 nm is about 10^{14}—10^{15} g^{-1} (see Table 6).

4. Influence of doping impurities on active sites of the oxide surface

Doping impurities are introduced into the oxide matrix to control the electrophysical properties of the material. Doping with donor impurities are used in resistive sensors based on highly dispersed broad-band semiconductor oxides of the n-type to increase electric conductivity. As a rule, these impurities are cations with a higher oxidation state than that of the matrix cations but with close ion radii in the corresponding crystallographic positions; doping with fluoride anions is used more rarely. In the materials based on SnO_2, Sb^V is applied most widely, whereas cations M^{III} (M = Ga, In) are used in the materials based on ZnO.[14,15,93] For the content of dopants in the oxide matrix structure within solubility, the electrophysical parameters of the matrix correlate with the impurity concentration, but the properties of the surface do not change substantially. At a higher content, dopants can be distributed between the surface and volume of matrix grains. The properties of the oxide surface depend on the impurity concentration, and the volume properties of the semiconductor remain unchanged.

The properties of nanocrystalline oxides SnO_2(Sb), ZnO(Ga), and ZnO(In) were examined in this review. In these oxides, the concentration of donor impurities was varied in the range

$$x = [M^{(2)}]/([M^{(2)}] + [M^{(1)}]) = 0—10 \text{ at.}\%,$$

Table 6. Concentration of paramagnetic centers (C_p) on the surface of nanocrystalline tin(IV) and zinc oxides doped with various amounts (C) of donor impurities of Ga and modified by catalytic additives of Pd and Ru (1 wt.%)

Matrix	T_{ann}/°C	C (at. %)	Modifier	C_p/μmol m^{-2}		
				$OH^{\bullet}$	O_2^-	$V_O^{\bullet}$
SnO_2	300	—	—	$2.6 \cdot 10^{-6}$	$1.4 \cdot 10^{-5}$	$3.4 \cdot 10^{-4}$
			Pd	$4.9 \cdot 10^{-6}$	$8.7 \cdot 10^{-6}$	—
			Ru	$2.1 \cdot 10^{-6}$	$1.5 \cdot 10^{-5}$	—
ZnO	250	—	—	—	—	$5.8 \cdot 10^{-5}$
		0.5	—	—	—	$6.8 \cdot 10^{-2}$
		1.0	—	—	—	$1.6 \cdot 10^{-1}$
		2.6	—	—	—	$8.4 \cdot 10^{-3}$
		4.3	—	—	—	$6.4 \cdot 10^{-3}$

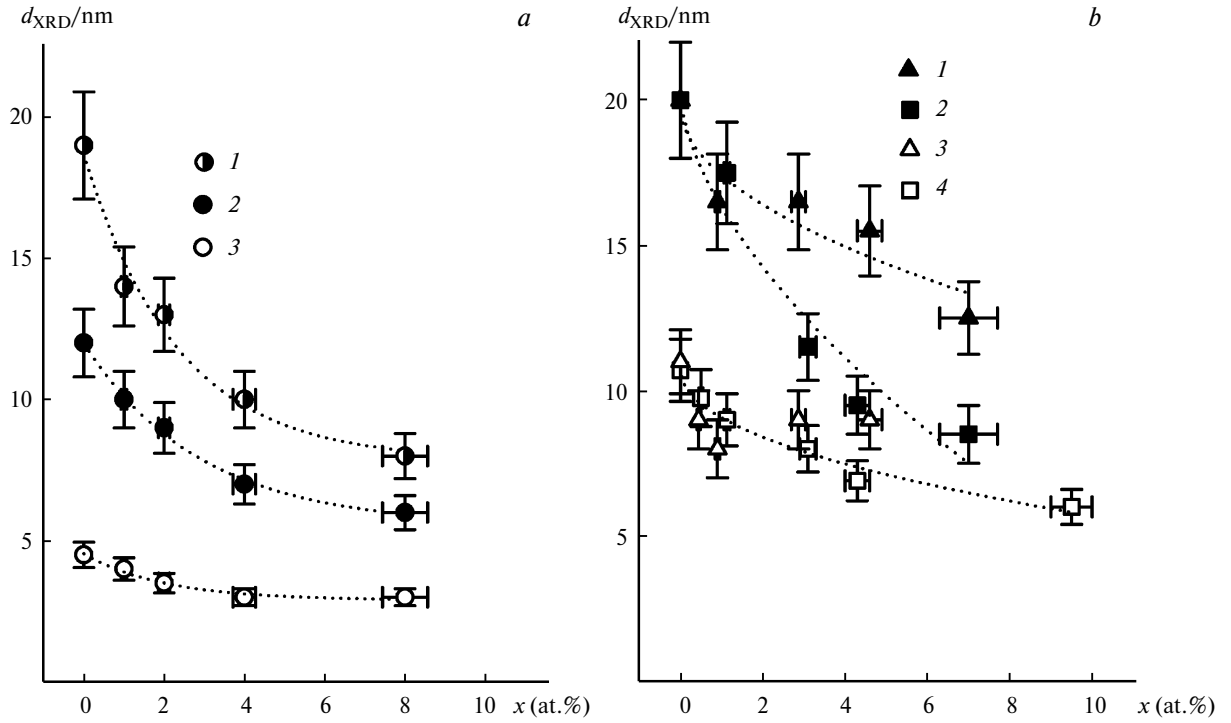

Fig. 13. Influence of the annealing temperature and content of dopants (x) on the size of crystalline grains (d_{XRD}) of nanocrystalline oxides SnO_2(Sb) (*a*) and ZnO(Ga) and ZnO(In) (*b*): (*a*) T_{ann} = 700 (*1*), 500 (*2*), and 300 °C (*3*); (*b*) ZnO(In), T_{ann} = 450 °C (*1*); ZnO(Ga), T_{ann} = 450 °C (*2*); ZnO(In), T_{ann} = 250 °C (*3*); and ZnO(Ga), T_{ann} = 250 °C (*4*).[106]

where $M^{(1)}$ = Sn, Zn; $M^{(2)}$ = Sb, Ga, In. In all cases, the introduction of dopants does not result in the formation of new crystalline phases. The influence of the content of donor impurities on the microstructure parameters of the semiconductor matrix is shown in Fig. 13. At a constant annealing temperature of the materials SnO_2(Sb), ZnO(Ga), and ZnO(In), the size of crystalline grains of the matrix decreases with an increase in the content of dopants. This can be due to the fact that within the solubility limits in the oxide matrix doping cations can retard ion diffusion and induce microstresses of the structure. In addition, if the content of dopants is higher than their solubility, impurities in the oxide structure can form segregation on the grain surface, which also prevents ion diffusion and retards the growth of oxide particles under the isothermal annealing conditions.[19]

The solubility of antimony in nanocrystalline tin dioxide is estimated as 3—6 at.% on the basis of the dependence of the conductivity on the concentration of the introduced impurity.[114—117] The structural methods of analysis are inefficient for studying the antimony distribution in nanocrystalline SnO_2, because cationic substitution does not affect the unit cell parameters due to the close sizes of Sb^V and Sn^{IV} (0.65 and 0.69 Å, respectively[118]). An impurity in SnO_2(Sb) cannot be visualized by contrast using electron microscopy, because the atomic masses of Sn and Sb are close. According to the data of Mössbauer spectroscopy, EXAFS, and XANES, antimony in low concentrations is incorporated into the SnO_2 structure in the form of Sb^V and shifts to the surface as Sb^{III} if the doping level increases.[119] The experimental difficulties in studying the distribution of gallium in zinc oxide are caused by the same fundamental factors. Taking into account the electric conductivity and optical properties, the solubility of Ga and In in nanocrystalline ZnO can be estimated as 1 at.%.[120,121] The uniform impurity distribution was revealed in zinc oxide doped with 1 at.% gallium, since the intensities of the Ga K-line in the EDX spectrum are comparable for different regions and when using different scales (Fig. 14). Owing to the significant difference in the atomic masses of In and Zn, the impurity distribution in ZnO(In) can be visualized by TEM, scanning transmission electron microscopy (STEM), and EDX mapping: it is shown that at the content >1 at.% indium forms amorphous segregations (presumably in the form of oxide) on the surface of agglomerated particles of zinc oxide (Fig. 15).

4.1. Influence of dopants on the acidity and hydration of the surface. The segregation on the oxide surface of doping cations differed in the charge state from the cations of the matrix, primarily affects the acidic properties, which appear, in particular, during chemisorption of water.

Doping of nanocrystalline SnO_2 with antimony in a concentration of 1—8 at.% results, as a whole, in a decrease in the acidity of the surface.[106] One of the modern approaches to quantitative ranging of various

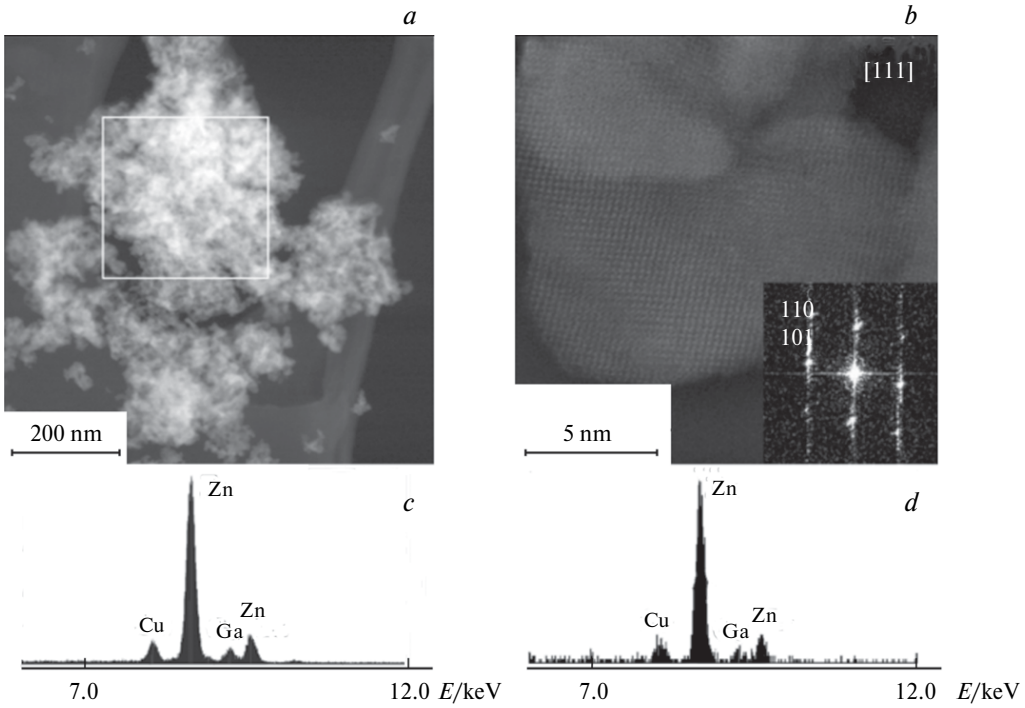

Fig. 14. TEM images (*a*, *b*) of samples of nanocrystalline zinc oxide doped with 4 at.% Ga and the corresponding EDX spectra (*c, d*): agglomerate of nanoparticles (*a, c*) and individual nanoparticle with the wurtzite structure (*b*, *d*).[97]

metal oxides according to their Lewis acidity[122] is based on the concept of so-called optical basicity (Λ).[123] According to this concept, the Lewis acidity of the cations that form oxide is inversely proportional to their optical basicity. The calculated[122] values of optical basicity for the Sb^V and Sn^{IV} cations in the octahedral oxygen environment are 0.985 and 0.870, respectively. The lower density of the positive charge on the Sb^V cations, as compared to the Sn^{IV} cations of the matrix, leads to a decrease in water chemisorption on the surface and the concentration of hydrate derivatives formed in this process. This is indicated by a decrease in the intensity of the absorption bands of stretching vibrations of OH groups and bending vibrations of H_2O molecules in the IR spectra of SnO_2(Sb) (Fig. 16). However, the concentrations of the Brønsted and Lewis acidic sites estimated from the data of TPD of ammonia vary insignificantly within the inaccuracy range (see Table 3).

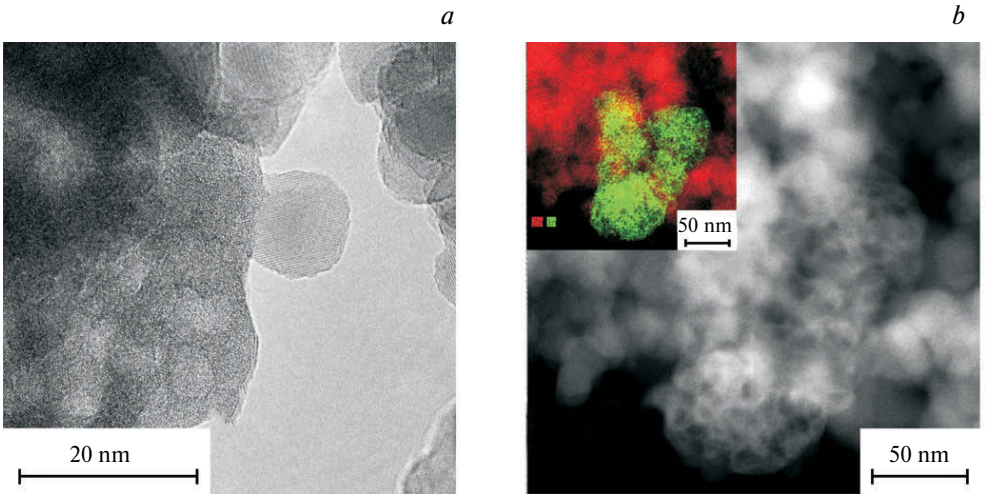

Fig. 15. TEM (*a*) and STEM (*b*) images nanocrystalline zinc oxide doped with 5 at.% In. Inset: EDX map of the composition of the detection region (dark is Zn, light is In).[97]

Note. Figures 15, 16, 21, and 23 are available in full color on the web page of the journal (http://www.link.springer.com).

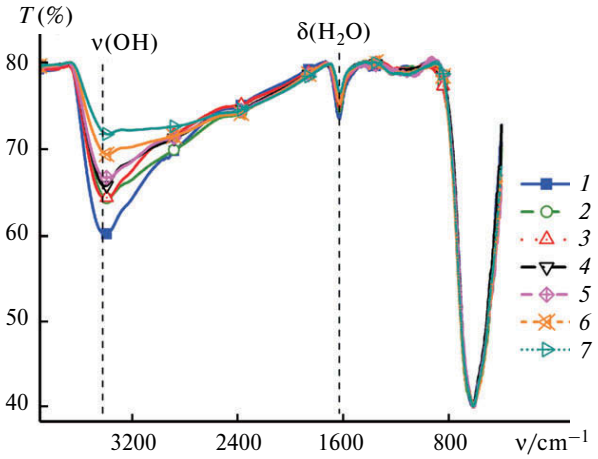

Fig. 16. IR absorption spectra of nanocrystalline tin dioxide doped with various amounts of antimony: [Sb]/[Sb+Sn] = 0 (*1*), 1 (*2*), 2 (*3*), 3 (*4*), 4 (*5*), 6 (*6*), and 7 at.% (*7*).[106]

Doping of zinc oxide with Ga^{III} and In^{III} cations exerts an opposite effect: the acidity of the ZnO(M) surface increases with an increase in the gallium and indium content.[61,97,106] This is confirmed by the results of TPD of ammonia: at the dopant content ≤0.5 at.% the spectra do not almost differ from those for undoped ZnO (Fig. 17). Evidently, impurities in this concentration exert no effect on the acidity of the surface, since they are components of the crystal structure of zinc oxide. Although the total amount of acidic sites in ZnO(Ga) and ZnO(In) does not change within the inaccuracy range being 2—3 μmol m^{-2}, the fraction of the Brønsted sites increases with an increase in the content of dopants higher than 1 at.%. In this case, the peak of ammonia desorption from the Lewis sites shifts to low temperatures, which indicates a decrease in their acidic strength (see Fig. 17). This fact can be caused by the fact that the surface M^{III} cations favor water chemisorption and the respective increase in the amount of acidic OH sites. This is confirmed by an increase in the bands of stretching vibrations of O—H in the IR absorption spectra of doped zinc oxide (Fig. 18, *a*, *b*). In turn, binding with water molecules and OH groups can weaken the Lewis acidity of surface cations, which makes it possible to explain the TPD results.[61,97] The data of IR diffuse reflectance spectroscopy under the conditions of *in situ* ammonia adsorption directly indicate an increase in the acidity of the surface with an increase in the dopant content in ZnO(M): the intensity of the absorption bands of stretching and bending NH_4 groups formed by ammonia bound to the Brønsted OH sites and NH_3 molecules linked to the Lewis sites (Fig. 18, *c*).[106]

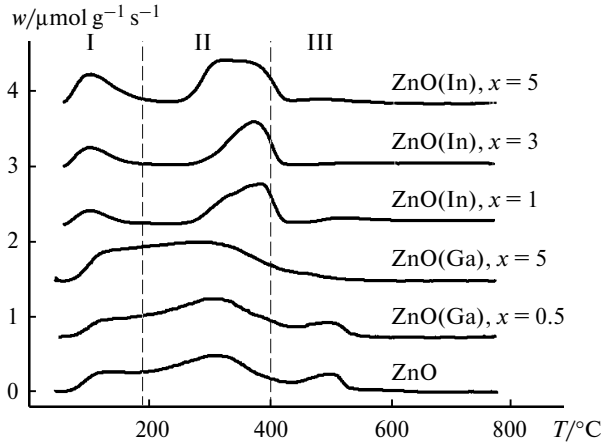

Fig. 17. Temperature dependences of the specific rate of ammonia desorption (*w*) during TPD from the surface of nanocrystalline zinc oxide doped with various amounts of gallium and indium. The regions of weak (I), medium (II), and strong acidic sites (III) are distinguished.[61]

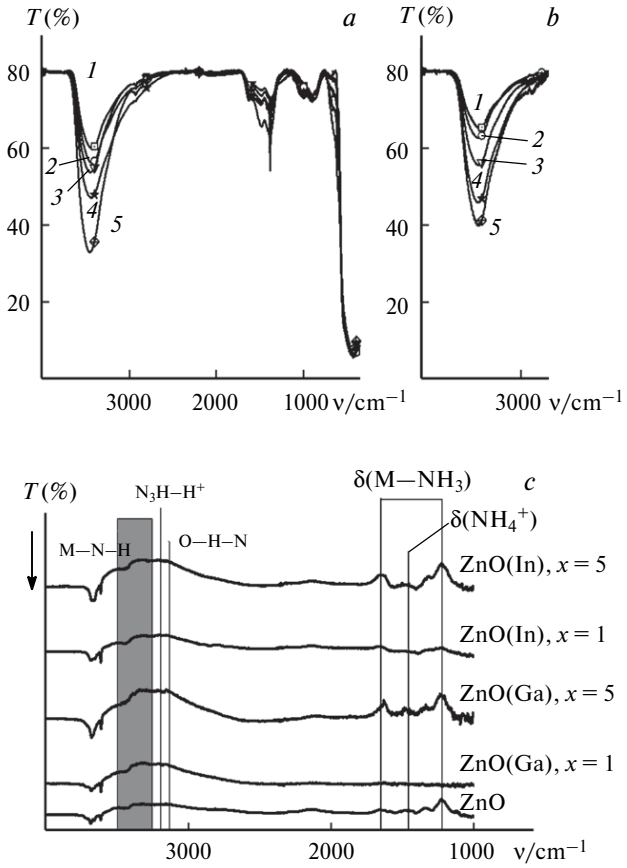

Fig. 18. IR absorption spectra (*a*, *b*) of nanocrystalline zinc oxide doped with various amounts of gallium (*a*) and indium (*b*) and IR diffuse reflectance spectra of similar samples under the conditions of *in situ* adsorption of 200 ppm NH_3 at room temperature (*c*); (*a*, *b*) *x* = [M]/[M+Zn] = 0 (*1*), 0.5 (*2*), 1 (*3*), 3 (*4*), and 5 at.% (*5*).[61]

4.2. Influence of dopants on the concentration and predominant form of chemisorbed oxygen. According to the results of analysis by the TPR-H_2 method, the concentration of chemisorbed oxygen on the surface of nano-

crystalline tin oxide doped with 0.5—8 at.% antimony is 10—15 μmol m^{-2} (see Table 4) without a pronounced dependence on the impurity amount.

The TPR spectra of zinc oxide doped with 1 at.% gallium or indium are identical to the spectrum of undoped ZnO. This effect confirms that impurities in this concentration do not affect the properties of the surface and, most likely, incorporate into the volume of the matrix grains. As the dopant content increases, new absorption peaks appear at $T = 300$—600 °C (Fig. 19), which is higher than the temperature range of reduction of surface-bound oxygen. It is most likely that they correspond to the reduction of segregations Ga_2O_3 and In_2O_3 on the zinc oxide surface. The amount of chemisorbed oxygen estimated from the hydrogen uptake at $T = 100$—300 °C somewhat increases with an increase in the concentration of dopants in ZnO(Ga), ZnO(In) (see Table 4). This can be caused by the fact that the impurity cations M^{III} form donor sites favoring the chemisorption of acceptor oxygen molecules.

The state of surface-bound oxygen can be studied indirectly by analysis of the dependence of the electric conductivity of the material on the partial pressure of O_2. The restriction of this method is that the obtained information concerns only ionosorbed oxygen in the form of O_2^-, O^-, or O^{2-} and the model of conductivity based on a series of assumptions[33] is used to determine their relative amount. The study of oxygen ionosorption in the case of nanocrystalline ZnO(Ga) and ZnO(In) showed that molecular O_2^- (100—200 °C) or atomic O^- (200—400 °C) ionosorbates can exist on the oxide surface depending on the temperature.[61] The influence of the dopants is manifested only in the low-temperature range: at $T = 100$—200 °C molecular ionosorption in the form of O_2^- predominates on the surface of the samples doped with gallium and indium, whereas on the surface of undoped zinc oxide the fractions of O_2^- and O^- are equivalent (Fig. 20). It is assumed that the acid-base interaction of the M^{III} surface cations with O_2 molecules takes place in the case of ZnO(M).[61]

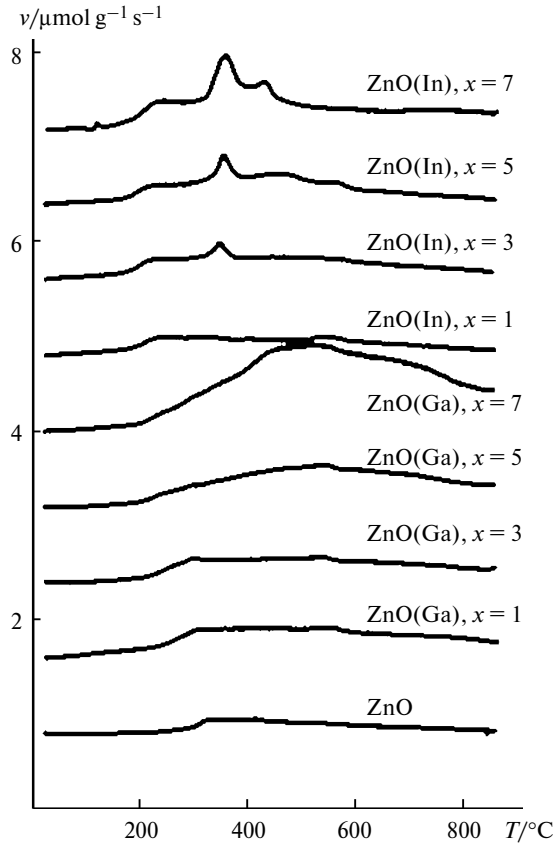

Fig. 19. TPR spectra of samples of zinc oxide annealed at different temperatures and doped with various amounts of gallium and indium; v is the specific rate of H_2 uptake.[106]

4.3. Influence of dopants on the type and concentration of paramagnetic centers. Doping additives affect most strongly the concentration of paramagnetic donor centers (oxygen vacancies) in the materials based on zinc oxide.[97] These sites are the single type of paramagnetic centers in the doped samples of nanocrystalline zinc oxide detected by the ESR method from the signal with $g = 1.956$ in the corresponding spectra (Fig. 21).

As the dopant concentration in ZnO(Ga) increases from 0 to 1 at.%, which corresponds to the solubility limit of gallium in zinc oxide, the signal intensity of the donor states reaches a maximum. With the further increase in the doping level, the concentrations of these paramagnetic centers somewhat decrease and depend weakly on the gallium content (Fig. 22). This nonmonotonic behavior of the concentration dependence can be explained by the fact that with increasing the dopant content higher than 1 at.% the donor states transform into non-paramagnetic states, for example, *via* the formation

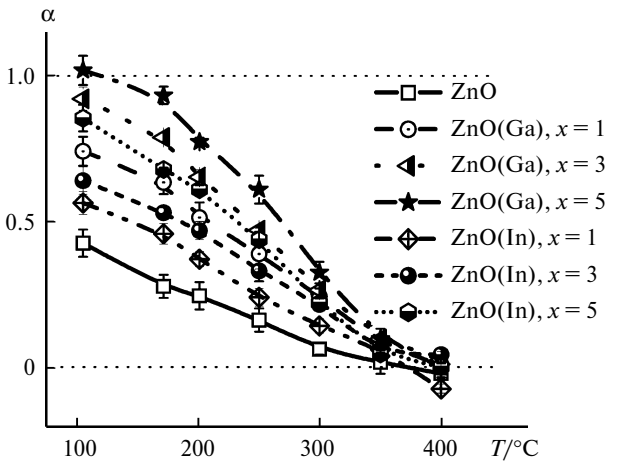

Fig. 20. Predominant form of chemisorbed oxygen *vs* concentration of impurities in nanocrystalline materials ZnO(Ga) and ZnO(In) at different temperatures; $\alpha = [O_2^-] - [O^-]$ is the fraction of ionosorbate O_2^-.[61]

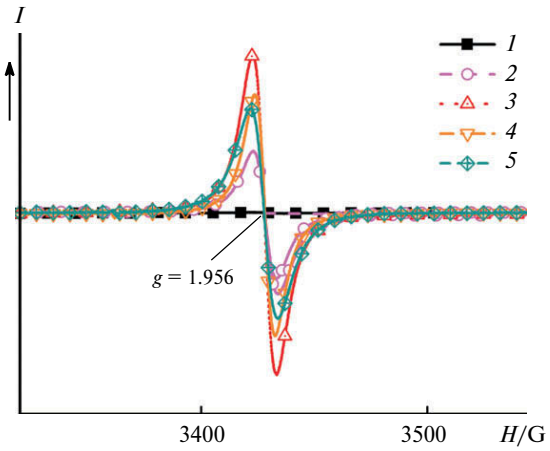

Fig. 21. ESR spectra of nanocrystalline zinc oxide doped with various amounts of gallium; x = [Ga]/[Ga+Zn] = 0 (*1*), 0.5 (*2*), 1 (*3*), 3 (*4*), and 5 at.% (*5*).[97]

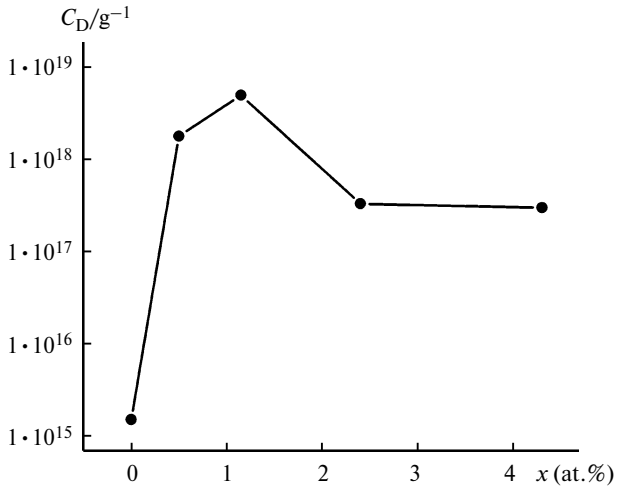

Fig. 22. Concentration of donor sites (g = 1.956) (C_D) *vs* gallium content in doped nanocrystalline zinc oxide[87]; x = [Ga]/[Ga+Zn].

of non-paramagnetic pairs of donor states. If assuming that the donor defects corresponding to paramagnetic centers with g = 1.956 are formed owing to the incorporation of doping cations into crystal structure of the matrix, it can be concluded that the maximum in Fig. 22 at x = 1 at.% Ga corresponds to the solubility of gallium in zinc oxide. With the further increase in its content, gallium can occupy positions on the surface of ZnO particle and suppress the formation of oxygen vacancies.

5. Influence of catalytic modifiers on active sites

The concept of chemical modification is the formation on the semiconductor matrix surface of new active sites with specific adsorbability and/or reactivity toward target gases. Numerous studies showed that the modification of the surface of semiconductor oxides improved their sensor properties: sensitivity, selectivity, dynamics of response, and stability.[17] An approach to choosing modifiers was developed as a result of the systematic study of the sensor sensitivity of nanocrystalline SnO_2 modified by diverse additives (noble metals, oxides of transition metals and lanthanides).[19] The essence of the approach is that the reactivity of the modifier should correspond to the chemical properties of the target gas. For example, if the gas has the Lewis basicity (NH_3, amines). Then it is reasonable to modify the sensor surface by additives with pronounced acidic properties (MoO_3, WO_3, V_2O_5).

Unlike the acid-base additives, the action of catalytic modifiers is the intensification of oxidation of analyzed gas molecules with chemisorbed oxygen on the material surface rather than the enhancement of adsorption. This occurs owing to a decrease in the activation energy of the reaction responsible for sensor signal formation and leads not only to an increase in the sensor sensitivity but also to a decrease in the working temperature necessary for this process.[124—128] The choice of selective modifiers is based on the concept about the mechanism of action of the heterogeneous catalysts.[18] The activity and specificity of a catalyst in oxidation processes are determined by the energy of adsorption of molecules of gas-reducing agent and oxygen and the energies of bonding with intermediates and reaction products. Transition metals of Groups 8, 9, and 10 have an optimum chemisorption energy toward various gases, which is caused by their electronic structure.[129] Transition metals of the beginning of the series (less occupied d-sublevel), metals of the main subgroups, and rare-earth elements are characterized by strong chemisorption of gases (with oxygen, up to the formation of new phases) due to vacant orbitals.[18] On the contrary, elements with the completely occupied d-sublevel (Group 11) are less prone to chemisorption of gases, and their catalytic activity is caused by the formation of vacancies in the d-sublevel, especially for nanodispersed metals.[129,130] An optimum catalytic modifier for a specific gas-reducing agent can be selected if considering the dependence of the catalytic activity of the metals in the oxidation of the target gas on the bonding energy with adsorbates. For instance, Pd and Pt are the optimum catalysts in CO oxidation, since the energy of oxygen chemisorption on them (340—360 kJ mol^{-1}) is close to the bonding energy of these metals with CO.[131,132] Palladium and platinum are among the most efficient modifiers for improving sensor properties toward CO.[126,133—136] Gold is of the same interest,[127,137,138] but its activity is determined by the size effect rather than the chemisorption energy. Other metals catalytically active in CO oxidation, such as Rh, Ru, and Ni, found no wide use as modifiers of sensor materials because, under the operation conditions of sensors, they tend to form stable oxide phases with the catalytic properties different from those of the metals.[131,139]

Systems oxide—Ru—NH_3 represent an example of the correspondence of the catalytic properties of the modifier and sensor properties of the modified oxide. On the one hand, the catalysts based on ruthenium are the most active and selective catalysts of synthesis, decomposition, and oxidation of ammonia.[140,141] This is caused the optimum energy of the Ru—N bond providing low activation barriers of transitions from chemisorbed NH_3 to intermediate species (NH_2—, NH=, N≡) and its oxidation products (N_2, NO_x).[142,143] On the other hand, the ruthenium-modified semiconductor oxides (ZnO, SnO_2) possess excellent sensitivity and selectivity toward NH_3.[144—146] It is shown that ammonia oxidation to nitrogen oxides catalyzed by the modifier plays the determining role in the formation of a sensor signal in these systems[146] (Scheme 1).

Scheme 1

$$NH_3 + 4\,O^-_{surf} \xrightarrow{RuO_2} NO_{surf} + 3\,OH_{surf} + 4\,e^-$$

$$O^-_{surf} \rightleftarrows$$

$$NO^-_{2,surf} \rightleftharpoons NO_2\,(g) + e^-$$

Oxygen does not inhibits the modifier, because oxide RuO_2 formed in air contains on the surface coordinately unsaturated Ru^{IV} cations accessible for binding NH_3 molecules and, hence, this oxide almost does not differ in catalytic properties from metallic ruthenium.[147,148]

The influence of the catalytic modifiers PdO_x and RuO_y (1 wt.%) on the type and concentration of active sites on the surface of nanocrystalline SnO_2 will be considered further. The modification was conducted by the impregnation of tin dioxide with alcohol solutions of Pd^{II} and Ru^{III} acetylacetonates followed by the thermal treatment in air.[67,146]

5.1. Active sites formed by catalytic modifiers. The active sites formed by the catalytic modifiers are clusters or nanoparticles of noble metals or their oxides localized on the surface of the semiconductor matrix. This was experimentally confirmed by the TEM and STEM studies of the nanocomposites.[67,127,134,146] The clusters can be detected if either the atomic masses of the modifier and the major element of the oxide matrix (for example, for the modification of tin dioxide with gold or nickel, Fig. 23, *a*), or sizes of the clusters of the modifier and support particles (Fig. 23, *b*) differ considerably. On the contrary, it is difficult to visualize additives by methods of transmission

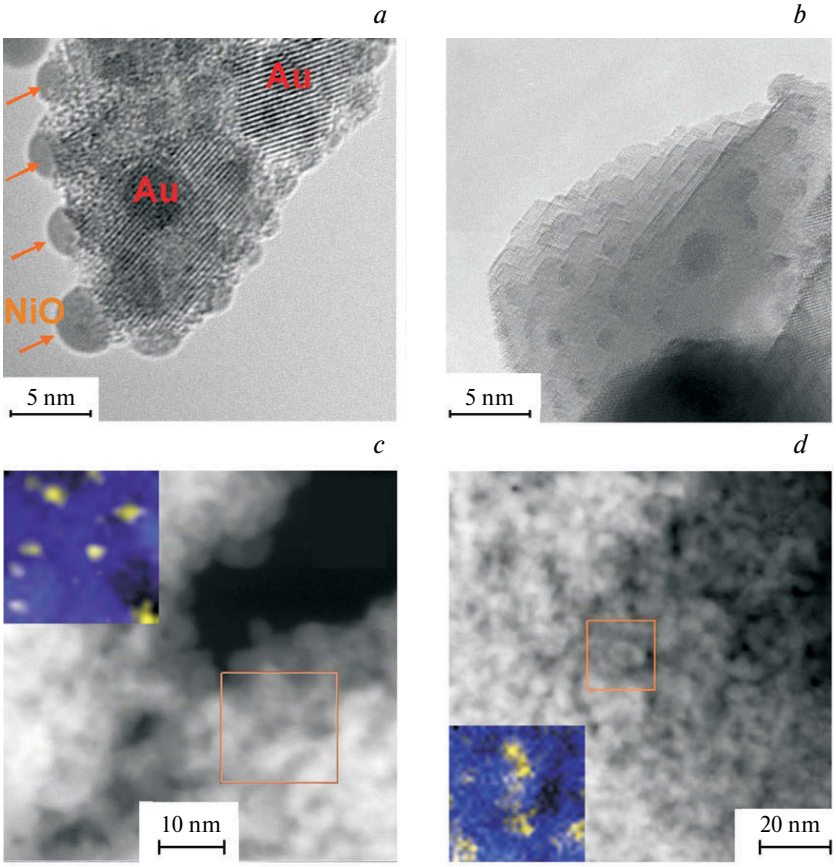

Fig. 23. High-resolution TEM images of nanocrystalline SnO_2 (d = 3—6 nm) modified by gold and nickel oxide (*a*) and platinum oxide clusters on the tin dioxide surface with the particle size d = 16—20 nm (*b*). STEM images of nanocomposites SnO_2/PdO_x (*c*) and SnO_2/RuO_y (*d*) based on nanocrystalline tin dioxide (d = 3—6 nm); insets: EDX maps of the isolated region (blue is Sn, yellow is modifier element).[68]

electron microscopy when nanocrystalline SnO_2 (particle size <10 nm) is modified by noble metals of the same period (Ru, Rh, Pd).[149] Scanning of the elemental composition of the surface in terms of energy dispersive X-ray microanalysis (EDX mapping) is informative when studying the modifier distribution in these systems. Figures 23, *c, d* exemplify the maps of the cationic composition of the surface of SnO_2/PdO_x and SnO_2/RuO_y nanocomposites composed by scanning the Sn L, Pd L, and Ru L signals and show that the modifiers form clusters 1—5 nm in size even when supporting a minor amount (1 wt.%) of the additives on the surface of highly dispersed SnO_2 (particle size 3—6 nm).[67,146] The catalytic clusters cover not isolated nanoparticles of SnO_2 but their agglomerates, whose sizes can range from several tens to hundreds of nanometers.

When describing the active sites formed by modifiers, it is important to determine the oxidation state of the latter. This depends, first of all, on the nature of the introduced additive. For the noble metals used, the affinity to form oxides decreases in the series Ru, Rh, Pd, Pt, and Au. This is caused by a decrease in the energy of the metal—oxygen bond, energy of the crystal lattice, thermal stability, and absolute enthalpy of formation of oxides of the indicated metals. Ruthenium and rhodium on the surface of nanocrystalline oxides exist in the oxidized state as RuO_2 ($\Delta_f H = -(150—200)$ kJ mol^{-1}) or Rh_2O_3 ($\Delta_f H \approx -(100—150)$ kJ mol^{-1}), respectively.[145,150] It was shown by the ESR method that ruthenium in the SnO_2/RuO_y nanocomposites (1 wt.%) prepared by the impregnation with a solution of $Ru(acac)_3$ can be in the mixed-valence state, where structured RuO_2 clusters contain a fraction of Ru^{III}.[109,151] Gold, oxide of which Au_2O_3 is an endothermic compound,[150] exists in the zero-valent state on the surface of sensor materials even in the form of small clusters (1—3 nm).[152,153] Palladium and platinum that occupy an intermediate position can exist both in the metallic state and as oxides PdO, PtO, and PtO_2 ($\Delta_f H \approx -(50—100)$ kJ mol^{-1}).[134,154] In this case, the oxidation state depends on the method of synthesis of the nanocomposite, morphology and particle size of the modifier, and conditions: temperature and composition of the gas phase. The investigations of the state of palladium deposited on SnO_2 show that the modifier in low concentrations (0.1—0.2 wt.%) is distributed over the surface at the atomic level, which facilitates its interaction with chemisorbed oxygen to form PdO.[15,155] When the content of palladium is increased to 1—3 wt.%, it forms three-dimensional clusters on the SnO_2 surface,[15] and their oxidation starts in the presence of oxygen already at 200 °C. As a result, mixed-valence clusters PdO_x containing Pd^{II} as the major form ($x = 0.7—0.8$) along with zero-valent palladium are formed.[105,155] The Pd^{II} cations can be incorporated into the support lattice on the Sn^{IV} positions,[15] but heating above 400 °C is necessary for the beginning of Pd^{II} diffusion into the near-surface layer of SnO_2.[156] The detailed study of the composition of the nanocomposites based on SnO_2/PdO_x (1 wt.%) by the XPS, ESR, XANES, and EXAFS methods revealed than the PdO_x clusters consisting of amorphous PdO also contain Pd^0 atoms and a minor fraction of Pd^{III} cations presumably stabilized at the boundary of the clusters and support.[109,151] The further increase in the amount of supported palladium results in the percolation of metallic clusters, formation of continuous layers of Pd and, finally, formation of the near-surface solid solution Sn—Pd (two—five monolayers of the additive).[15] The particle size similarly affects the state of platinum on the surface of nanocrystalline SnO_2: clusters <3—4 nm in size were shown to be PtO_2 and larger clusters represent zero-valent Pt^0.[157] According to the XPS data, in the nanocomposites containing 1 wt.% platinum and obtained by the impregnation method using $Pt(acac)_2$, platinum exists as PtO, which is characteristic of small Pt clusters (<2 nm).

5.2. Influence of modifiers on intrinsic active sites of the oxide. In addition to the formation of new active sites, modifiers affect intrinsic surface sites of the semiconductor oxide: catalytic clusters specifically change their concentration and reactivity of the surface of the material as a whole. This predetermines the character of interaction of nanocomposites with gases, which affects the operation conditions of the gas sensor. Let us consider how additives of palladium and ruthenium oxides (1 wt.%) affect the active sites of nanocrystalline tin dioxide. As shown by the TPR results, the shift of the maximum of the low-temperature hydrogen uptake to the low-temperature range indicates an increase in the activity of the oxidative surface sites in catalytically modified SnO_2 (Fig. 24). The quantitative influence of the modifiers is manifested in that the palladium additives (and, to a higher extent, the ruthenium additives) favor an increase in the concentration of chemisorbed oxygen on the SnO_2 surface (see

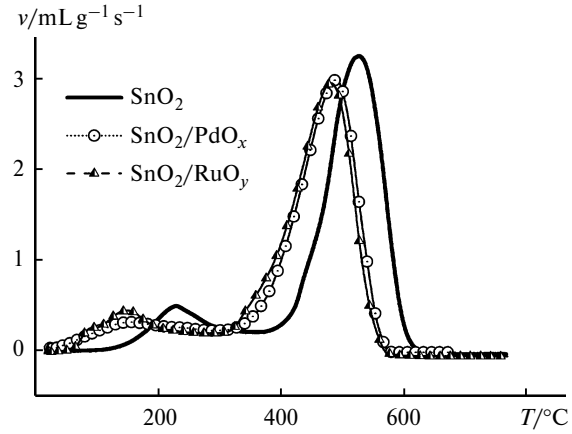

Fig. 24. Temperature dependence of the specific rate of hydrogen uptake (v) during TPR of nanocrystalline SnO_2 modified by catalytic additives.[68]

Table 4). Their concentration in the modified materials by 3—5 times exceeds the surface concentration of PdO_x or RuO_y. This indicates that the clusters of platinum metal oxides form new oxidative sites and also favor the accumulation of chemisorbed oxygen on the surface.

According to the data of TPD of ammonia, the introduction of catalytic additives induces a change in the acidity of the SnO_2 surface. Modification with palladium oxide results in a systematic increase in the concentration of the Brønsted OH sites on the surface of materials with different microstructure parameters (see Table 3). The peaks of NH_3 desorption from the Lewis sites appear at lower temperatures than those in the case of the unmodified oxide, so that the corresponding TPD signals lie in the range corresponding to acidic sites of medium strength (Fig. 25). This can indicate the weakening of the Lewis acidity of the SnO_2 surface under the action of PdO_x and RuO_y additives or can reflect the desorption of the products of catalytic ammonia oxidation.[109,146]

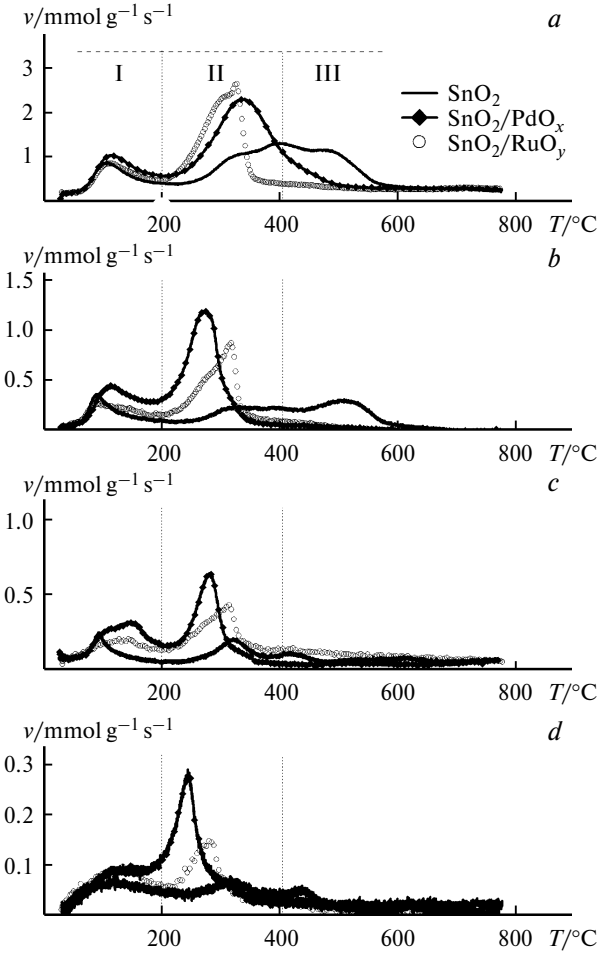

Fig. 25. Temperature dependences of the specific rate of NH_3 desorption (v) during TPD from the surface of nanocrystalline SnO_2 with different microstructure parameters and catalytic modifiers: (*a*) $d(SnO_2) = 3$—6 nm, $S_{BET} = 100$—110 m^2 g^{-1}; (*b*) $d(SnO_2) = 10$—12 nm, $S_{BET} = 20$—25 m^2 g^{-1}; (*c*) $d(SnO_2) = 16$—20 nm, $S_{BET} = 5$—10 m^2 g^{-1}; and (*d*) $d(SnO_2) = 26$—35 nm, $S_{BET} = 1$—5 m^2 g^{-1}. The regions of weak (I), medium (II), and strong acidic sites (III) are distingished.[109]

The influence of the modifiers on the paramagnetic centers appears in the fact that the signal of the donor sites is not detected in the ESR spectra of modified tin dioxide, which can be caused by the acceptor action of the PdO_x and RuO_y clusters themselves or by the promotion of oxygen chemisorption favoring the complete ionization of oxygen vacancies $V_O^{\bullet}$.[85] The relative concentrations of surface sites O_2^- and $OH^{\bullet}$ (see Table 6) change slightly upon modification by ruthenium oxide. However, under other equivalent conditions, the concentration of hydroxyl sites $OH^{\bullet}$ on the SnO_2/PdO_x surface is twice as large and that of the oxygen sites O_2^- is 1.5 times lower than those in the case of SnO_2. This effect is enhanced for the hydration of SnO_2/PdO_x, so that the ESR spectrum of the material kept in wet air contains no signal of O_2^- (Fig. 26). It is most likely that the PdO_x clusters favor the transformation of the oxygen sites into the hydroxyl sites in the presence of water vapors.[83,153]

The composition of the HHL of the surface of nanocrystalline SnO_2 changes under the action of the catalytic additives.[105,109] This is expressed quantitatively as an increase in the concentration of molecular and dissociated derivatives of adsorbed water (see Table 5), which is confirmed by the data of IR spectroscopy (Fig. 27) and thermogravimetry (Fig. 28). The IR spectra also indicate the changes in the qualitative composition of the hydroxyl layer: the modification of SnO_2 by palladium or ruthenium oxide favors an increase in the fraction of bridging hydroxyl groups OH...OH joined by hydrogen bonds among the dissociated hydrate species (OH groups) (see Fig. 27, Table 1). This can be caused by an increase in the mobility of protons of the OH groups under the action of modifiers, as its occurs in the case of increasing the Brønsted acidity on the SnO_2/PdO_x surface.

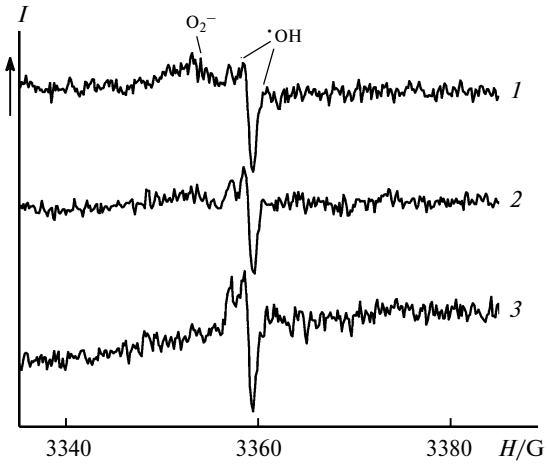

Fig. 26. ESR spectra of nanocrystalline materials SnO_2 (*1*), SnO_2/PdO_x (*2*), and SnO_2/PdO_x kept in wet air (*3*).[109]

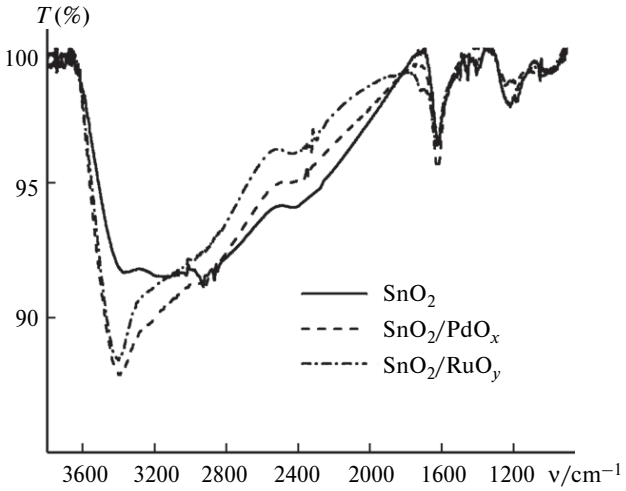

Fig. 27. IR absorption spectra of the materials based on nanocrystalline tin dioxide modified by catalytic additives.[109]

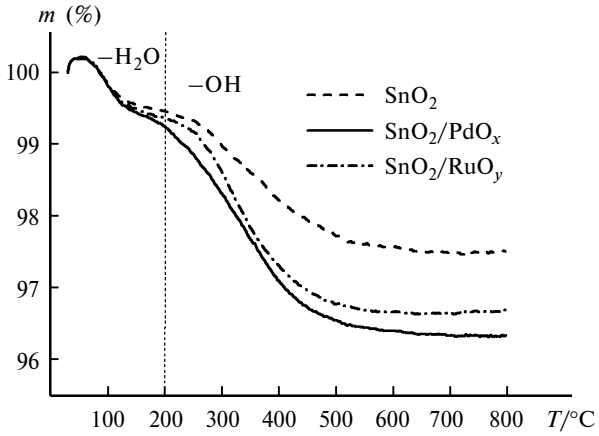

Fig. 28. Thermograms of the materials based on nanocrystalline tin dioxide modified by catalytic additives.[109]

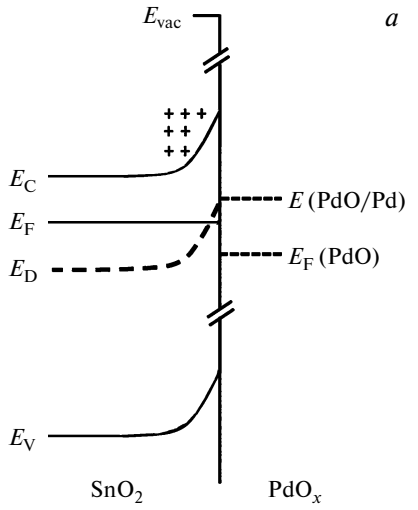

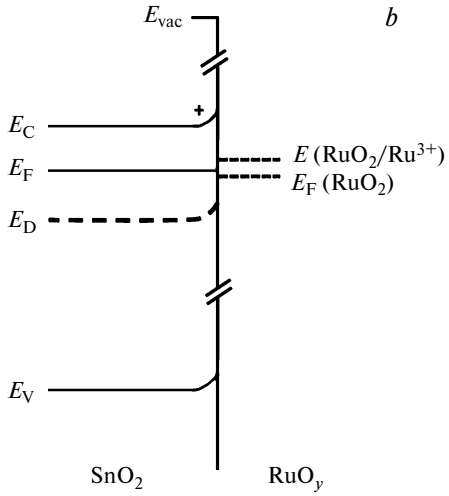

Fig. 29. Scheme of formation of the depleted layer in the near-surface region of SnO_2 on contact with PdO_x clusters (levels corresponding to the work function of PdO and potential of the PdO/Pd) pair (*a*) and RuO_y (*b*); E_{vac}, E_C, E_F, E_D, and E_V are levels of vacuum, conduction band, Fermi, donor states, and valence band, respectively.[109]

Note that modifiers exert different effects on the amount of different active sites. Unlike ruthenium oxide resulting in the accumulation of chemisorbed oxygen, the PdO_x clusters exhibit the hydrating effect, namely, favor an increase in the concentration of surface hydrate species: molecular-adsorbed water and OH groups, including the hydroxyl groups that are Brønsted acidic sites, and paramagnetic $OH^{\bullet}$ centers (see Tables 3—6). It is assumed than the increase in the chemisorption of H_2O under the action of palladium oxide is induced by the electronic interaction with the support. At the concentration of the modifier (1 wt.%), the PdO_x clusters mainly contain bivalent (~70% of the total amount) and zero-valent palladium. The work function of PdO oxide is 6.0 eV.[157] In addition, these two states can form redox pair PdO/Pd, the energy level of which lies by ~5.5 eV lower than the vacuum level.[158] Since the work function of tin dioxide (4.8 eV) is lower than these values, a depleted layer is formed in the semiconductor region contacting with the PdO_x clusters (Fig. 29, *a*). The electron-deficient character of the near-boundary region of the support favors the adsorption of H_2O donor molecules and their dissociation, which, according to Eq. (6), is accompanied by the formation of OH groups and paramagnetic centers $OH^{\bullet}$ on the SnO_2/PdO_x surface. A lower hydrating effect of ruthenium oxide is caused by its weak electron-acceptor action: the work function of RuO_2 is[159] 5.0—5.1 eV, and in contrast with SnO_2 the effect of depletion of the support in electrons is less pronounced (Fig. 29, *b*) than that at the SnO_2—PdO_x boundary.

6. Oxygen exchange

Various forms of oxygen can participate in processes of interaction of semiconductor oxides with gases responsible for their sensor sensitivity: chemisorbed oxygen and structural anions (anions incorporated in the crystal lattice of oxide) in the near-surface layer and in the volume of oxide particles. An efficient method of investigation of these interactions is temperature-programmed isotope exchange $^{18}O/^{16}O$ under the dynamic conditions.[160] This method is experimentally performed by passing a gas mixture of isotopic oxygen molecules $^{16}O_2$, $^{16}O^{18}O$, and $^{18}O_2$ in argon through the oxide heated in the reactor with a constant rate with the simultaneous determination of the isotope composition of the outlet gas by mass spectrometry. The initial isotope composition of the gas can be close to the random distribution of molar fractions $^{16}O_2 : {}^{16}O^{18}O : {}^{18}O_2 \approx 1 : 2 : 1$ (so-called equilibrium mixture) or can deviate from it considerably (nonequilibrium mixture). The temperature dependences of the molar fractions of isotopic oxygen molecules and the atomic fraction of ^{18}O in the outlet gas calculated from these dependences are analytical data. The mathematical description of these dependences makes it possible to determine the mechanism and to estimate the kinetic parameters of oxygen exchange.[67,68,160]

6.1. Influence of the SnO_2 microstructure on the oxygen exchange. The temperature dependences of the molar fractions of isotope oxygen molecules $^{16}O_2$ (f_{32}), $^{16}O^{18}O$ (f_{34}), and $^{18}O_2$ (f_{36}) in the gas passed through the reactor with the nanocrystalline samples of SnO_2 with various microstructure parameters[67] are presented in Fig. 30. The deviation of $f_i(T)$ from the initial values indicates the onset of oxygen exchange between O_2 of the gas phase and oxide. For highly dispersed SnO_2 (particle size 3—6 nm), this occurs at $T \approx 430$ °C, whereas for a coarsely crystalline material (particle size 35—50 nm) the onset of oxygen exchange is observed at $T \approx 520$ °C, indicating a lower activity of the latter. The temperature dependences of the molar fraction of $^{16}O^{18}O$ $f_{34}(T)$ and atomic fraction of ^{18}O $f_{18}(T)$ in the outlet gas flow are presented in Fig. 31. A decrease in the atomic fraction of ^{18}O after the exchange onset indicates that the major process is the heteroexchange involving the oxygen atoms of the oxide. The simulation of the curves $f_{18}(T)$ and $f_{34}(T)$ (see Fig. 31) showed that the so-called simple heteroexchange of a gas molecule with one oxygen atom of the crystal structure of oxide[67] was the rate-determining process in the case of unmodified SnO_2 (Scheme 2).

The total amount of oxygen capable of exchanging with the gas phase, which was estimated by the integration of the $f_{18}(T)$ curves, increases from 4 to 100 at.% with a decrease in the average particle size of SnO_2 from 35—50 to 3—6 nm.[67,68] The kinetic parameters determined in the framework of the model of simple heteroexchange are presented in Table 7. In the case of coarsely crystalline samples of SnO_2, the intensity of the exchange is low and, therefore, its kinetic parameters were not determined.

Scheme 2

$$^{18}O_2\ (g) + {}^{16}O\ (s) \rightleftharpoons {}^{16}O^{18}O\ (g) + {}^{18}O\ (s)$$

$$^{16}O^{18}O\ (g) + {}^{16}O\ (s) \rightleftharpoons {}^{16}O_2\ (g) + {}^{18}O\ (s)$$

The total amount of oxygen capable of exchanging with the gas phase in highly dispersed SnO_2 was estimated as $(7\pm0.6) \cdot 10^{21}$ atom g^{-1}, which is consistent (within the error) with the stoichiometric content of oxygen in SnO_2 ($8.0 \cdot 10^{21}$ atom g^{-1}). Thus, almost the whole oxygen in the composition of highly dispersed SnO_2 can be substituted by the O atoms in the gas phase. Note that tin dioxide even in the nanodispersed state is usually considered as a material with the rigid cation-anionic framework and an insignificant mobility of the oxygen sublattice is implied when describing the formation of oxygen vacancies.[15] The low-temperature peak (see Fig. 31, *a*, dashed line) corresponding to the state of oxygen with a high activity in the heteroexchange can be distinguished in the $f_{18}(T)$ dependence of highly dispersed SnO_2. The oxygen amount is $(1.6\pm0.4) \cdot 10^{21}$ atom g^{-1}, which coincides with the estimated concentration of structural oxygen on the SnO_2 surface ($95\ m^2\ g^{-1} \times 1.4 \cdot 10^{19}$ atom $m^{-2} \approx 1.4 \cdot 10^{21}$ atom g^{-1}). Therefore, oxygen on the material surface undergoes complete substitution at the exchange onset, whereas at high temperatures the main process is

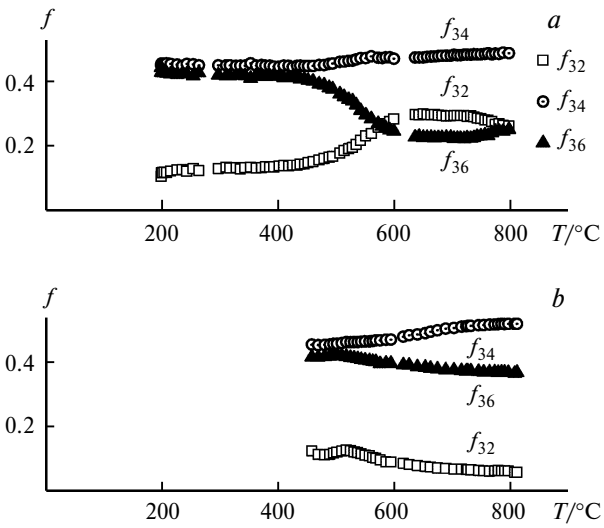

Fig. 30. Temperature dependences of the molar fraction of molecules $^{16}O_2$ (f_{32}), $^{18}O^{16}O$ (f_{34}), and $^{18}O_2$ (f_{36}) in gas after the interaction with tin dioxide samples with different microstructure parameters: (*a*) d = 3—6 nm, S_{BET} = 100—110 $m^2\ g^{-1}$ and (*b*) d = 26—35 nm, S_{BET} = 1—5 $m^2\ g^{-1}$.[67]

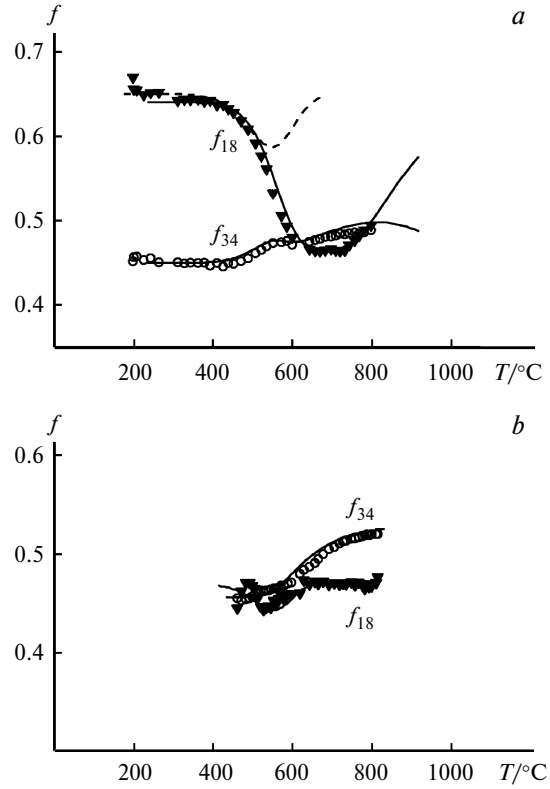

Fig. 31. Experimental (points) and calculated (lines) temperature dependences of the atomic fraction of ^{18}O (f_{18}) and molar fraction of $^{18}O^{16}O$ (f_{34}) in gas after the interaction with tin dioxide with the particle size $d(SnO_2)$ = 3—6 (*a*) and 26—35 nm (*b*). Dashed line corresponds to the exchange of surface oxygen.[67]

the substitution of anions in the crystallite bulk. The fraction of surface atoms in the total amount of oxygen capable of exchanging is $1.6 \cdot 10^{21}/(8.0 \cdot 10^{21}) = 0.2$.

6.2. Influence of catalytic modifiers on the oxygen exchange on SnO_2. The study of the influence of additives PdO_x and RuO_y deposited on the surface of highly dispersed SnO_2 showed that the catalytic clusters intensified the oxygen exchange of the oxide matrix with the gas phase, and the ruthenium additives exerted a stronger effect.[68] This appears primarily as a decrease in the temperature of exchange onset to 310 °C for SnO_2/PdO_x and to 200 °C for SnO_2/RuO_y compared to unmodified SnO_2 (430 °C). The decrease in the atomic fraction of ^{18}O after the beginning of the exchange (Fig. 32) indicates heteroexchange occurring on the surface of the modified samples as in the case of SnO_2.

The influence of modifies also reflects the exchange of surface oxygen. The corresponding peak on the $f_{18}(T)$ dependences appears as a low-temperature shoulder in the case of SnO_2/PdO_x and is distinctly resolved for SnO_2/RuO_y (see Fig. 32). This fact, as well as the shifts of the peaks toward low temperatures, indicates that the mobility of surface oxygen increases in the series $SnO_2 < SnO_2/PdO_x < SnO_2/RuO_y$. Note that the concentration of oxidative sites on the sample surface increases in the same sequence (see Table 4).

The modeling of the oxygen exchange on the basis of the experimental dependences $f_{18}(T)$ and $f_{34}(T)$ (see Fig. 32) showed its double mechanism being a combination of the simple (as on unmodified SnO_2) and complicated heteroexchange in which the gas molecule exchange with two oxygen atoms of the oxide[61] (Scheme 3).

Scheme 3

$$^{18}O_2\ (g) + 2\ ^{16}O\ (s) \rightleftharpoons {}^{16}O_2\ (g) + 2\ ^{18}O\ (s)$$

$$^{18}O_2\ (g) + 2\ ^{16}O\ (s) \rightleftharpoons {}^{16}O^{18}O\ (g) + {}^{16}O\ (s) + {}^{18}O\ (s)$$

$$^{16}O^{18}O\ (g) + 2\ ^{16}O\ (s) \rightleftharpoons {}^{16}O_2\ (g) + {}^{16}O\ (s) + {}^{18}O\ (s)$$

The kinetic parameters of both mechanisms are compared in Table 7. The comparison of the data for the simple heteroexchange of various samples shows that for modified SnO_2 the exchange *via* this mechanism is caused by the free surface of the matrix and the action of supported clusters PdO_x and RuO_y appears only as a twofold increase in the rate of the simple heteroexchange. On the

Table 7. Main parameters of oxygen exchange for the materials of pure and modified tin dioxide[67,68]

Compound	T_0[a]	Rate of heteroexchange (300 °C)		D[b]/m^2 s^{-1}	E_a[c]/kJ mol^{-1}			f[d]
		simple	complex		I	II	III	
SnO_2-1000	520	—	—	—	—	—	—	4
SnO_2-300	430	$1.3 \cdot 10^{12}$	—	$6.1 \cdot 10^{-24}$	130	—	80	60
SnO_2-300/PdO_x	310	$2.6 \cdot 10^{12}$	$5.7 \cdot 10^{14}$	$1.9 \cdot 10^{-22}$	130	110	80	54
SnO_2-300/RuO_y	200	$2.6 \cdot 10^{12}$	$3.6 \cdot 10^{17}$	$3 \cdot 10^{-21}$	130	130	60	46

[a] Temperature of exchange onset.
[b] Diffusion coefficient (300 °C).
[c] Activation energy of simple (I) and complicated heteroexchange (II) and diffusion (III).
[d] Fraction of substituted oxygen of the total content of O.

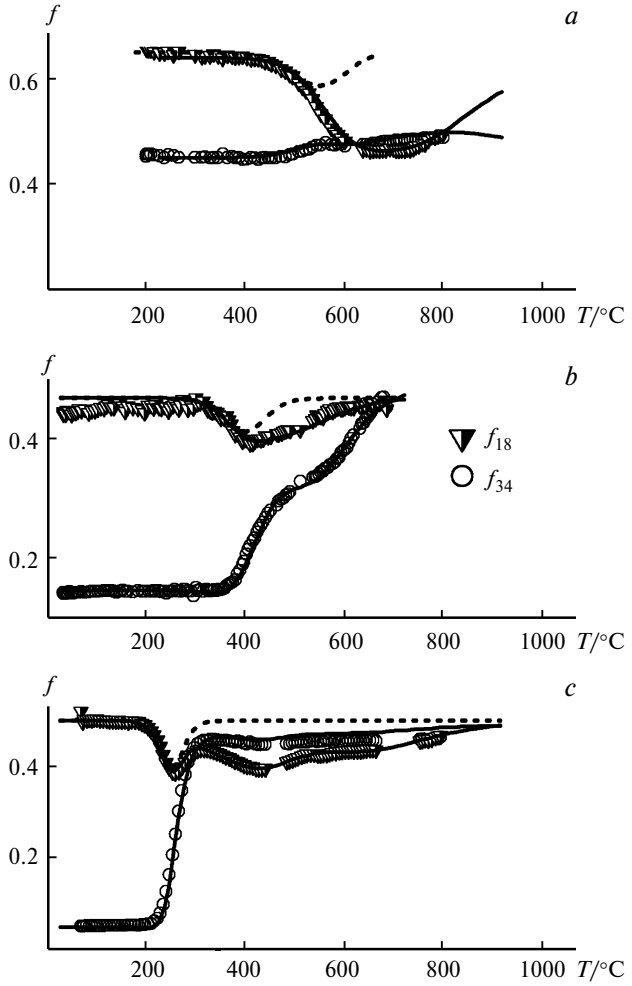

Fig. 32. Experimental (points) and calculated (lines) temperature dependences of the atomic fraction of ^{18}O (f_{18}) and molecular fraction of $^{18}O^{16}O$ (f_{34}) in gas after the interaction with nanocrystalline tin dioxide unmodified (*a*) and modified by palladium oxide (*b*) and ruthenium oxide (*c*). Dashed line corresponds to the exchange of surface oxygen.[68]

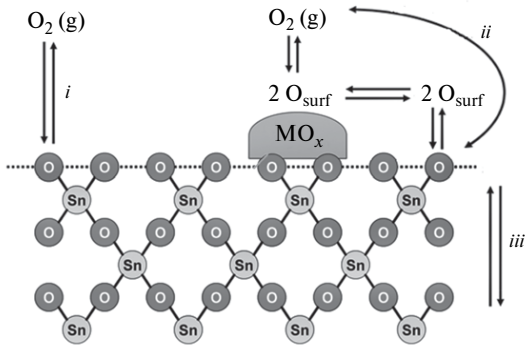

Fig. 33. Influence of catalytic modifiers, clusters of palladium or ruthenium oxides, on the mechanism of oxygen exchange of tin dioxide with the gas phase[68]; *i* and *ii* designate simple and complicated heteroexchange, respectively; *iii* is diffusion of O.

contrary, the complicated heteroexchange characterized by substantially higher rate and diffusion coefficient and lower activation energies of exchange and diffusion is completely caused by the presence of modifiers. Unlike the simple heteroexchange occurring *via* the Riedel—Eley mechanism, the mechanism of complicated heteroexchange includes the preliminary dissociation of molecular oxygen on the material surface followed by the substitution of lattice anions by adsorbed O atoms. The spillover effect often observed on the noble metal (Pt, Pd) clusters supported on the oxide support[160—162] is based on these processes. If assuming that the effect of PdO_x and RuO_y nanoparticles supported on the SnO_2 surface and taking into account its interpretation in terms of the temperature-programmed isotope exchange, then the heteroexchange *via* the spillover mechanism can be presented by Fig. 33. If the dissociation of O_2 is the rate-determining step because of the high energy of O—O bond (493 kJ mol^{-1} in the gas[18]), then, from the kinetic point of view, this complex of processes is equivalent to the mechanism of complicated heteroexchange (see Scheme 3). Thus, the influence of the supported PdO_x and RuO_y nanoparticles on the reaction of SnO_2 with gaseous O_2 is reduced to the formation of sites of dissociative adsorption and routes of the fast migration of atomic oxygen to the matrix surface.

Thus, the study of the isotope exchange showed that the modifiers of the nanocrystalline SnO_2 surface intensified the interaction of the material with oxygen *via* the spillover effect. Possibly, this is related to the influence of the PdO_x and RuO_y modifiers on the concentration of chemisorbed oxygen; moreover, both the activity in the oxygen exchange and the content of oxidation sites increase in the series $SnO_2 < SnO_2/PdO_x < SnO_2/RuO_y$. The spillover effect implies that the clusters of the modifiers form the dissociative adsorption sites of O_2 molecules and routes of migration of the formed O atoms to the support surface (see Fig. 33). As a result, not only the total content of chemisorbed oxygen species increases on the surface of the modified material, but also their reactivity is enhanced due to an increase in the fraction of the most reactive species (atomic forms), although the detection of them by any method of surface investigation failed. The higher the metal affinity to oxygen, the more intense the adsorption and dissociation of molecular oxygen on the modifier clusters. For example, the RuO_y clusters consisting mainly of RuO_2 favor an increase in the adsorbed oxygen concentration on the tin dioxide surface to a higher extent than PdO_x does (see Table 4). They also activate the oxygen exchange (the temperature of the exchange onset for SnO_2/RuO_y is 200 °C, while that for SnO_2/PdO_x is 310 °C). This correlates with a lower enthalpy of formation of RuO_2 ($\Delta_f H$ = = −(150—200) kJ mol^{-1}) compared to that of PdO ($\Delta_f H$ = −(50—100) kJ mol^{-1})[149] and a higher energy of the metal—oxygen bond.

7. Sensor properties toward gases CO, NH_3, and NO_2

At present, a change in the electrophysical properties of semiconductors depending on the gas phase composition are described in the framework of two different models: ionosorption and changing the amount of oxygen vacancies. The ionosorption model takes into account only the effects related to the electric potential of the surface and regions of special charge formed due to the chemisorption of molecules from the gas phase. The model of oxygen vacancies describes the sensor properties of semiconductor metal oxides on the basis of concepts about a change in the deviation of their composition from stoichiometry.

It is assumed in terms of the ionosorption model that the sensor signal is formed due to a change in the density of the localized surface charge of the semiconductor in the course of the following processes[15]:

(a) chemisorption of air oxygen

$$\beta/2\ O_2\ (g) + \alpha e^- \rightleftharpoons O_{\beta(ads)}{}^{-\alpha}, \qquad (15)$$

where $\beta = 1$ and 2 for the atomic and molecular species, respectively; $\alpha = 1$ and 2 for the singly and doubly charged ions, respectively; e^- is electron with a sufficient energy for surmounting the barrier formed by the negatively charged surface; and $O_{\beta(ads)}{}^{-\alpha}$ is the chemisorption oxygen species;

(b) reaction of gas-reducing agent R (for example, CO, NH_3) with chemisorbed oxygen

$$\beta\ R\ (g) + O_{\beta(ads)}{}^{-\alpha} \longrightarrow \beta\ RO\ (g) + \alpha e^-, \qquad (16)$$

where RO (g) is the oxidation product of gas-reducing agent R (CO_2, N_2);

(c) chemisorption of the gas-oxidant (for example, NO_2)

$$NO_2\ (g) + e^- \rightleftharpoons NO_{2(ads)}{}^-. \qquad (17)$$

Oxygen chemisorption from the gas phase on the surface of oxide semiconductors results in the formation of a double electrical layer and a surface acceptor level in semiconductors with conductivity of the n-type.[163] The volume charge formed in the near-surface layer due to the reaction induces the bending of conduction band (E_C), valence band (E_V), and donor (E_D) and acceptor (E_A) levels near the surface (Fig. 34).

The reaction with molecules of the gas-reducing agent (see Eq. (16)) results in a decrease in the concentration of chemisorbed oxygen, an increase in the concentration of the carriers, a decrease in the surface charge, and a de-

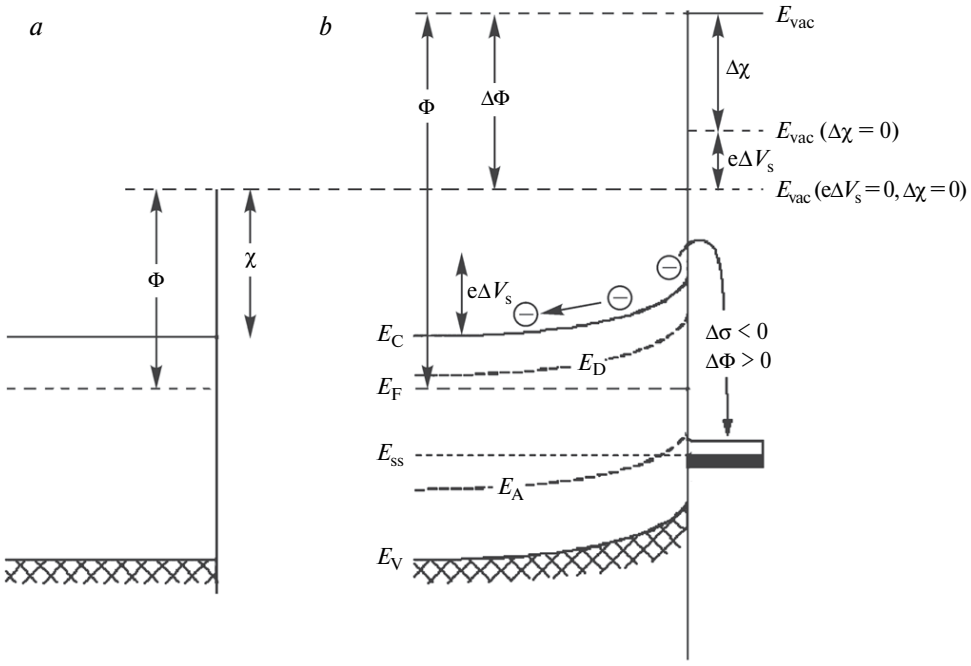

Fig. 34. Scheme of the band structure of an n-type semiconductor under the adsorption conditions: (*a*) band diagram of the semiconductor volume; (*b*) band diagram of the near-surface layer of the semiconductor under the adsorption conditions of gas (electron acceptor); Φ is the work function, χ is the electron affinity; E_{ss} and E_A are the levels of surface and acceptor states, respectively; eΔV_s is the change in the surface energy barrier during ionosorption of gas molecules, and Δσ is the change in the surface charge.[24]

crease in the extension of the depleted layer and intergranular barrier. All these processes are accompanied by an increase in the conductivity. For the chemisorption of the gas-oxidant (NO_2) with a higher electron affinity than that of oxygen, on the contrary, the depletion of semiconductor grains in charge carrier is enhanced, the surface barrier increases, and the conductivity decreases.

The model of oxygen vacancies[164] is applied for the description of the process of sensor signal formation in an inert atmosphere in the presence of gas-reducing agents, for example, CO,[32] CH_4,[76] and H_2 (see Ref. 45). It is assumed that the oxygen anions from the crystal structure of semiconductor oxide are directly involved in the oxidation of molecules of gas-reducing agents on the material surface, which can be expressed using the Kröger—Vink notation

$$O_O^{\times} + R \rightleftharpoons V_O^{\times} + RO \rightleftharpoons V_O^{\bullet} + e' + RO \rightleftharpoons \rightleftharpoons V_O^{\bullet\bullet} + 2\,e' + RO, \qquad (18)$$

where R is a molecule of the gas-reducing agent, and RO is the oxidation product of gas R. Experimental data confirming the reactivity of lattice O^{2-} anions are few.[165] For instance, the formation of Sn^{II} cations accompanying ionized oxygen vacancies was proved by Mössbauer spectroscopy for the interaction of nanocrystalline SnO_2 with CO (1 vol.%) in nitrogen at elevated temperature.[166] There are data that signals of carbonate groups, whose formation is independent of the oxygen concentration in the gas phase and is not accompanied by CO_2 evolution, appear in the IR spectra of tin dioxide interacting with CO at 300 °C. The formation of these carbonates can be due[56] to the interaction of CO with lattice oxygen on the SnO_2 surface

$$CO + O^{2-} \rightleftharpoons CO_3^{2-}. \qquad (19)$$

It seems reasonable to use investigation methods under the *in situ* conditions for studying mechanisms of interaction of the sensor materials with gases. Raman spectroscopy[167] and IR diffuse reflectance spectroscopy,[92,168] as well as chromatographic and mass spectrometric analyses of the formed gases,[169] provide information about the adsorption sites, routes of chemisorption of gas molecules, and their transformations on the surface. Additional data can be obtained from measurements of the electrophysical properties, for example, examination of the electron work function by the Kelvin method or by synchronous measurements of the electric conductivity and work function. According to the band model (see Fig. 34), the reversible chemisorption processes change the position of the Fermi level relative to the vacuum level, *i.e.*, work function of electron (Φ), and the charged surface states (ionosorbates) are responsible for the change in height of the surface barrier (eV_s), which determines the response of electric resistance, and the uncharged surface states (chemisorbates) are responsible for the change in the electron affinity (χ)[62]

$$\Delta\Phi = -e\Delta V_s + \Delta\chi = kT\ln(R_{air}/R_{gas}) + \Delta\chi, \qquad (20)$$

where Δ is the change in the corresponding parameter due to the interaction with the gas, and R_{air} and R_{gas} are the resistances of the material in pure air and in the presence of the determined gas, respectively. Since $\Delta\chi$ is directly proportional to the concentration of formed dipolar chemisorbates, the combined measurements of the resistance and work function make it possible to estimate the intensity of both collective and local interactions of the semiconductor with the gases that simultaneously determine the electrical signal.[168] Impedance metry allows one to determine a change in both electron and ionic (proton) conductivity during the interaction with gases.[105]

7.1. Role of the nature of active sites. The oxidation of CO and NH_3 on the surface of unmodified tin(IV) and zinc oxides at different temperatures can be presented[106] by Scheme 4.

Scheme 4

$$2\,CO\,(g) + O^-_{2,surf} \longrightarrow CO^-_{3,surf} + CO\,(g)$$

$$\longrightarrow 2\,CO_2\,(g) + e^- \quad (150\ ^\circ C < T < 200\ ^\circ C)$$

$$CO\,(g) + O^-_{surf} \longrightarrow CO^-_{2,surf} \longrightarrow 2\,CO_2\,(g) + e^- \quad (T > 200\ ^\circ C)$$

$$\updownarrow +O^-_{surf}$$

$$CO^{2-}_{3,surf}$$

$$4\,(NH_3OH)_{surf} + 6\,O^-_{2,surf} \longrightarrow$$

$$\longrightarrow 2\,N_2\,(g) + 4\,OH_{surf} + 6\,H_2O_{surf} + 3\,e^- \quad (150\ ^\circ C < T < 200\ ^\circ C)$$

$$2\,(NH_3{-}Sn^{IV})_{surf} + 6\,O^-_{surf} \longrightarrow$$

$$\longrightarrow N_2\,(g) + 2\,(OH{-}Sn^{IV})_{surf} + 6\,e^- \quad (T > 200\ ^\circ C)$$

The formation of intermediate and final carbonate species on the SnO_2 surface was confirmed by IR spectroscopy.[56,75,92] It was taken into account in the scheme of the reaction with ammonia that at these temperatures NH_3 molecules are chemisorbed on the OH groups, which are predominant hydrate species at these temperatures, and on surface cations.[168] The fact that ammonia oxidation on the surface of unmodified oxides ceases at the

stage of N_2 formation is consistent with the concepts of other authors[125,126,142] and results of analysis of the reaction products of these oxides with ammonia.[146]

Modification of nanocrystalline SnO_2 by catalytic additives of PdO_x and RuO_y favors an increase in the sensor sensitivity and selectivity toward CO and NH_3, respectively.[105,146,150,170] The catalytic effect also appears as a shift of the maximum of the sensor signal to the range of lower temperatures (Fig. 35). The results of combined measurements of the electron work function and electric conductivity showed that the modifiers in these systems provided a specific increase in the reactivity of the surface towards gases CO and NH_3.[168] It was concluded on the basis of the data of IR diffuse reflectance spectroscopy that the active sites being catalytic clusters themselves are primarily responsible for this phenomenon.[168]

The positions of bands corresponding to the carbonyl group vibrations, which were observed only for the interaction of CO and SnO_2/PdO_x (Fig. 36), indicate that they are attributed to the CO molecules chemisorbed on

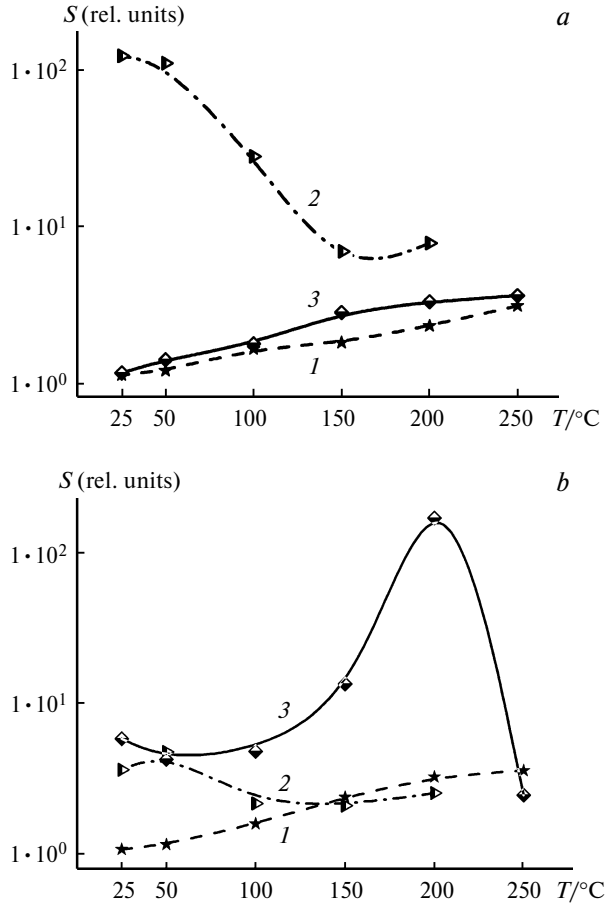

Fig. 35. Temperature dependences of the sensor signal (S) of the materials based on nanocrystalline SnO_2 toward CO (*a*) and NH_3 (*b*) (50 ppm): SnO_2 (*1*), SnO_2/PdO_x (*2*), and SnO_2/RuO_y (*3*).[151]

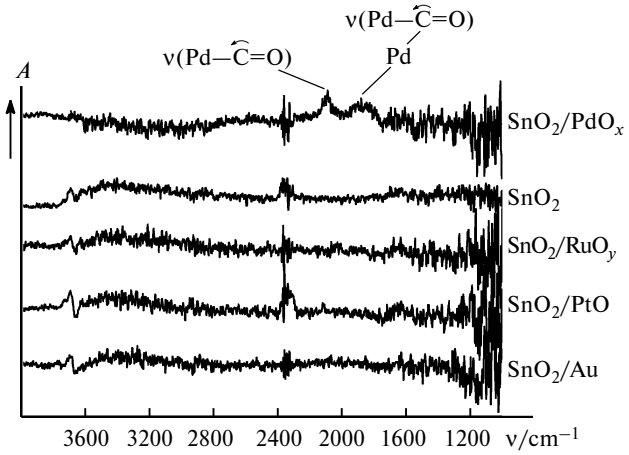

Fig. 36. IR diffuse reflectance spectra of nanocrystalline tin dioxide modified by various catalytic additives under the conditions of *in situ* interaction with CO (100 ppm) at room temperature[168]; A is absorbance.

the Pd atoms in the linear (2090 cm^{-1}) and bridging (1910—1840 cm^{-1}) configurations. The shift toward lower wave numbers relative to the gas-phase (2143 cm^{-1}) or physically adsorbed molecules (2138 cm^{-1}) is caused by the π-dative interaction with palladium that weakens the C—O bond.[42] No spectral changes occur in the presence of CO at elevated temperature (200 °C). Thus, the specific chemisorption of CO on the PdO_x clusters takes place only at $T < 150$ °C. The formation of adsorbed sites necessary for this process can be induced by the partial reduction of the PdO_x clusters, which was confirmed by the XPS data about an increase in the $Pd^0 : Pd^{II}$ ratio in the presence of CO.[105] In addition, as shown by the results of studies by IR spectroscopy and impedance metry,[105,168] the sensitivity of SnO_2/PdO_x to CO at low temperatures is caused by the participation of surface OH groups in the oxidation of chemisorbed molecules.

Thus, the role of PdO_x clusters in the specific interaction of SnO_2/PdO_x with CO at $T < 150$ °C can be reduced to the following points[105,168]:

— gas molecules are oxidized directly on the surface of the PdO_x clusters, due to which the modifier is partially reduced and the fraction zero-valent Pd increases

$$PdO_x + CO \rightleftharpoons Pd + (1 + x)/2\ CO_2; \qquad (21)$$

— strong chemisorption of CO molecules occurs on Pd^0, which is the essence of the catalytic action since is accompanied by intramolecular bond weakening and thus facilitates its cleavage and subsequent transformations of chemisorbed molecules

$$Pd^0 + CO \rightleftharpoons Pd^{\delta+}—CO^{\delta-}; \qquad (22)$$

— the action of clusters PdO_x on the SnO_2 surface increases the concentration of active hydroxyl species

(paramagnetic centers $^{\bullet}OH$, associates of hydrogen-bound OH...OH groups) (see Tables 5 and 6) involved in the palladium-catalyzed oxidation of chemisorbed gas molecules

$$CO + OH \longrightarrow CO_2 + H^+ + e^-. \quad (23)$$

High sensitivity and selectivity of the sensor response of the SnO_2/RuO_y nanocomposites toward NH_3 at elevated temperature (150—200 °C) are consistent with the selective increase in the reactivity of the material surface under these conditions.[146,168] At room temperature ammonia is adsorbed on the surface OH groups and Sn^{IV} cations, which is indicated by the appearance of the corresponding peaks of bending vibrations of the NH_3—OH and NH_3—Sn^{IV} chemisorbates in the IR diffuse reflectance spectra (Fig. 37, *a*). On heating to $T = 200$ °C, on adsorption occurs only on the cationic (Lewis) sites (Fig. 37, *b*), since the Brønsted acid sites of the OH group are weak and, according to the TPD data, do not retain

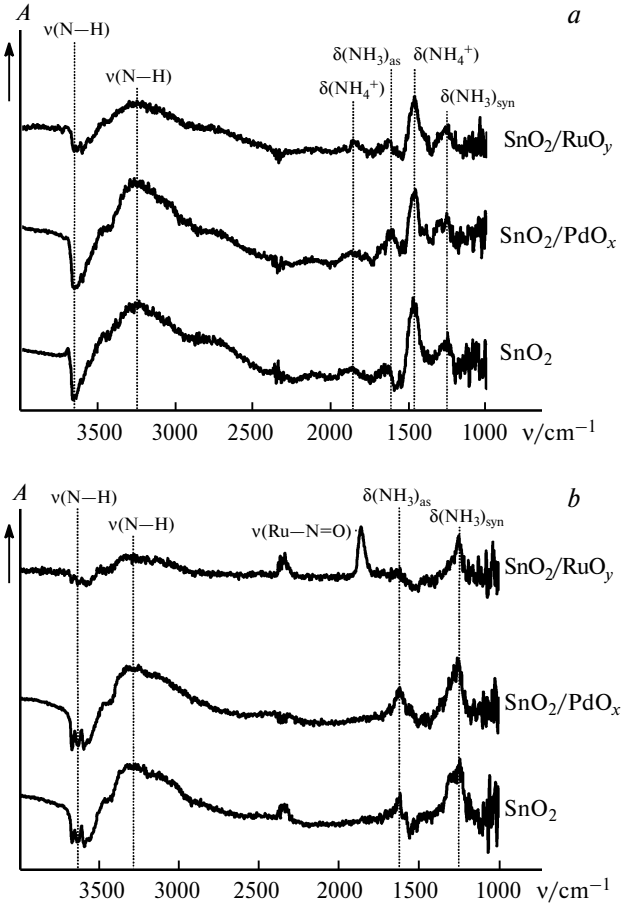

Fig. 37. IR diffuse reflectance spectra of the nanocrystalline materials SnO_2, SnO_2/PdO_x, and SnO_2/RuO_y under the conditions of *in situ* interaction with NH_3 (100 ppm) at room temperature (*a*) and at $T = 200$ °C (*b*).[168]

NH_3 molecules at this temperature. The appearance of the peak of stretching vibrations of the nitrosyl group linked to the ruthenium cation (1870 cm^{-1}) is the indication to the specific catalytic effect of RuO_y clusters in the course of ammonia oxidation (see Scheme 1). The corresponding absorption peak was assigned due to the study of the IR spectra of the SnO_2/RuO_y nanocomposites under NO adsorption conditions.[168] The presence of nitrogen dioxide NO_2 as the product of NH_3 oxidation on the SnO_2/RuO_y surface was also established by an analysis of the gas mixture formed upon this interaction.[146] In addition, clusters RuO_y on the surface of tin dioxide promote active sites of catalytic oxidation of ammonia, namely, chemisorbed oxygen, which is manifested as an increase in the concentration of chemisorbed oxygen on the SnO_2/RuO_y surface (see Table 4) and acceleration of the oxygen exchange of the support with the gas phase (see Table 7). Since the mechanism of interaction with O_2 includes the dissociative adsorption and spillover effect (see Fig. 33), and the temperature of oxygen exchange onset (200 °C) corresponds to the conditions of catalytic oxidation of NH_3, it can be assumed that the process considered involves active atomic species of chemisorbed oxygen.

7.2. Influence of the concentration of active sites. A comparison of the concentration of active sites and values of sensor signals of pure and chemically modified semiconductor oxides makes it possible to reveal the nature of active sites involved in the solid phase—gas interaction and to establish relationships composition—structural parameters—sensor properties of materials.[106]

The obtained experimental results indicate that the processes of chemisorption and redox interaction with the surface are prevailing in the formation of the sensor signal of semiconductor oxides SnO_2 and ZnO, depending on the nature and properties of molecules of the analyzed gas-oxidants or gas-reducing agents. The change in the sensor response of nanocrystalline zinc oxide toward NO_2 with a change in the amount of the doping impurity of gallium correlates with the concentration of paramagnetic donor centers[104] (Fig. 38). This fact confirms that the sensitivity to NO_2 is determined by chemisorption with capture of electrons (see Eq. (17)) provided by ionized oxygen vacancies. The plots of the change in the sensor sensitivity of doped zinc oxide toward H_2S and CO with an increase in the content of gallium and indium is monotonic (Fig. 39). This indicates that in the case considered the process of response formation is determined by the acid-base properties of the surface rather than electronic factors. The introduction of M^{III} additives into nanocrystalline zinc oxide results in a monotonic increase in the acidity of the surface (see Table 3), which also causes an enhanced content of hydroxyl groups. The intensity of the bands of O—H stretching vibrations in the IR absorption spectra, which was normalized to the inten-

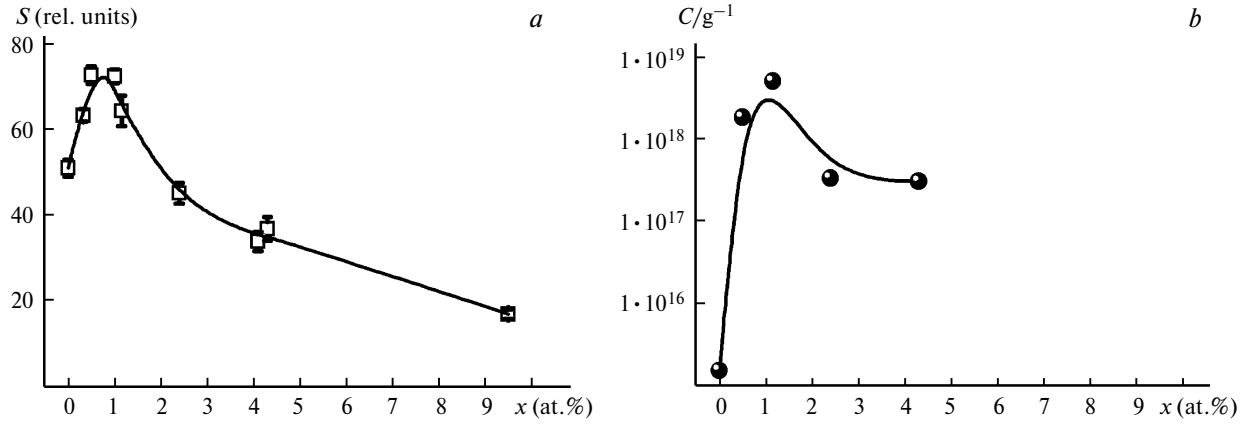

Fig. 38. Dependences on the gallium content x = [Ga]/[Ga+Zn] of the sensor signal (S) for the nanocrystalline materials ZnO(Ga) toward NO_2 (2 ppm) at 250 °C (*a*) and concentration (C) of paramagnetic donor centers in them (*b*).[104]

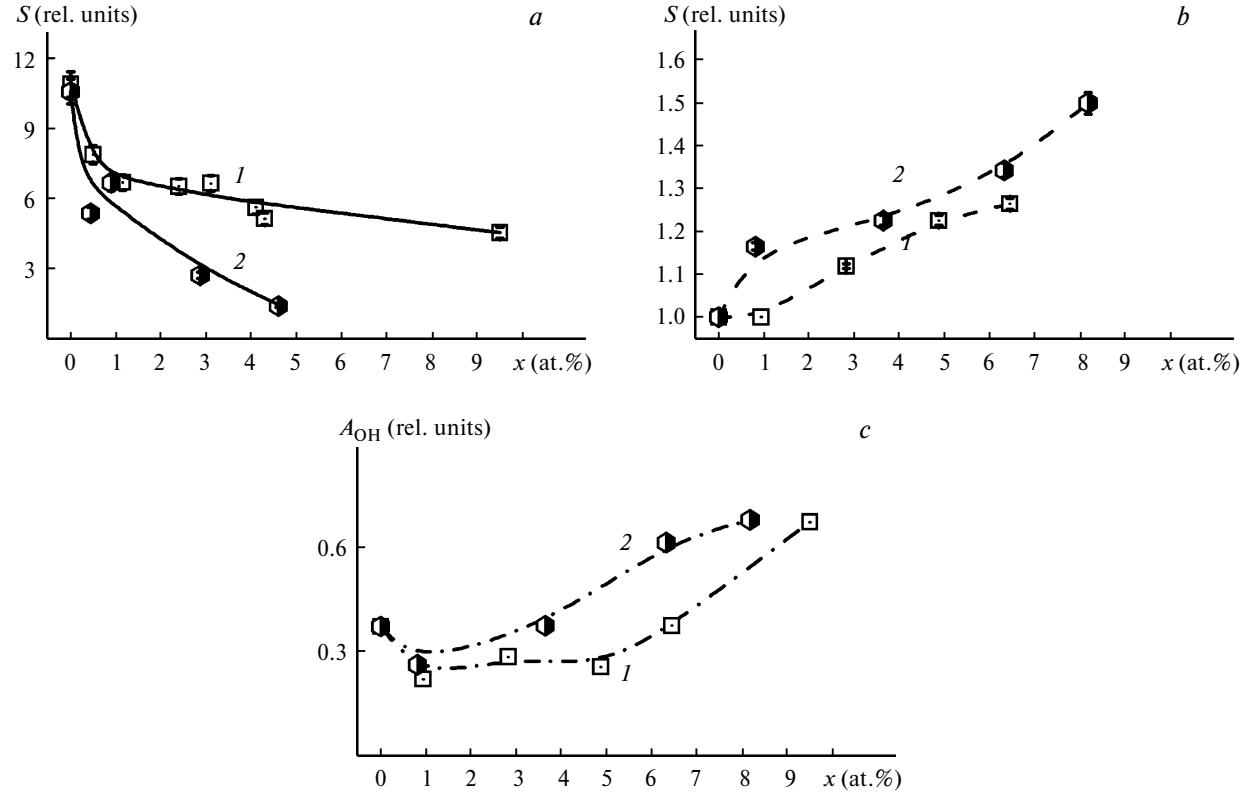

Fig. 39. Dependences on the concentration of dopants x = [M]/[M+Zn] of the sensor signals (S) for the nanocrystalline materials ZnO(Ga) (*1*) and ZnO(In) (*2*) toward H_2S (2 ppm) at 250 °C (*a*) and toward CO (5 ppm) at 150 °C (*b*) and of the normalized intensities (A_{OH}) of the IR absorption band of OH groups at ν = 3400 cm^{-1} (*c*).[106]

sity of the band of Zn—O lattice vibrations, was accepted as a measure of the amount of OH groups in Fig. 39. An increase in the sensor signal toward CO with an increase in the dopant content (see Fig. 39) is related, most likely, to the participation of OH groups in the oxidation of carbon monoxide on the ZnO(M) surface. At the same time, an increase in the acidity should prevent the chemisorption of acidic molecules H_2S, which can cause a decrease in the sensitivity to hydrogen sulfide with an increase in the dopant content.

For CO detection at room temperature, the sensitivity of tin dioxide modified by palladium oxide decreases upon the introduction of a doping impurity of Sb^V (Fig. 40). This can be related to a decrease in the content of surface

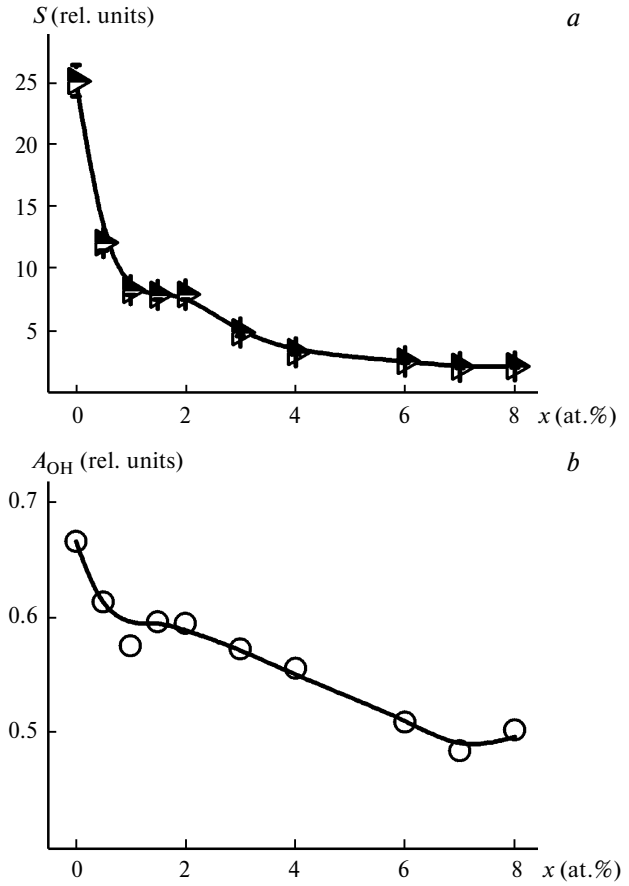

Fig. 40. Dependences on the antimony concentration x = = [Sb]/[Sb+Zn] of the sensor signal (S) for the nanocrystalline materials $SnO_2(Sb)/PdO_x$ toward CO (5 ppm) at room temperature (*a*) and normalized intensity of the IR absorption band of OH groups at $\nu = 3400$ cm^{-1} (*b*).[106]

OH groups under the effect of the dopant, since hydroxyl groups are among the sites responsible for the oxidation of CO (see Eq. (23)).

8. Conclusion

Gas sensitivity of nanocrystalline oxides is primarily determined by active sites on their surface. Semiconductor n-type oxides contain active sites diverse in adsorbability and reactivity: surface cations and anions, oxygen vacancies and other point defects, chemisorbed oxygen, and hydroxyl groups. This causes their nonselectivity toward various detected gases. Using tin(IV) and zinc oxides synthesized from salt solutions as examples, the influence of the synthesis conditions, microstructure parameters, and the content of doping impurities and modifiers of the surface on the properties and concentration of active sites was shown. The following types of active sites were detected on the oxide surface using a complex of investigation methods: Lewis acidic sites (surface cations), chemisorbed oxygen in the uncharged ($O_{2,chem}$) and ionized (O_2^-) forms, oxygen vacancies $V_O^{\bullet}$, chemisorbed water molecules, and hydroxyl groups, including Brønsted acidic sites and paramagnetic centers $^{\bullet}OH$. The total concentration of surface sites decreases with an increase in the particle size and a decrease in the specific surface of the oxides that occur during annealing at various temperature. Doping of oxides with donor additives in order to increase electric conductivity affects the concentration of donor defects and acid-base properties of the surface. The introduction of Ga^{III} or In^{III} into zinc oxide results in an increase in the concentration of donor paramagnetic centers (oxygen vacancies) at the content of dopants in the ZnO structure within solubility (1 at.%). Since donor sites are responsible for the chemisorption of molecules of gas-oxidants, this influence of dopants on their concentration is accompanied by the enhancement of the sensor sensitivity toward NO_2. When the content of dopants is higher than their solubility in zinc oxide, they are segregated on the matrix surface, which increases their acidity and concentration of hydroxyl groups on it. This can be related to an increase in the sensor sensitivity toward CO or its decrease toward the acidic H_2S molecules.

The most efficient method for enhancing selectivity of the sensor materials with gas-reducing agents is the formation on their surface of centers of the selective catalytic oxidation of detected molecules by the modification of the oxides with clusters of noble metals or their oxides. It was shown for nanocrystalline tin dioxide as an example that the high sensor sensitivity and selectivity toward CO and NH_3 are achieved by modification with palladium and ruthenium oxides, respectively. In the first case, the highest sensor signals were obtained at room temperature, which is great practical interest for the production of sensor to carbon monoxide operating without heating. At the optimum temperature of sensor sensitivity, on the one hand, the chemisorption of a sufficient amount of molecules of analyzed gases should be observed, and, on the other hand, the activation barrier of their oxidation on the sensitive material surface should be surmounted. In the SnO_2/PdO_x—CO system, this combination of factors is achieved at a temperature about room temperature due to specific chemisorption of CO molecules on Pd atoms accompanied by weakening of the C—O bond. The selective catalytic action of ruthenium oxide during NH_3 oxidation on the surface of SnO_2/RuO_y nanocomposites appears only at elevated temperatures (150—200 °C). An important factor determining conditions of interaction of modified materials with analyzed gases is the influence of catalytic clusters on intrinsic active sites of the semiconductor matrix. Modification by palladium and ruthenium oxides exerts different effects on the concentration and reactivity of active sites of nanocrystalline SnO_2. The

PdO_x clusters are shown to favor an increase in the concentration of hydroxyl groups, being some centers of CO oxidation at a temperature about room temperature. The ruthenium oxide clusters promote the interaction of the support matrix with oxygen, resulting in an increase in the concentration of chemisorbed forms of oxygen involved in the catalytic oxidation of ammonia on the modified material surface at elevated temperature.

This work was financially supported by the ERA. Net. Russ. Plus (Grant 096 FONSENS).

References

1. S. M. Repinskii, *Nano- i mikrosistemnaya tekhinika* [*Nano- and Microsystem Techniques*], 2001, **9**, 28 (in Russian).
2. S. Morrison, *The Chemical Physics of Surfaces*, Plenum Press, New York, 1977.
3. A. Davydov, *Molecular Spectroscopy of Oxide Catalyst Surfaces*, Wiley, Chichester, 2003, 643 pp.
4. N. Yamazoe, K. Shimanoe, *Sensors,* 2009, **21**, 1.
5. N. Yamazoe, *Sens. Actuators B*, 2005, **108,** 2.
6. S. M. Repinskii, *Nano- i mikrosistemnaya tekhinika* [*Nano- and Microsystem Techniques*], 2001, **10**, 7 (in Russian).
7. S. Nardis, D. Monti, C. Di Natale, A. D´Amico, P. Siciliano, A. Forleo, M. Epifani, A. Taurino, R. Rella, R. Paolesse, *Sens. Actuators B*, 2004, **103**, 339.
8. L. Huo, S. Gao, J. Zhao, H. Wang, S. Xi, *J. Mater. Chem.*, 2002, **12**, 392.
9. C. Di Natale, R. Paolesse, A. D´Amico, *Sens. Actuators B*, 2007, **121**, 238.
10. A. C. Lindhorst, S. Haslinger, F. E. Kuehn, *Chem. Commun.*, 2015, **51**, 17193.
11. E. T. Saka, Z. Biyiklioglu, *J. Organomet. Chem.*, 2013, **745—746**, 50.
12. R. A. Collins, K. A. Mohammed, *J. Phys. D: Appl. Phys.*, 1988, **21**, 154.
13. X. Li, Y. Jiang, G. Xie, H. Tai, P. Sun, B. Zhang, *Sens. Actuators B*, 2013, **176**, 1191.
14. C. O. Park, S. A. Akbar, *J. Mater. Sci.*, 2003, **38**, 4611.
15. M. Batzill, U. Diebold, *Prog. Surf. Sci.*, 2005, **79**, 47.
16. J. P. Cheng, J. Wang, Q. Q. Li, H. G. Liu, Y. Li, *J. Ind. Eng. Chem.*, 2016, **44**, 1.
17. A. Gurlo, N. Barsan, U. Weimar, in *Metal Oxides*, Ed. J. L. G. Fierro, CRC Press, Boca Raton, 2006, p. 683.
18. G. C. Bond, C. Louis, D. T. Thompson, *Catalysis By Gold*, Imperial College Press, London, 2006, 367 pp.
19. M. N. Rumyantseva, A. M. Gaskov, *Russ. Chem. Bull.*, 2008, **57**, 1106.
20. A. Marikutsa, M. Rumyantseva, A. Baranchikov, A. Gaskov, *Materials*, 2015, **8**, 6437.
21. S. S. Nalimova, Ph. D. (Chem.) Thesis, St. Petersburg State Electrotechn. Univ. "LETI" im. V. I. Ul´yanova (Lenina), 2013, 160 pp. (in Russian).
22. R. W. J. Scott, M. Mamak, K. Kwong, N. Coombs, G. A. Ozin, *J. Mater. Chem.*, 2003, **13**, 1406.
23. H. Teterycz, R. Klimiuewicz, M. Laniecki, B. W. Licznerski, *Proc. Int. Conf. "26th Intern. Spring Seminar on Electrnoics Technology" (Stara Lesna, Slovak Republic, May 8—11, 2003)*, Stara Lesna, 2003, p. 384.
24. N. Barsan, U. Weimar, *Electroceram.*, 2001, **7**, 143.
25. V. Rodrнguez-Gonzalez, R. Gomez, M. Moscosa-Santillan, J. Amouroux, *J. Sol-Gel Sci. Techn.*, 2007, **42**, 165.
26. N. B. Shali, S. Sugunan, *Mater. Res. Bull.*, 2007, **42**, 1777.
27. A. S. Khder, E. A. El-Sharkawy, S. A. El-Hakam, A. I. Ahmed, *Catal. Commun.*, 2008, **9**, 769.
28. A. C. B. dos Santos, W. B. Kover, A. C. Faro, Jr., *Appl. Catal. A*, 1997, **153**, 83.
29. S. S. Nalimova, S. V. Myakin, V. A. Moshnikov, *Glass Phys. Chem.*, 2016, **42**, 597.
30. G. K. Boreskov, *Kataliz: Voprosy teorii i praktiki: izbrannye trudy* [*Catalysis: Problems of Theory and Practice: Selected Works*], Nauka, Novosibirsk, 1987, 536 pp. (in Russian).
31. G. Gaggiotti, A. Galdikas, S. Kacilius, G. Mattogno, A. Setkus, *J. Appl. Phys.*, 1994, **76**, 4467.
32. M. I. Ivanovskaya, G. A. Branitskii, D. R. Orlik, S. I. Mal´chenko, A. I. Vrublevskii, *Zh. Neorg. Khim.*, 1992, **37**, 1147 [*Russ. J. Inorg. Chem.* (*Engl. Transl.*), 1992, **37**].
33. M. N. Rumyantseva, E. A. Makeeva, S. M. Badalyan, A. A. Zhukova, A. M. Gaskov, *Thin Solid Films*, 2009, **518**, 1283.
34. H. Noei, H. Qiu, Y. Wang, E. Loeffler, C. Woell, M. Muhler, *Phys. Chem. Chem. Phys.*, 2008, **10**, 7092.
35. Y. Wang, K. Jacobi, W.-D. Scholne, G. Ertl, *J. Phys. Chem. B*, 2005, **109**, 7883.
36. M. W. Abee, D. F. Cox, *Surf. Sci.*, 2002, **520**, 65.
37. J. F. McAleer, P. T. Moseley, J. O. W. Norris, D. E. Williams, *J. Chem. Soc., Faraday Trans.*, 1987, **83**, 1323.
38. Y. Zhang, A. Kolmakov, Y. Lilach, M. Moskovits, *J. Phys. Chem. B*, 2005, **109**, 1923.
39. T. Sahm, A. Gurlo, N. Barsan, U. Weimar, *Sens. Actuators B*, 2006, **118**, 78.
40. A. Gurlo, *Chem. Phys. Chem.*, 2006, **7**, 2041.
41. J. D. Prades, A. Cirera, J. R. Morante, J. M. Pruneda, P. Ordejon, *Sens. Actuators B*, 2007, **126**, 62.
42. K. I. Hadjiivanov, G. N. Vayssilov, *Adv. Catal.*, 2002, **47**, 307.
43. M. Egashira, M. Nakashima, S. Kawasumi, T. Seiyama, *J. Phys. Chem.*, 1981, **85**, 4125.
44. V. V. Kovalenko, A. A. Zhukova, M. N. Rumyantseva, A. M. Gaskov, V. V. Yushchenko, I. I. Ivanova, T. Pagnier, *Sens. Actuators B*, 2007, **126**, 52.
45. Y. Yamaguchi, K. Tabata, E. Suzuki, *Surf. Sci.*, 2003, **526**, 149.
46. S. Jina, K. Kwon, C. Park, H. Chang, *Catal. Today*, 2011, **164**, 176.
47. G. Neri, A. Bonavita, G. Micali, G. Rizzo, N. Pinna, M. Niederberger, J. Ba, *Sens. Actuators B*, 2008, **130**, 222.
48. D. E. Williams, K. F. E. Pratt, *J. Chem. Soc., Faraday Trans.*, 1998, **94**, 3493.
49. C. Woell, *Progress in Surface Science*, 2007, **82**, 55.
50. Y. Wang, B. Meyer, X. Yin, M. Kunat, D. Langenberg, F. Traeger, A. Birkner, C. Woell, *Phys. Rev. Lett.*, 2005, **95**, 266104.
51. B. Meyer, D. Dominik Marx, O. Dulub, U. Diebold, M. Kunat, D. Langenberg, C. Woell, *Angew. Chem., Int. Ed.*, 2004, **43**, 6642.
52. K. Tanabe, *Solid Acids and Bases: Their Catalytic Properties*, Kodansha Ltd., Tokyo, 1970, 175 pp.

53. S. Sugunan, B. Varghese, *React. Kinet. Catal. Lett.*, 1997, **62**, 157.
54. R. G. Pavelko, H. Daly, C. Hardacre, A. A. Vasiliev, E. Llobet, *Phys. Chem. Chem. Phys.*, 2010, **12**, 2639.
55. M. Huebner, R. G. Pavelko, N. Barsan, U. Weimar, *Sens. Actuators B*, 2011, **154**, 264.
56. M. I. Baraton, in *Proc. of the NATO Advanced Study Institute on Sensors for Environment, Health and Security: Advanced Materials and Technologies*, Vichy, France, 2007, p. 31.
57. M. Habgood, N. Harrison, *Surf. Sci.*, 2008, **602**, 1072.
58. N. Yamazoe, J. Fuchigami, M. Kishikawa, T. Seiyama, *Surf. Sci.*, 1979, **86**, 335.
59. K. Tabata, T. Kawabe, Y. Yamaguchi, Y. Nagasawa, *Catal. Surv. Asia*, 2003, **7**, 251.
60. G. L. Shen, R. Casanova, G. Thornton, *Vacuum*, 1992, **43**, 1129.
61. N. A. Vorobyeva, A. V. Marikutsa, M. N. Rumyantseva, V. F. Kozlovskii, D. G. Filatova, A. M. Gaskov, *Inorg. Mater.*, 2016, **52**, 578.
62. A. Oprea, N. Barsan, U. Weimar, *Sens. Actuators B*, 2009, **142**, 470.
63. Z. Zhu, R. C. Deka, A. Chutia, R. Sahnoun, H. Tsuboi, M. Koyama, N. Hatakeyama, A. Endou, H. Takaba, C. A. Del Carpio, M. Kubo, *J. Phys. Chem. Solids*, 2009, **70**, 1248.
64. H. Chon, J. Pajares, *J. Catal.*, 1969, **14**, 257.
65. W. Hirschwald, P. Bonasewicz, L. Ernst, M. Grade, D. Hofmann, S. Krebs, R. Littbarski, G. Neumann, M. Grunze, D. Kolb, H. J. Schulz, in *Current Topics in Materials Science*, Vol. **7**, Ed. E. Kaldis, North-Holland Publishing Company, Amsterdam, 1981, p. 143.
66. F. Morazzoni, R. Scotti, S. Volonte, *J. Chem. Soc.*, *Faraday Trans.*, 1990, **86**, 1587.
67. D. D. Frolov, Y. N. Kotovshchikov, I. V. Morozov, A. I. Boltalin, A. A. Fedorova, A. V. Marikutsa, M. N. Rumyantseva, A. M. Gaskov, E. M. Sadovskaya, A. M. Abakumov, J. *Solid State Chem.*, 2012, **186**, 1.
68. A. Marikutsa, M. Rumyantseva, D. Frolov, I. Morozov, A. Boltalin, A. Fedorova, I. Petukhov, L. Yashina, E. Konstantinova, E. Sadovskaya, A. Abakumov, Y. Zubavichus, A. Gaskov, *J. Phys. Chem. C*, 2013, **117**, 23858.
69. S. Harbeck, A. Szatvanyi, N. Barsan, U. Weimar, V. Hoffmann, *Thin Solid Films*, 2003, **436**, 76.
70. M. Batzil, U. Diebold, *Phys. Chem. Chem. Phys.*, 2007, **9**, 2307.
71. D. Koziej, N. Barsan, U. Weimar, J. Szuber, K. Shimanoe, N. Yamazoe, *Chem. Phys. Lett.*, 2005, **410**, 321.
72. N. Barsan, U. Weimar, *J. Phys.: Condens. Matter.*, 2003, **15**, 813.
73. A. Helwig, G. Muller, G. Sberveglieri, M. Eickhoff, *J. Sensors*, 2009, **2009**, 620720.
74. C. S. Rout, M. Hegde, A. Govindaraj, C. N. Rao, *Nanotechnology*, 2007, **18**, 205504.
75. D. Koziej, N. Barsan, K. Shimanoe, N. Yamazoe, J. Szuber, U. Weimar, *Sens. Actuators B*, 2006, **118**, 98.
76. W. Schmid, N. Barsan, U. Weimar, *Sens. Actuators B*, 2004, **103**, 362.
77. Y. Yan, M. M. Al-Jassim, *Phys. Rev. B*, 2005, **72**, 235406.
78. C. Canevali, N. Chiodini, F. Morazzoni, R. Scotti, *J. Mater. Chem.*, 2000, **10**, 773.
79. E. A. Konstantinova, I. S. Pentegov, A. V. Marikutsa, M. N. Rumyantseva, A. M. Gaskov, P. K. Kashkarov, *Phys. Stat. Sol. C*, 2011, **8**, 1957.
80. S.-C. Chang, *J. Vac. Sci. Technol.*, 1980, **17**, 366.
81. J. M. Smith, W. E. Vehse, *Phys. Lett. A*, 1970, **31**, 147.
82. L. A. Kappers, O. R. Gilliama, S. M. Evans, L. E. Halliburton, N. C. Giles, *Nucl. Instrum. Meth. B*, 2008, **266**, 2953.
83. B. Schallenberger, A. Hausmann, *Z. Phys. B*, 1976, **23**, 177.
84. D. Galland, A. Herve, *Solid State Commun.*, 1974, **14**, 953.
85. N. Lopez, J. D. Prades, F. Hernandez-Ramirez, J. R. Morante, S. Mathur, *Phys. Chem. Chem. Phys.*, 2010, **12**, 2401.
86. J. Maier, W. Gopel, *J. Solid State Chem.*, 1988, **72**, 293.
87. M. Epifani, J. D. Prades, E. Comini, E. Pellicer, M. Avella, P. Siciliano, G. Faglia, A. Cirera, R. Scotti, F. Morazzoni, J. R. Morante, *J. Phys. Chem. C*, 2008, **112**, 19540.
88. F. Hernandez-Ramirez, J. D. Prades, A. Tarancon, S. Barth, O. Casals, R. Jimenez-Diaz, E. Pellicer, J. Rodriguez, J. R. Morante, M. A. Juli, S. Mathur, A. Romano-Rodriguez, *Adv. Funct. Mater.*, 2008, **18**, 2990.
89. G. Heiland, D. Kohl, in *Chemical Sensor Technology*, Ed. T. Seiyama, Kodansha, Tokyo, 1988, p. 15.
90. E. A. Konstantinova, A. V. Marikutsa, M. N. Rumyantseva, D. M. Deigen, S. V. Zabotnov, M. N. Martyshov, A. S. Vorontsov, P. A. Forsh, P. K. Kashkarov, *Nauchnoe obozrenie* [*Scientific Review*], 2013, **9**, 297 (in Russian).
91. J. E. Wertz, J. R. Bolton, *Electron Spin Resonance*, McGraw Hill Book Company, New York, 1972, 378 pp.
92. D. Koziej, K. Thomas, N. Barsan, F. Thibault-Starzyk, U. Weimar, *Catal. Today*, 2007, **126**, 211.
93. K. Ellmer, in *Handbook of Transparent Conductors*, Eds D. S. Ginley, H. Hosono, D. C. Paine, Springer, New York, 2010, p. 193.
94. K. I. Hagemark, P. E. Toren, *J. Electrochem. Soc.*, 1975, **122**, 992.
95. E. Ziegler, A. Heinrich, H. Oppermann, G. Stoever, *Phys. Stat. Sol. (A)*, 1981, **66**, 635.
96. A. F. Kohan, D. Morgan, C. G. Van de Walle, *Phys. Rev. B*, 2000, **61**, 15019.
97. N. Vorobyeva, M. Rumyantseva, D. Filatova, E. Konstantinova, D. Grishina, A. Abakumov, S. Turner, A. Gaskov, *Sens. Actuators B*, 2013, **182**, 555.
98. F. Runge, W. Goepel, *Z. Phys. Chem. Neue Folge*, 1980, **123**, 173.
99. K. M. Sancier, *Surf. Sci.*, 1970, **21**, 1.
100. C. Drouilly, J.-M. Krafft, F. Averseng, H. Lauron-Pernot, D. Bazer-Bachi, C. Chizallet, V. Lecocq, G. Costentin, *Appl. Catal. A*, 2013, **453**, 121.
101. C. Drouilly, J.-M. Krafft, F. Averseng, S. Casale, D. Bazer-Bachi, C. Chizallet, V. Lecocq, H. Vezin, H. Lauron-Pernot, G. Costentin, *J. Phys. Chem. C*, 2012, **116**, 21297.
102. V. A. Nikitenko, *J. Appl. Spectrosc.*, 1992, **57**, 783.
103. D. M. Hofmann, A. Hofstaetter, F. Leiter, H. Zhou, F. Henecker, B. K. Meyer, S. B. Orlinskii, J. Schmidt, P. G. Baranov, *Phys. Rev. Lett.*, 2002, **88**, 045504.
104. F. Morazzoni, R. Scotti, P. Di Nola, C. Milani, D. Narducci, *J. Chem. Soc., Faraday Trans.*, 1992, **88**, 1691.

105. A. V. Marikutsa, M. N. Rumyantseva, L. V. Yashina, A. M. Gaskov, *J. Solid State Chem.*, 2010, **183**, 2389.
106. A. Marikutsa, M. Rumyantseva, A. Gaskov, *Proc. Eng.*, 2016, **168**, 1082.
107. K. Atherton, G. Newbold, J. A. Hockey, *Discuss. Faraday Soc.*, 1971, **52**, 33.
108. K. Ozawa, K. Edamoto, *Surf. Rev. Lett.*, 2002, **9**, 717.
109. A. V. Marikutsa, M. N. Rumyantseva, E. A. Konstantinova, T. B. Shatalova, A. M. Gaskov, *J. Phys. Chem. C*, 2014, **118**, 21541.
110. F. Boccuzzi, E. Borello, A. Chiorino, A. Zecchina, *Chem. Phys. Lett.*, 1979, **61**, 617.
111. J. Saussey, J.-C. Lavalley, C. Bovet, *J. Chem. Soc., Faraday Trans. 1*, 1982, **78**, 1457.
112. B. M. Keyes, L. M. Gedvilas, X. Li, T. J. Coutts, *J. Cryst. Growth*, 2005, **281**, 297.
113. F. Boccuzzi, E. Borello, A. Zecchina, A. Bossi, M. Camia, *J. Catal.*, 1978, **51**, 150.
114. T. J. Liu, Z. G. Jin, L. R. Feng, T. Wang, *Appl. Surf. Sci.*, 2008, **254**, 6547.
115. R. Noonuruk, N. Vittayakorn, W. Mekprasart, J. Sritharathikhun, W. Pecharapa, *J. Nanosci. Nanotechnol.*, 2015, **15**, 2564.
116. J. Liu, X. Liu, Z. Zhai, G. Jin, Q. Jiang, Y. Zhao, C. Luoa, L. Quan, *Sens. Actuators B*, 2015, **220**, 1354.
117. P. Yao, *Desalination*, 2011, **267**, 170.
118. R. D. Shannon, *Acta Crystallogr.*, 1976, **A32**, 751.
119. J. Rockenberger, U. zum Felde, M. Tischer, L. Troeger, M. Haase, H. Weller, *J. Chem. Phys.*, 2000, **112**, 4296.
120. N. A. Vorobyeva, M. N. Rumyantseva, P. A. Forsh, A. M. Gaskov, *Semiconductors*, 2013, **47**, 650.
121. N. A. Vorobyeva, M. N. Rumyantseva, R. B. Vasiliev, V. F. Kozlovskii, Yu. M. Soshnikova, D. G. Filatova, A. E. Baranchikov, V. K. Ivanov, A. M. Gaskov, *Russ. J. Inorg. Chem.*, 2014, **59**, 403.
122. E. Bordes-Richard, *Top. Catal.*, 2008, **50**, 82.
123. J. A. Duffy, M. D. Ingram, *J. Am. Chem. Soc.*, 1971, **93**, 6448.
124. A. Cabot, J. Arbiol, J. R. Morante, U. Weimar, N. Barsan, W. Gopel, *Sens. Actuators B*, 2000, **70**, 87.
125. V. Aroutiounian, *Int. J. Hydrogen Energy*, 2007, **32**, 1145.
126. N. S. Ramgir, Y. K. Hwang, S. H. Jhung, I. S. Mulla, J.-S. Chang, *Sens. Actuators B*, 2006, **114**, 275.
127. B. Bahrami, A. Khodadadi, M. Kazemeini, Y. Mortazavi, *Sens. Actuators B*, 2008, **133**, 352.
128. N. Yamazoe, Y. Kurokawa, T. Seiyama, *Sens. Actuators*, 1983, **4**, 283.
129. M. Haruta, *CATTECH*, 2002, **6**, 102.
130. A. K. Santra, D. W. Goodman, *J. Phys.: Condens. Matter*, 2002, **14**, 31.
131. V. I. Savchenko, G. K. Boreskov, A. V. Kalinkin, A. N. Salanov, *Kinet. Catal.*, 1983, **24**, 983.
132. H. Over, M. Muhler, *Prog. Surf. Sci.*, 2003, **72**, 3.
133. R. Rella, P. Siciliano, S. Capone, M. Epifani, L. Vasanelli, A. Licciulli, *Sens. Actuators B*, 1999, **58**, 283.
134. J. C. Belmonte, J. Manzano, J. Arbiol, A. Cirera, J. Puigcorbe, A. Vila, N. Sabate, I. Gracia, C. Cane, J. R. Morante, *Sens. Actuators B*, 2006, **114**, 881.
135. G. Korotcenkov, V. Brinzari, Y. Boris, M. Ivanov, J. Schwank, J. Morante, *Thin Solid Films*, 2003, **436**, 119.
136. R. Dolbec, M. A. El Khakania, *Appl. Phys. Lett.*, 2007, **90**, 173114.
137. P. Manjula, S. Arunkumar, S. V. Manorama, *Sens. Actuators B*, 2011, **152**, 168.
138. N. S. Ramgir, Y. K. Hwang, S. H. Jhung, H. K. Kim, J.-S. Hwang, I. S. Mulla, J.-S. Chang, *Appl. Surf. Sci.*, 2006, **252**, 4298.
139. A. K. Santra, D. W. Goodman, *Electrochim. Acta*, 2002, **47**, 3595.
140. S. F. Yina, B. Q. Xub, X. P. Zhouc, C. T. Au, *Appl. Catal. A*, 2004, **277**, 1.
141. B. Lorenzut, T. Montini, C. C. Pavel, M. Comotti, F. Vizza, C. Bianchini, P. Fornasiero, *CHEMCATCHEM*, 2010, **2**, 1096.
142. R. Schloegl, *Angew. Chem., Int. Ed.*, 2003, **42**, 2004.
143. G. Jones, T. Bligaard, F. Abild-Pedersen, J. K. Norskov, *J. Phys. Condens. Matter*, 2008, **20**, 064239.
144. V. V. Krivetskiy, A. Ponzoni, E. Comini, S. M. Badalyan, M. N. Rumyantseva, A. M. Gaskov, *Inorg. Mater.*, 2010, **46**, 1100.
145. M. S. Wagh, G. H. Jain, D. R. Patil, S. A. Patil, L. A. Patil, *Sens. Actuators B*, 2006, **115**, 128.
146. A. Marikutsa, V. Krivetskiy, L. Yashina, M. Rumyantseva, E. Konstantinova, A. Ponzoni, E. Comini, A. Abakumov, A. Gaskov, *Sens. Actuators B*, 2012, **175**, 186.
147. Y. Wang, K. Jacobi, W.-D. Scholne, G. Ertl, *J. Phys. Chem. B*, 2005, **109**, 7883.
148. A. Salomonsson, R. M. Petoral, K. Uvdal, C. Aulin, K. Per-Olov, L. Ojama, M. Strand, M. Sanati, A. Lloyd Spetz, *J. Nanoparticle Res.*, 2006, **8**, 899.
149. O. V. Safonova, G. Delabouglise, B. Chenevier, A. M. Gaskov, M. Labeau, *Mater. Sci. Eng. C*, 2002, **21**, 105.
150. S. J. Ashcroft, E. Schwarzmann, *J. Chem. Soc., Faraday Trans.*, 1972, **68**, 1360.
151. A. V. Marikutsa, M. N. Rumyantseva, A. M. Gaskov, E. A. Konstantinova, D. A. Grishina, D. M. Deygen, *Thin Solid Films*, 2011, **520**, 904.
152. S. Wang, Y. Zhao, J. Huang, Y. Wang, H. Ren, S. Wu, S. Zhang, W. Huang, *Appl. Surf. Sci.*, 2007, **253**, 3057.
153. G. Neri, A. Bonavita, C. Milone, S. Galvagno, *Sens. Actuators B*, 2003, **93**, 402.
154. J. T. Miller, A. J. Kropf, Y. Zhac, J. R. Regalbutoc, L. Delannoy, C. Louis, E. Bus, J. A. van Bokhoven, *J. Catal.*, 2006, **240**, 222.
155. D. Koziej, M. Hubner, N. Barsan, U. Weimar, M. Sikorazc, J.-D. Grunwaldt, *Phys. Chem. Chem. Phys.*, 2009, **11**, 8620.
156. K. D. Schierbaum, U. K. Kirner, J. F. Geiger, W. Gopel, *Sens. Actuators B*, 1991, **4**, 87.
157. M. Gaidi, J. L. Hazeman, I. Matko, B. Chenevier, M. N. Rumyantseva, A. M. Gaskov, M. Labeau, *J. Electrochem. Soc.*, 2000, **147**, 3131.
158. S. Matsushima, Y. Teraoka, N. Miura, N. Yamazoe, *Jpn J. Appl. Chem.*, 1988, **27**, 1798.
159. D.-J. Yun, S. Lee, K. Yong, S.-W. Rhee, *Appl. Phys. Lett.*, 2010, **97**, 073303.
160. E. M. Sadovskaya, Y. A. Ivanova, L. G. Pinaeva, G. Grasso, T. G. Kuznetsova, A. van Veen, V. A. Sadykov, C. Mirodatos, *J. Phys. Chem. A*, 2007, **111**, 4498.
161. D. Martin, D. Duprez, *J. Phys. Chem.*, 1996, **100**, 9429.

162. S. Bedrane, C. Descorme, D. Duprez, *Appl. Catal. A*, 2005, **289**, 90.
163. M. N. Rumyantseva, O. V. Safonova, M. N. Boulova, L. I. Ryabova, A. M. Gaskov, *Russ. Chem. Bull.*, 2003, **52**, 1217.
164. R. B. Vasiliev, S. G. Dorofeev, M. N. Rumyantseva, L. I. Ryabova, A. M. Gaskov, *Semiconductors*, 2006, **40**, 104.
165. A. Gurlo, R. Riedel, *Angew. Chem., Int. Ed.*, 2007, **46**, 3826.
166. O. Safonova, I. Bezverkhy, P. Fabrichnyi, M. Rumyantseva, A. Gaskov, *J. Mater. Chem.*, 2002, **12**, 1174.
167. M. N. Rumyantseva, A. M. Gaskov, N. Rosman, T. Pagnier, J. R. Morante, *Chem. Mater.*, 2005, **17**, 893.
168. A. Marikutsa, M. Rumyantseva, A. Gaskov, *J. Phys. Chem. C*, 2015, **119**, 24342.
169. V. V. Krivetskiy, M. N. Rumyantseva, A. M. Gaskov, *Russ. Chem. Rev.*, 2013, **82**, 917.
170. A. Marikutsa, M. Rumyantseva, A. Gaskov, *Chemosensors*, 2015, **3**, 241.

Received April 10, 2017;
in revised form July 5, 2017